



Fisheries and Oceans
Canada

Pêches et Océans
Canada

Ecosystems and
Oceans Science

Sciences des écosystèmes
et des océans

Canadian Science Advisory Secretariat (CSAS)

Research Document 2018/037

Québec Region

**Chemical and Biological Oceanographic Conditions in the Estuary and Gulf of
St. Lawrence during 2016**

M. Blais, L. Devine, C. Lehoux, P. S. Galbraith, S. Michaud, S. Plourde, and M. Scarratt

Fisheries and Oceans Canada
Institut Maurice-Lamontagne
850 route de la Mer, P.O. Box 1000
Mont-Joli, QC, G5H 3Z4

Foreword

This series documents the scientific basis for the evaluation of aquatic resources and ecosystems in Canada. As such, it addresses the issues of the day in the time frames required and the documents it contains are not intended as definitive statements on the subjects addressed but rather as progress reports on ongoing investigations.

Published by:

Fisheries and Oceans Canada
Canadian Science Advisory Secretariat
200 Kent Street
Ottawa ON K1A 0E6

[http://www.dfo-mpo.gc.ca/csas-sccs/
csas-sccs@dfo-mpo.gc.ca](http://www.dfo-mpo.gc.ca/csas-sccs/csas-sccs@dfo-mpo.gc.ca)



© Her Majesty the Queen in Right of Canada, 2018
ISSN 1919-5044

Correct citation for this publication:

Blais, M., Devine, L., Lehoux, C., Galbraith, P.S., Michaud, S., Plourde, S., and Scarratt, M. 2018. Chemical and Biological Oceanographic Conditions in the Estuary and Gulf of St. Lawrence during 2016. DFO Can. Sci. Advis. Sec. Res. Doc. 2018/037. iv + 57 pp.

Aussi disponible en français :

Blais, M., Devine, L., Lehoux, C., Galbraith, P.S., Michaud, S., Plourde, S., et Scarratt, M. 2018. Les conditions océanographiques chimiques et biologiques dans l'estuaire et le golfe du Saint-Laurent en 2016. Secr. can. de consult. sci. du MPO. Doc. de rech. 2018/037. iv + 61 p.

TABLE OF CONTENTS

ABSTRACT.....	IV
INTRODUCTION	1
METHODS.....	1
SAMPLE COLLECTION.....	1
SATELLITE REMOTE SENSING OF OCEAN COLOUR.....	2
VERTICALLY INTEGRATED VARIABLES.....	3
ZOOPLANKTON INDICES.....	3
SCORECARDS.....	4
OBSERVATIONS.....	5
PHYSICAL ENVIRONMENT	5
NUTRIENTS AND PHYTOPLANKTON.....	5
High-frequency monitoring sites	5
Gulf subregions	6
Remote sensing of ocean colour	7
ZOOPLANKTON.....	8
High-frequency monitoring sites	8
Gulf subregions	9
Copepod phenology	10
Scorecards.....	10
DISCUSSION.....	11
ENVIRONMENTAL CONDITIONS	11
PHYTOPLANKTON	12
ZOOPLANKTON.....	13
SUMMARY	15
ACKNOWLEDGEMENTS	16
REFERENCES	16
TABLES.....	19
FIGURES.....	20
APPENDICES.....	56

ABSTRACT

An overview of chemical and biological oceanographic conditions in the Gulf of St. Lawrence (GSL) in 2016 is presented as part of the Atlantic Zone Monitoring Program (AZMP). AZMP data as well as data from regional monitoring programs are analyzed and presented in relation to long-term means in the context of a strong warming event that began in 2010. Nitrate inventories in 2016 were mostly below normal in the 0–50 m layer, due to a mild early winter, but strongly above normal in the deeper layer (particularly in the southern and eastern GSL). According to satellite imagery, phytoplankton biomass averaged annually (March–November) over the GSL was slightly below the long-term average. A dominance of small cells (flagellates and dinoflagellates) within phytoplankton assemblages, as observed at Shediac Valley station, could explain why annual biomass was generally low. Nevertheless, spring bloom magnitude and amplitude were generally higher than the climatology (1999–2010). Spring bloom maximum biomass even reached a record high in the western GSL. Positive diatom anomalies at Rimouski station were responsible for the strong biomass found there all year-round (April–October), and high diatom abundance could also explain the strong phytoplankton biomass retrieved elsewhere in western GSL during spring. The spring bloom occurred earlier and lasted longer than normal in the Magdalen Shallows and Cabot Strait, while timing was normal and duration was shorter in the northern GSL. Zooplankton biomass in 2016 was among the lowest recorded so far throughout the GSL, mainly due to the decreased abundance of *Calanus finmarchicus*, which showed the earliest stage development observed so far at Rimouski station. The large calanoid index was above normal for the first time since 2006 in the western GSL due to a high abundance of *C. hyperboreus*. The positive anomalies observed since 2008 for the abundances of small calanoids, cyclopoids, warm-water-associated copepods, *Pseudocalanus* spp., and non-copepod species continued in 2016. They were possibly due to a combination of warm water and reduced competition since abundances of *Calanus* spp. were generally low.

INTRODUCTION

The Atlantic Zone Monitoring Program (AZMP) was implemented in 1998 (Therriault et al. 1998) with the aim of (1) increasing Fisheries and Oceans Canada's (DFO) capacity to understand, describe, and forecast the state of the marine ecosystem and (2) quantifying the changes in the ocean's physical, chemical, and biological properties and the predator–prey relationships of marine resources. AZMP provides data to support the sound development of ocean activities. A critical element in the observational program of AZMP is an annual assessment of the distribution and variability of nutrients and the plankton communities they support.

A description of the spatiotemporal distribution of nutrients (nitrate, silicate, phosphate), chlorophyll concentrations, and oxygen dissolved in seawater provides important information on water-mass movements and on the locations, timing, and magnitude of biological production cycles. A description of phytoplankton and zooplankton distribution provides important information on the organisms forming the base of the marine food web. An understanding of plankton production cycles is an essential part of an ecosystem approach to fisheries management.

The AZMP derives its information on the state of the marine ecosystem from data collected at a network of sampling locations (high-frequency monitoring sites, cross-shelf sections) in each DFO region (Québec, Gulf, Maritimes, Newfoundland; see Figure 1 for Québec region locations) sampled at a frequency of weekly to once annually. The sampling design provides basic information on the natural variability in physical, chemical, and biological properties of the Northwest Atlantic continental shelf: cross-shelf sections provide detailed geographic information but are limited in their seasonal coverage while critically placed high-frequency monitoring sites complement the sampling by providing more detailed information on annual scale changes in ecosystem properties.

In this document, we review the chemical and biological oceanographic (lower trophic levels) conditions in the Gulf of St. Lawrence (GSL) in 2016. Overall, temperature conditions were warmer than normal during the whole year, likely due to a mild early winter and a very low sea-ice cover (the third lowest seasonal maximum ice volume since 1969; Galbraith et al. 2017). Record high sea-surface temperatures were registered for the Estuary for the May–November period (since 1985). Deep-water temperatures have continued to increase with record highs at depths of 250 m and 300 m. The bottom areas covered by waters warmer than 6°C decreased in Anticosti and Esquiman Channels, while it increased sharply in the central GSL and made its first appearance in the northwest GSL (Galbraith et al. 2017). This report describes the 2016 production cycles and community composition of phytoplankton and zooplankton in this context.

METHODS

SAMPLE COLLECTION

All sample collection and processing steps meet and often exceed the standards of the AZMP protocol (Mitchell et al. 2002). Field measurements included in this report were collected along seven sections during surveys done in March (winter), June (summer), and October–November (fall) of each year and at two high-frequency monitoring sites (Fig. 1). In this document, the seven sections were grouped into three subregions to better correspond to the spatial scales addressed by AZMP in other regions:

-
1. western GSL (wGSL): this region is generally deep (> 200 m) and cold in summer. It is strongly influenced by freshwater runoff from the St. Lawrence River and cold and dense waters from the Laurentian Channel. It includes TESL, TSI, and TASO sections;
 2. southern GSL (sGSL): this region is shallow (< 100 m) and much warmer in summer. It is under the influence of the Gaspé Current and includes TIDM section only;
 3. eastern GSL (eGSL): this region, with deep channels and a relatively wide shelf (< 100 m), is characterized by higher surface salinity and is directly influenced by the intrusion of water from the Labrador and Newfoundland shelves. It includes TCEN, TDC, and TBB sections.

Table 1 provides details about the 2016 sampling surveys and Figure 2 gives the sampling effort at the high-frequency sampling sites. Rimouski station (depth 320 m) has been sampled since 1991 as part of a research project—about weekly throughout the summer, less frequently in early spring and late fall, and rarely in winter (except for physical variables during the March survey; nutrients have been sampled during the March survey since 2001). It has been included in AZMP’s annual review of environmental conditions since 2004 to represent conditions in the St. Lawrence Estuary (SLE) and the northwest GSL. Since the beginning of the AZMP, Shediac Valley station (depth 84 m) has represented conditions in the southern GSL and SLE outflow. While the goal is to sample Shediac Valley station twice a month, the frequency is closer to monthly and even more rarely during January–April because of its remoteness. Sampling at sections and high-frequency monitoring sites includes a CTD profile (temperature, salinity, fluorescence, dissolved oxygen, pH) as well as water sampling using Niskin bottles. Water from the Niskin bottles is collected for the analysis of chlorophyll *a* (chl *a*; method of Welschmeyer 1994 or Holm-Hansen et al. 1965), nutrients, and phytoplankton identification. Finally, zooplankton were sampled with bottom-to-surface ring net tows (75 cm diameter, 200 µm mesh) for identification and biomass measurements.

Since 1996, a survey of the winter surface mixed layer of the GSL has been conducted in early to mid-March using a Canadian Coast Guard (CCG) helicopter (shipboard sampling in 2016); surface nutrients (2 m) were added to the sampling protocol in 2001 (Galbraith 2006, Galbraith et al. 2006). Additional depths were also sampled in March 2016 because sampling was carried out from a CCG ship rather than from a helicopter. This survey has added a considerable amount of data to the previously sparse winter sampling in the region. Seventy-four stations were sampled between 29 Feb. and 14 March 2016.

SATELLITE REMOTE SENSING OF OCEAN COLOUR

Near-surface phytoplankton biomass has been estimated from ocean colour data collected by the Sea-viewing Wide Field-of-view Sensor ([SeaWiFS](#)) satellite launched by NASA in late summer 1997, by the Moderate Resolution Imaging Spectroradiometer ([MODIS](#)) “Aqua” sensor launched by NASA in July 2002, and most recently by the Visible Infrared Imaging Radiometer Suite ([VIIRS](#)) satellite, which was launched in October 2011. In this report, VIIRS data for the 2012–2016 period and MODIS data for the 2008–2011 period are combined with SeaWiFS data from September 1997 until December 2007 to construct composite time series of surface chl *a* in four GSL subregions (northwest and northeast GSL [NWGSL, NEGSL], Magdalen Shallows, Cabot Strait; see Fig. 3 for locations). Note that in our previous report (Devine et al. 2017), MODIS data were used from January 2008 through June 2015 and VIIRS data were used for the remainder of 2015. The performance of the MODIS satellite to estimate chl *a* has been compared with that of SeaWiFS for some regions of the globe. Although differences in sensor design, orbit, and sampling between MODIS and SeaWiFS cause some differences in calculated chl *a* values (Gregg and Rousseaux 2014), the biases associated with these

satellites are overall not significantly greater than algorithm uncertainties, particularly in non-turbid waters (Zibordi et al. 2006, Arun Kumar et al. 2015). Recent studies comparing all three sensors indicate that they provide consistent global ocean colour data records, with similar patterns and magnitudes and generally high cross-sensor fidelity, reflecting the strong performance of these sensors (Wang et al. 2013, Barnes and Hu 2016).

All selected subregions for the imagery data are located outside of the St. Lawrence River plume because data in regions influenced by this freshwater are unreliable due to turbidity and riverine input of terrestrially derived coloured matter. Composite satellite images were provided by BIO's remote sensing unit (Bedford Institute of Oceanography, DFO, Dartmouth, NS) in collaboration with NASA's GSFC (Goddard Space Flight Center). Basic statistics (mean, range, standard deviation) were extracted from two-week average composites with a 1.5 km spatial resolution for SeaWiFS and MODIS, and a 1 km spatial resolution for VIIRS.

A shifted Gaussian function of time model was used to describe characteristics of the spring phytoplankton bloom based on the combined satellite data (Zhai et al. 2011). Four different metrics were computed to describe the spring bloom characteristics: start date (day of year), cycle duration (days), magnitude (the integral of chl *a* concentration under the Gaussian curve), and amplitude (maximum chl *a*). In addition, the mean chl *a* biomass during spring (March to May), summer (June to August), and fall (September to November) as well as its annual average (March to November) were computed. For each of these eight metrics, we computed normalized annual anomalies (see Scorecard section below) to evaluate evidence of temporal trends among the different statistical subregions.

VERTICALLY INTEGRATED VARIABLES

Chlorophyll *a* and nutrient data collected along the AZMP sections and the high-frequency monitoring sites were integrated over various depth intervals (i.e., 0–100 m for chl *a*; 0–50 m and 50–150 m for nutrients) using trapezoidal numerical integration. The surface (0 m) data were actually the shallowest sampled values and the closest sampled depth to the lower integration limit was used in the calculation. Zooplankton indices (described below) were integrated using sampled depth. In previous reports, integrated nitrate values from the winter survey were calculated using surface concentrations (2 m) × 50 m; it was assumed that nitrate concentrations are homogeneous in the winter mixed layer at that time of the year. In 2016, the vertical profiles of nutrients at Rimouski station revealed that nitrate concentrations were indeed relatively homogenous in the upper 50 m of the water column (around 14 mmol m⁻³; see Results) The nutrient inventory in the upper (0–50 m) water column was also relatively homogenous elsewhere in the GSL during the March 2016 survey (data not shown), confirming the initial assumption.

ZOOPLANKTON INDICES

In this document, we provide a detailed description of the seasonal patterns for different zooplankton indices, mostly at Rimouski and Shediac Valley stations, but also for the three GSL subregions described above. In recent years, the number and type of zooplankton indices as well as the way they are reported have been rationalized with the aim of standardizing research documents among AZMP regions. For the high-frequency monitoring sites, we thus present total zooplankton biomass, total copepod abundance, and the relative contributions of the copepod species making up 95% of the identified taxa by abundance. In addition, we include *Pseudocalanus* spp. (Rimouski station only) and *Calanus finmarchicus* abundances and stage composition. Because of its importance to the total zooplankton biomass in the GSL, a detailed description of *Calanus hyperboreus* has been added for Rimouski and Shediac Valley stations. We also present the spring and fall total zooplankton biomass and total abundance of *C.*

finmarchicus, *C. hyperboreus*, and *Pseudocalanus* spp. for the three GSL subregions since they have distinct oceanographic regimes.

Changes in zooplankton phenology were described using *C. finmarchicus* as an indicator. We used the time series at Rimouski station because adequate sampling and stage identification started there more than 20 years ago (1994). From 1994 to 2004, *C. finmarchicus* copepodite stage abundance was determined using samples collected with 333 μm (CIV–CVI) and 73 μm (CI–III) mesh nets that were analyzed for seven years of the time series (see Plourde et al. 2009 for details). In other years before 2004 for which 73 μm samples were not analyzed, the abundance of CI–III in the 333 μm samples was adjusted based on a comparison done with a similar net (S. Plourde, DFO, Mont-Joli, QC, unpublished data). The phenology of *C. finmarchicus* was described using the following steps: (1) stage abundance data (ind. m^{-2}) were normalized (x/x_{max}) within each year for CI–III, CIV, CV, and CVI (male and female) and (2) relative stage proportions were smoothed using a Loess algorithm.

We finally present several zooplankton indices that reflect either different functional groups with different roles in the ecosystem or groups of species indicative of cold- or warm-water intrusions and/or local temperature conditions specific to the GSL. These indices are for large calanoids (dominated by *Calanus* spp. and *Metridia* spp.), small calanoids (depending of the region, this group can be dominated by species such as *Pseudocalanus* spp., *Acartia* spp., *Temora longicornis*, and *Microcalanus* spp.), cyclopoids (dominated by *Oithona* spp. and *Triconia* spp.; the latter is a poecilostomatoid that is included in this category because of its ecological characteristics), warm-water species (*Metridia lucens*, *Centropages* spp., *Paracalanus* spp., and *Clausocalanus* spp.), and cold/arctic species (*Calanus glacialis* and *Metridia longa*). Anomalies were computed for these groups (see Scorecard section below) for both high-frequency monitoring sites and GSL subregions.

SCORECARDS

Standardized anomalies of standard chemical and biological indices presented in scorecards were computed for the high-frequency monitoring sites, sections, and oceanographic regions. These anomalies are calculated as the difference between the variable's average for the season (i.e., chlorophyll and nutrient indices) or for the complete year (i.e., zooplankton indices) and the variable's average for the reference period (usually 1999–2010, but a longer reference period is often used for physical variables); this number is then divided by the reference period's standard deviation. These anomalies are presented as scorecards with positive anomalies depicted as shades of red, negatives as blues, and neutral as white. A standard set of indices representing anomalies of nutrient availability, phytoplankton biomass and bloom dynamics, and the abundance of dominant copepod species and groups (*C. finmarchicus*, *Pseudocalanus* spp., total copepods, and total non-copepods) are produced for each AZMP region. To visualize northwest Atlantic shelf-scale patterns of environmental variation, a zonal scorecard including observations from all of the AZMP regions is presented in DFO (2017).

Annual estimates of the mean abundance of key zooplankton at both the fixed stations and as an overall average in each GSL subregions are based on general linear models (GLMs) of the form

$$\begin{aligned}\text{Log}_{10}(\text{Abundance}+1) &= \alpha + \beta_{\text{YEAR}} + \delta_{\text{MONTH}} + \varepsilon \text{ for the fixed stations and} \\ \text{Log}_{10}(\text{Abundance}+1) &= \alpha + \beta_{\text{YEAR}} + \delta_{\text{STATION}} + \gamma_{\text{SEASON}} + \varepsilon \text{ for the sections,}\end{aligned}$$

as in Pepin et al. (2013) and Johnson et al. (2016). *Abundance* is in units of ind/m^{-2} , α is the intercept, and ε is the error. The GLM is applied to the three subregions separately. For the fixed stations, β and δ are the categorical effects for year and month effects, respectively. For the sections, β , δ , and γ take into account the effect of year, station, and season, respectively.

An estimate of the least-square mean based on type III sums of squares was used as the measure of the overall year effect. Results of the GLM analysis for high-frequency monitoring stations and sections are shown in Appendices 1 and 2, respectively. This year, we log-transformed density values to compute zooplankton anomalies in order to deal with the skewed distribution of the observations. One was added to the *Abundance* term to include observations with a value = 0. It should also be noted that the functional group zooplankton indices were integrated using bottom depth rather than sampled depth prior to 2015 (e.g., Devine et al. 2015). Thus, numbers in the scorecard might not exactly match previous values even though anomaly patterns have not changed.

OBSERVATIONS

PHYSICAL ENVIRONMENT

The temperature and salinity of the 2016 water column are described in Galbraith et al. (2017) in detail. Stratification is one of the key parameters controlling primary production. For this reason, we introduce a new figure on the upper water column stratification at the high-frequency monitoring stations (Fig. 4). Higher-than-normal stratification values are shown in blue in this figure because they are usually caused by lower salinity in the upper layer. The onset of water column stratification started earlier than the climatological average at Rimouski station, as evidenced by the strong 0–50 m density gradient ($\Delta\sigma$) in April (Fig. 4). At Shediac Valley station, the upper water column stratification strength was similar to the climatology (Fig. 4).

NUTRIENTS AND PHYTOPLANKTON

Distributions of the primary dissolved inorganic nutrients (nitrate, silicate, phosphate) included in AZMP's observational program strongly co-vary in space and time (Brickman and Petrie 2003). For this reason and because the availability of nitrogen is most often associated with phytoplankton growth limitation in coastal waters of the GSL, emphasis in this document is given to variability in nitrate concentrations and inventories, even though distribution of other nutrients is also briefly discussed. In this document, we use the term "nitrate" to refer to nitrate+nitrite ($\text{NO}_3^- + \text{NO}_2^-$).

High-frequency monitoring sites

The main highlights of 2016 in terms of nutrient and phytoplankton biomass are well illustrated in Figure 5 for both high-frequency monitoring sites. At Rimouski station, the nitrate drawdown that occurred during spring was associated with an unprecedented spring phytoplankton bloom (Fig. 5a, c, e). Moreover, a second bloom occurred in early fall (Fig. 5c) and was responsible for another important nitrate drawdown in the surface layer at that period (Fig. 5a). At Shediac Valley station, sampling was sparse and almost nonexistent during wintertime and early spring (Fig. 5b, d), rendering difficult the detection of seasonal patterns. From June until November, surface nitrate inventories and phytoplankton biomass were generally near normal values. However, in May, both nitrate inventory and chl *a* were below the climatology (Fig. 5b, d), which could be due to a change in spring bloom phenology.

Detailed nitrate and chl *a* vertical profiles and/or vertical anomaly patterns are shown in Figures 6 and 7 for Rimouski and Shediac Valley stations, respectively. Following the spring phytoplankton bloom decline in May, the increase of chl *a* concentrations below 50 m suggests a strong export of organic material from the surface to deeper layers (Fig. 6). Mid-layer (50–150 m) nitrate inventories were above the 1999–2010 average most of the year at Rimouski station (Fig. 6), and sporadic intrusion of this nutrient-rich mid-layer into the surface layer during the

season might explain why phytoplankton biomass remained high. Such intrusions can clearly be seen from the nitrate profile through the productive season (Fig. 6). Consequently, a pattern of low near-surface nitrate concentrations and concomitant strong pulses of chl *a* scattered with higher nitrate/lower chl *a* values can be distinguished from May until September, and this is similar to observations made in previous years (Fig. 6). The spring–neap tidal forcing has been hypothesized as a potential mechanism behind these nutrient upwelling events, but this requires further investigation. Deep nitrate concentrations were mostly below the long-term average at both Rimouski (320 m, Fig. 6) and Shediac Valley station (75 m, Fig. 7).

Annual (May–Oct.) averaged total phytoplankton cell abundance at Rimouski station was higher than normal for the first time since 2009, and the positive diatom anomaly was the highest recorded over the time series (Fig. 8). Dinoflagellate abundance was well below normal, continuing a pattern observed since 2011. In 2016, the relative abundance of diatoms almost reached 80% in April, whereas in the climatology their relative abundance is below 10% in April and reaches ca. 65% in May, suggesting that the bloom occurred about a month earlier than the climatology (Fig. 9). Figure 10 illustrates the phenology of phytoplankton assemblages and its inter-annual variability. The diatom-dominated bloom that peaked in August 2016 was among the strongest late summer/early fall diatom blooms on record (Fig. 10). This figure also suggests that a community change from a flagellate-dominated system to a diatom-dominated system occurred in 2011 (no data in 2010), and the community composition of recent years is more like that observed from 1997 to 2003. From 2004 to 2009, the community was mostly dominated by flagellated cells (including dinoflagellates) (Fig. 10).

At Shediac Valley station, the contribution of diatoms was relatively low throughout the year, and the contribution of dinoflagellates to the fall bloom was particularly noticeable, nearly 20% (Fig. 9). Flagellates were the dominant phytoplankton group throughout the year, except during the two phytoplankton blooms (Fig. 9). While diatom abundance was below normal, the dinoflagellate, flagellate, and ciliate abundances showed positive anomalies in 2016, bringing the annual (April–October) average total phytoplankton abundance to near-normal values (Fig. 11). However, these seasonal patterns and annual anomalies must be interpreted carefully considering that only eight phytoplankton samples were analyzed at this station in 2016 and the absence of sampling in April, when the spring diatom bloom usually occurs.

Gulf subregions

A general overview of the seasonal distribution of nutrient and phytoplankton biomass anomalies in the GSL is presented in Figure 12. Surface layer nitrate inventories were near or below normal at the onset of the productive season and remained relatively low throughout the rest of the season, particularly in sGSL and eGSL, where spring nutrient drawdown (computed as the difference in nitrate inventory between March and June) was near normal (Fig. 12). In wGSL, spring nutrient drawdown was mostly below normal, which was likely responsible for the small positive nitrate anomalies observed there during summer and fall (Fig. 12). Nitrate inventories were averaged for spring and fall over each section and water column layer (mean S+F) to serve as an indicator of the average annual nutrient pool available during the productive season. The average nitrate inventories in the deep layer mostly showed positive anomalies in northern GSL, while average nitrate inventories in the CIL were generally above average in wGSL and below average in eGSL (Fig. 12). Phytoplankton biomass anomalies combined for summer and fall showed a distribution pattern different from the one observed for nitrate anomalies in the surface and CIL layers. Indeed, chl *a* negative anomalies averaged over the productive season were generally associated with positive nitrate anomalies in wGSL, while the reverse situation occurred in eGSL and sGSL (Fig. 12).

There were some inconsistencies between the observations at the high-frequency monitoring stations and along sections. During summer and fall, near-normal nitrate and chl *a* concentrations were measured along TESL while negative annual 0–50 m nitrate inventory anomalies and positive annual 0–100 m chl *a* anomalies occurred at Rimouski station (Figs. 5, 12). Moreover, while positive chl *a* anomalies were recorded along TIDM during summer and fall, biomass stayed near or below average at Shediac Valley station (Figs. 5, 12). These inconsistencies are likely related to the timing of the PMZA surveys relative to the spring bloom phenology, and so we must be cautious with our interpretation.

Detailed nutrient and phytoplankton biomass seasonal distributions are illustrated in Figure 13 to Figure 19. No matter the season, surface nutrient inventories were highest in the Estuary and around the Gaspé Peninsula, as it is generally expected from the climatology (Figs. 13, 14, 15). As estuarine waters are mixed and diluted towards the GSL (mostly in the southern part), nutrient concentrations decrease as does the N:P ratio. The change of limiting nutrient—from phosphate in freshwater environments to nitrogen in marine environments—caused the N:P ratio drop from the Estuary to the Gulf. As expected, silicate and phosphate concentrations followed patterns very similar to nitrate in terms of distribution and anomalies (Figs. 13, 14, 15). Nutrient inventories within the CIL during summer and fall also tend to be higher in the Estuary and around the Gaspé Peninsula as well as in deep regions of the GSL, where it is likely influenced by nutrient-rich bottom waters (Figs. 16, 17).

Similar to the 2001–2015 climatology, the most important nitrate drawdown between March and June occurred around the Gaspé Peninsula (Fig. 18), suggesting that this region is among the most productive areas in the GSL during springtime. In June, phytoplankton biomass hotspots were located in the Estuary and in sGSL, the latter being associated with strong positive anomalies (Fig. 19). Chl *a* concentrations had largely decreased in October–November compared with June in wGSL and sGSL, but were slightly higher during late fall than during spring in eGSL. During late fall, the strongest chl *a* concentrations were measured in sGSL (Fig. 19).

Remote sensing of ocean colour

Satellite ocean colour data provide large-scale images of surface phytoplankton biomass (chl *a*) over the whole NW Atlantic. We used two-week satellite composite images of four GSL subregions (NWGSL, NEGSL, Magdalen Shallows, and Cabot Strait; see Fig. 3) to supplement our ship-based observations and provide seasonal coverage and a large-scale context over which to interpret our survey data. The ocean colour imagery provides information about the timing and spatial extent of the spring and fall blooms but does not provide information on the dynamics that take place below the top few metres of the water column. In addition, satellite ocean colour data for the St. Lawrence Estuary are largely contaminated by suspended particulates and coloured dissolved organic matter that render these data too uncertain to be used. Knowledge of phytoplankton dynamics and subsurface information in the St. Lawrence Estuary are gathered using the high-frequency sampling at Rimouski station and the broad-scale oceanographic surveys.

Satellite imagery suggests that the phenology of the phytoplankton spring bloom varied among the different GSL subregions (Figs. 20, 21). In Cabot Strait and Magdalen Shallows, the spring bloom started in early March and peaked during the first half of April while it started in late March – early April and peaked during the second half of April in the northern GSL (Fig. 20). In the two southernmost regions, the spring bloom occurred earlier and lasted longer, and its magnitude was greater than the long-term average (Figs. 20, 22). In NWGSL and NEGSL, timing of the spring bloom was similar to the long-term average but its duration was shorter (Figs. 20, 22). A strong positive chl *a* anomaly in the NWGSL was observed during the second

half of April (Figs. 20, 21); it was associated with the highest spring bloom amplitude ever recorded at this location at this time of the year (Fig. 22). The high chl *a* concentration measured in April at Rimouski station confirmed the occurrence of such a high chl *a* peak in wGSL (Fig. 5). Phytoplankton biomass integrated over springtime (March to May) was near normal, with the exception of the positive anomaly in the NWGSL (Fig. 22). Summer (June to August) and fall (September to November) biomasses were mostly below the long-term average (Figs. 22, 23). However, this contrasts with the *in situ* observations at Rimouski station that indicated that a strong fall bloom took place in the Estuary (Fig. 5). Overall, the annual (March to November) phytoplankton biomass was mostly below the long-term average except in NWGSL, where the spring bloom was strong enough to overshadow the relatively low summer and fall biomass (Fig. 22).

The chl *a* anomalies calculated from the satellite imagery during the same periods as the surveys (1–15 June and 16–31 Oct. 2016) generally matched field observations. In wGSL, the below-normal summer biomass measured onboard (Fig. 12) agrees with a spring bloom that was shorter than the long-term average in NWGSL (Fig. 22). In the Magdalen Shallows (sGSL) and Cabot Strait (eGSL), the longer-than-average bloom duration and greater-than-average bloom magnitude (Fig. 22) corroborate the above-average biomass concentration measured in sGSL and eGSL during the surveys (Fig. 12). Overall, the composite images show mostly negative anomalies in early June (Fig. 21) and near-normal values in late October (Fig. 23) that correspond well with field data (Fig. 12). The minor local discrepancies between methods are likely attributable to the difference in chl *a* vertical integration. As noted above, satellite imagery records only the near-surface layer, whereas the shipboard data integrate the top 100 m of the water column.

ZOOPLANKTON

High-frequency monitoring sites

In 2016, the zooplankton biomass at Rimouski station was slightly below normal during spring and similar to the long-term average for most of the summer. Biomass was highest during late summer, still relatively near the climatology, and then decreased to values lower than the long-term average during fall (Fig. 24a). Overall, the zooplankton biomass was below the climatology at Rimouski station. Similarly, lower-than-average annual biomass was also seen at Shediac Valley station in 2016, especially during spring and early summer, while the highest biomass was observed in July. Only during fall was the biomass higher than the climatology, at least for the two samples collected after mid-October (Fig. 24b). Sampling frequency at Shediac Valley station was much lower compared to Rimouski station (9 vs. 34) and might not reveal a comprehensive seasonal pattern.

Total copepod abundance was much higher than the long-term average at Rimouski station in 2016 from May until the end of the year, with the seasonal variability in the copepod assemblage notably different from the long-term climatology (Fig. 25a). While *Calanus glacialis* and *Paraeuchaeta norvegica* appear in the climatology, they were no longer in the top 95% in 2016; they were replaced by *Acartia* spp., the Aetideidae group, and *Metridia lucens*. A maximum abundance almost one order of magnitude greater than the climatology occurred in June and early July and was associated with an increase in the relative abundance of *Oithona similis* (Fig. 25a, c). In addition, the relative abundance of *Microcalanus* spp., *Triconia borealis*, *Pseudocalanus* spp., and deep-dwelling species from family Aetideidae were all above the climatology for most of the year. The relative abundance of the normally dominant and large-sized *Calanus* spp. was thus considerably reduced relative to the climatology (Fig. 25b, c). At Shediac Valley station, the seasonal variability of total copepod abundance in 2016 was similar

to the long-term average during spring and early summer but then showed variations of larger amplitude than normal during late summer and fall (Fig. 26a). Copepod abundance was particularly low in September in comparison with the climatology (Fig. 26a). As expected from the climatology, *O. similis* dominated copepod abundance most of the year (Fig. 26b, c). An increase in the relative abundance of *Pseudocalanus* spp. and the presence of new taxa in the ten most abundant copepod taxa, such as *Triconia borealis* and *Metridia lucens*, were mirrored by a striking decrease in the relative abundance of *Calanus* spp. compared to the 1999–2010 climatology (Fig. 26b, c). In 2016, *Calanus glacialis* was not part of the ten most abundant taxa. This large decrease in the relative abundance of *Calanus* spp. compared to the long-term average at both sites is driven by both an increase in abundance of small taxa (*Pseudocalanus* spp. at both stations; *Microcalanus* spp. and *O. similis* at Rimouski station) and a decrease in *Calanus* spp. abundance at both sites (Fig. 26b, c).

During most of the year, *C. finmarchicus* abundance was relatively stable and below the long-term seasonal average at Rimouski station, with the exception of two observations in June that were overwhelmingly dominated by early copepodite stages (CI–CIII) in proportions greater than the climatology (Fig. 27a-c). Late summer and fall increases in the proportion of adults and CI–CIII suggest the possible occurrence of a second and third generation (Fig. 27c). At Shediac Valley station, the seasonal variability of copepodite stage structure was generally similar to the climatology, but July was marked by the near absence of early stages (Fig. 27f). It resulted in a total abundance of *C. finmarchicus* well below the climatology during summer, when a high peak of abundance is usually observed (Fig. 27d).

The abundance of the large-bodied *C. hyperboreus* was generally above the seasonal climatology in 2016 at Rimouski station, with maximum abundance observed in late summer/early fall (Fig. 28a). The 2016 copepodite stage structure was roughly similar to the climatology, but with a greater contribution of stage CIV and lower contributions of CV and CVI stages during summer and fall (Fig. 28b, c). At Shediac Valley station, *C. hyperboreus* abundance was below the seasonal average during spring and summer and about the same as in 1999–2010 during fall (Fig. 28d). Copepodite stage structure was also similar to the long-term average, but no specimen was detected prior to May and no samples were collected after early November, which limits our capacity to describe the seasonal pattern of stage composition at this site (Fig. 28e, f). Overall, the stable stage structure from July onward at both sites indicates a population in diapause, mainly at stage CIV.

The abundance of *Pseudocalanus* spp. at Rimouski station in 2016 was well above the climatology from May until November, with an exceptionally high peak of abundance dominated by the CI–CIII stages observed in June (Fig. 29a) that coincided with the two observations of high abundance in early stages of *C. finmarchicus* (Fig. 27a). The seasonal pattern of *Pseudocalanus* spp. stage structure was similar to the climatology during the whole year. The timing of the early stage peak during spring was slightly earlier than the climatology, with an increased proportion of early copepodite stages (CI–CIII; Fig. 29b, c). At Shediac Valley station in 2016, two observations made during summer showed abundances that were well above the climatology. Abundance was similar to the long-term average afterwards (Fig. 29d). No data were collected during late fall and no stage analysis was carried out for this species at Shediac Valley station.

Gulf subregions

For a second consecutive year, the average total zooplankton biomasses during the spring and fall 2016 surveys were nearly the same for both seasons and among the lowest seen over the 2000–2016 period in all three GSL subregions (Fig. 30). The abundance of *C. finmarchicus* was low during fall but not in spring, when abundance was near the overall average in all subregions

(Fig. 31). In 2016, *C. hyperboreus* abundances were higher than normal in the wGSL, even reaching a record high since 2000 during spring. However, this large taxon showed a record low abundance during spring in sGSL and was near average for both seasons in eGSL (Fig. 32). The abundances of *Pseudocalanus* spp. in wGSL have seemed to increase slowly over the years, and 2016 was no exception. In eGSL and sGSL, among the highest abundances of the time series were recorded during spring, and abundances were near average during fall (Fig. 33). The very high abundance of *Pseudocalanus* spp. during spring in sGSL is particularly striking, being almost twice as high as the highest abundance measured so far (Fig. 33). The patterns of interannual variability for these three key copepod species generally agree well with those observed at the high-frequency monitoring stations (cf. Rimouski station and wGSL, Shediac Valley station and sGSL), considering the generally low abundance of *C. finmarchicus* (Fig. 27a, d) and the extremely high abundance of *Pseudocalanus* spp. during spring at both stations (Fig. 29a, d). Moreover, the high abundance of *C. hyperboreus* in wGSL during the June survey is consistent with its higher-than-normal abundance during summer at Rimouski station (Fig. 28a).

Copepod phenology

We present a detailed seasonal pattern of the relative proportions of *C. finmarchicus* copepodite stages, a key copepod species, at Rimouski station from 1994 to 2016 as an indicator of changes in the developmental timing of zooplankton in the GSL (Fig. 34). Overall, there is an obvious ongoing trend towards earlier population development for *C. finmarchicus* at Rimouski station (Fig. 34). The earliest stage development since the beginning of the time series was observed in 2016. The pulse of adult stage (CVI) in early May was the earliest observed since 1994, suggesting that timing of the emergence from diapause was also the earliest seen so far. Early development of the 2016 cohort allowed the occurrence of a second generation, as revealed by the large contribution of adult stage to the population in July–August (Fig. 34).

Scorecards

A synthesis of standard AZMP zooplankton indices (abundances of *C. finmarchicus*, *Pseudocalanus* spp., total copepods, non-copepods) was performed using annual standardized abundance anomalies and is presented as a scorecard (Fig. 35). These anomalies in 2016 showed a continuation of patterns initiated in 2009 for *C. finmarchicus* and *Pseudocalanus* spp. and in 2006 for total copepods and non-copepods. In 2016, *C. finmarchicus* annual abundance anomalies were predominantly negative, while the annual abundance of *Pseudocalanus* spp. and total zooplankton (both copepods and non-copepods) were above the long-term average across the GSL. The greatest positive anomalies for the *Pseudocalanus* spp. and total copepod indices occurred at Rimouski station while the positive anomaly of the total non-copepod index was greatest in eGSL (Fig. 35).

The annual standardized abundance anomalies for six additional zooplankton indices (*C. hyperboreus* and five zooplankton groups: small calanoids, large calanoids, cyclopoids, warm-water species, and cold/arctic species) are presented in Figure 36. Again this year, these annual anomalies were relatively coherent among the high-frequency sampling sites (Rimouski and Shediac Valley stations) and their associated GSL subregions (Fig. 36). The abundance of small calanoids, cyclopoids, and warm-water copepod species all showed positive anomalies everywhere in the GSL in 2016, as has been generally observed since 2008 for small calanoids (mostly due to *Pseudocalanus* spp.; see Fig. 35) and warm-water copepod species. However, 2016 represents a first year of widespread positive anomaly for cyclopoids (including *Triconia/Oncaea*) (Fig. 36). The positive abundance anomalies of warm-water copepod species were the highest recorded so far in wGSL and at Rimouski station in 2016 (Fig. 36), where the

abundance of *M. lucens* was slightly higher than in the climatology (Fig. 25b, c). *M. lucens* was also the main contributor to the positive anomalies of warm-water copepods elsewhere in the GSL, along with *Centropages* spp. in sGSL and *Paracalanus* spp. in eGSL.

Strong negative anomalies have mostly been observed for large calanoids in sGSL (including Shediac Valley station) since 2009. Negative anomalies were also observed during 2016 in sGSL, but they were not as strong as they have been in the past (Fig. 36). Other GSL subregions have either shown near-normal or negative anomalies since 2009, but to a lesser extent than in sGSL. In 2016, wGSL showed positive anomalies for large calanoids and *C. hyperboreus*, the latter also being more abundant than the long-term average at Rimouski station and in eGSL (Fig. 36). In addition, a positive anomaly was observed for the first time since 2010 in wGSL for cold copepod species. In eGSL, the positive anomaly for cold species continues the trend started in 2007 (Fig. 36). It must be noted that indices of warm-water and cold/arctic species are based on generally rare taxa, implying that relatively minor changes in abundance could result in large variations in their anomalies.

DISCUSSION

ENVIRONMENTAL CONDITIONS

Besides the effect of water column stratification on phytoplankton dynamics, thermal properties of the surface, intermediate (Cold Intermediate Layer [CIL], 30–125 m), and deep-water masses play a role in defining zooplankton dynamics (Plourde et al. 2002). Galbraith et al. (2017) reported on the physical conditions that prevailed in the GSL during 2016. We briefly summarize here their main findings. Among them was the observation of a mild early winter; the surface mixed layer was not near freezing over the entire GSL, which led to the third lowest maximum volume in sea-ice cover since 1969. From May to November, sea-surface temperatures averaged over the GSL were near normal or above normal and were at record highs in the Estuary. CIL temperature was also generally warmer than usual. The summed normalized anomalies of different composite climate indices for the three layers of the GSL's water column revealed that all layers (surface, intermediate, and deep) showed warmer-than-usual conditions, with the most striking warming occurring in the deep water. The annual average freshet of the St. Lawrence River combined with tributaries to the Estuary was slightly above normal in 2016. This document reports on the chemical and biological conditions in the GSL in the context of these conditions.

Overall, surface nitrate inventories were near or below the long-term average in March over the GSL. Winter mixing is a critical process for bringing nutrient-rich deep water to the surface. In the GSL, this winter convection is partly caused by buoyancy loss (cooling and reduced freshwater runoff), brine rejection associated with sea-ice formation, and wind-driven mixing prior to ice formation (Galbraith 2006). However, surface waters stayed relatively warm through the winter and sea-ice formation was minimal, suggesting lower winter convection than normal, which likely resulted in water column stratification that was stronger than usual during early spring. Thus, it seems that weak winter convection did not allow a complete replenishment of surface water nutrients prior to the spring bloom in most areas of the GSL.

High deep-water (> 200 m) nutrient anomalies have been observed since 2012 in all areas but the Estuary region; these are associated with high temperature and salinity intrusions into the GSL from Cabot Strait (Galbraith et al. 2017). These higher-than-average deep inventories are probably associated with a combination of a thermocline that is higher in the water column, stronger stratification during late summer and fall, and a water mass composition that has a greater contribution of slope water than Labrador Shelf water (Galbraith et al. 2017). The

upwelling of such nutrient-rich water could supply primary producers during the productive season. However, the warming of bottom waters and their above-normal nutrient levels may also affect acidification that has been previously reported in the region (Mucci et al. 2011), with potential negative consequences on fisheries and aquaculture activities as well as on overall productivity and biodiversity in the GSL.

PHYTOPLANKTON

The weak winter mixing and consequent low nutrient inventory at the onset of the spring bloom could suggest relatively low spring productivity in the GSL. However, according to satellite imagery, spring (March to May) biomass was near normal throughout the GSL. The spring chl *a* biomass was even above normal in NWGSL, and field data collected at Rimouski station confirmed the occurrence of a strong phytoplankton bloom. In the Magdalen Shallows and Cabot Strait, the bloom started earlier than the climatology, and field data from Rimouski station indicated that the bloom also began earlier in the Estuary. The timing of the spring bloom in the St. Lawrence Estuary is known to be largely influenced by both runoff intensity and freshwater-associated turbidity (Levasseur et al. 1984, Therriault and Levasseur 1985; Zakardjian et al. 2000, Le Fouest et al. 2010, Mei et al. 2010). The slightly above-normal spring freshet combined with a thinner cold winter surface mixed layer in 2016 likely resulted in early stratification of the upper water column in the Estuary; this could explain the early start of primary production in the Estuary, especially considering the reduced ice cover (Ferland et al. 2011; Le Fouest et al. 2005). Low ice cover and early stratification due to weak winter convection could possibly be responsible for an early start of primary production elsewhere in the GSL and explain the observations made in the Magdalen Shallows and Cabot Strait. Moreover, satellite observations revealed that the spring bloom started in late February in the Cabot Strait region, before the March AZMP survey. Thus, in sGSL and eGSL, where most of the negative anomalies in the winter nitrate inventory were measured, an early start of the spring bloom prior to the March survey could partly explain the concomitant near-average spring biomass and low nutrient inventory. A low zooplankton spring biomass, as observed throughout the GSL in 2016, and reduced grazing pressure could also allow the growth of phytoplankton to near normal values despite a low spring nutrient inventory.

Despite a relatively normal spring biomass, chl *a* was mostly below average for the remainder of the year in the GSL, with the exception of the late summer/early fall bloom observed at Rimouski station. Diatoms are typically found in nutrient-rich, well-mixed environments because they mainly rely on nitrate to fulfill their nitrogen requirement; smaller-sized cells such as flagellates and dinoflagellates are associated with nutrient-poor, stratified environments and mostly use reduced forms of nitrogen, such as ammonium (Levasseur et al. 1984, Li and Harrison 2008). Thus, the warm, stratified, low-nutrient environment that prevailed over most of the GSL in 2016 was favourable to flagellated phytoplankton communities. Interestingly, the relative abundances of flagellates and dinoflagellates were above the long-term average at Shediac Valley station from April to November in 2016, and the diatom/flagellate and diatom/dinoflagellate ratios showed negative anomalies. The AZMP program has not regularly documented the taxonomic composition of the phytoplankton community elsewhere in the GSL, and we must be cautious when generalizing these results to other GSL subregions. Nevertheless, flagellate-dominated communities could be responsible for low phytoplankton biomass during summer and fall 2016 in the GSL.

At Rimouski station, phytoplankton biomass was generally dominated by diatoms until late fall during 2016. Diatoms were responsible for the strong spring and late summer blooms recorded at this site, and perhaps in wGSL during spring. A second phytoplankton bloom can occur when late summer/early fall winds are strong enough to break stratification and upwell deep nutrient-

rich waters to the sea surface, especially considering the widespread positive anomaly of deep-water nitrate inventories observed in 2016. Observations of the vertical profiles of salinity (see Fig. 73 in Galbraith et al. 2017) and nitrate recorded at Rimouski station showed that the strong fall bloom was preceded by the intrusion of saltier, nutrient-rich water from greater depths into the surface layer. The interannual variability of the seasonal phytoplankton assemblage shows that diatoms have made up the greatest proportion of the total abundance from late spring to early fall from 2011 to 2016, while they represented a relatively low proportion (< 50%) of total abundance from 2003 to 2009 (Fig. 10). Interestingly, the 2011–2016 period is associated with near- or above-average surface nitrate inventories during fall in wGSL, while nutrient inventories during fall were generally below average during the 2003–2009 period (Fig. 12). Thus, environmental parameters altering the onset of stratification and its strength throughout the productive season could possibly play a critical role in determining annual phytoplankton biomass, community composition, and the possibility for the occurrence of a second bloom.

ZOOPLANKTON

Among the most striking features in 2016 was the very low zooplankton biomass for a second consecutive year during spring and fall throughout the GSL. It was likely associated with the decrease in large-sized zooplankton species abundance, particularly in sGSL. However, against this general backdrop of decreased *Calanus* spp. abundance, large calanoid abundance was above the climatology in wGSL, mostly due to *C. hyperboreus*. It has been hypothesized that high spring freshwater runoff from the St. Lawrence River could result in a lower transport of *Calanus* species in sGSL (Runge et al. 1999, Galbraith et al. 2017). In 2016, the freshet was slightly above normal and could therefore partly explain the negative anomaly of large calanoids in sGSL despite their relatively high abundance in the source region (wGSL). Life cycle strategies are different among large copepod species, and the timing of reproduction relative to the freshet—considering its influence on water mass circulation and transport—could explain dissimilarities in the distribution pattern of these species. Change in bottom water masses entering the GSL through Cabot Strat (Galbraith et al. 2017) is another hypothesis that could explain low abundance of large calanoids in sGSL. Additionally, at Shediac Valley station, and possibly elsewhere in sGSL, the diatom contribution to the spring and summer phytoplankton assemblage was below the long-term average in 2016, which may have contributed to the negative anomaly of the large calanoid index observed there.

The predation pressure exerted on large calanoids by the massive cohort of the local redfish stock (*Sebastes mentella*), first detected in 2013 and seen again in 2016 in the northern GSL (Bourdages et al. 2017), could also have contributed to the generally low zooplankton biomass in 2016. Small redfish (< 25 cm) feed predominantly on large calanoids and other small crustaceans (Gonzalez et al. 2000) and may represent a new predatory threat strong enough to exert a significant top-down pressure on populations of large calanoids in the GSL in recent years. The large energy-rich copepod *C. finmarchicus* exhibited another year of widespread negative anomalies (Rimouski and Shediac Valley stations, eGSL), but to a lesser extent than in 2015. As redfish individuals grow older and their distribution deepens, they might change their feeding behaviour and select larger prey (Brassard et al. 2017), reducing pressure on *C. finmarchicus* compared to what has been observed in the last few years. *Calanus hyperboreus*, with its larger size and its deeper distribution (Plourde et al. 2003), might become a more suitable prey later in the ontogeny of redfish and might be therefore less affected by redfish predation. However, studies on the effect of redfish predation on large calanoid populations are lacking in the GSL to validate these hypotheses.

Despite low zooplankton biomass, the overall zooplankton abundance increased as did the abundances of both copepod and non-copepod species (larval stages of benthic invertebrates,

many carnivores that feed on other zooplankton, and small particle-feeding taxa), suggesting a general shift towards smaller zooplankton species with potential implications for the pelagic food web and pelago–benthic coupling. The change towards a dominance of smaller taxa was initiated in 2008, as seen from the small calanoid index, and was mainly attributable to *Pseudocalanus* spp. During spring 2016, *Pseudocalanus* spp. abundance was above normal in all GSL subregions. The sustained below-normal abundance of *C. finmarchicus* (since 2009) throughout the GSL may have favoured the recruitment of *Pseudocalanus* spp. in spring and early summer by diminishing competition for adequate food, especially considering the low contribution of diatoms to the spring bloom—on which both copepods rely—observed at Shediac Valley station. Reverse anomaly patterns can be seen for these two copepod species over the study period (1999–2016; Fig. 35) and may suggest that competition is occurring between the species. *Calanus hyperboreus* usually accounts for a large part of biomass during spring in sGSL, and its abundance was among the lowest recorded during spring 2016. This could further reduce competition for *Pseudocalanus* spp. in this region.

The year-round warm temperature of the whole water column in 2016 may also have driven some changes in community composition. Warm-water copepod species showed the strongest overall positive anomaly of the time series in 2016, particularly in wGSL and at Rimouski station. At Rimouski and Shediac Valley stations, these anomalies were mostly driven by *Metridia lucens* in 2016, which has replaced cold/arctic species such as *C. glacialis* among the dominant copepod species. *M. lucens* is a strong vertical migrator that is mostly associated with temperate conditions. Thus, it might have benefited from a warmer and saltier deep layer as well as from warmer conditions at the surface that have become typical in the GSL in recent years. Despite warm conditions, the northern GSL showed positive anomalies for cold/arctic copepod species due to relatively high abundances of *M. longa* (data not shown). Their mesopelagic early copepodite stages are known to exploit sinking phytoplankton aggregates and associated microfauna (Grønvik and Hopkins 1984, Plourde et al. 2002). Vertical profiles of phytoplankton biomass recorded at Rimouski station show a large sinking of organic material following the spring bloom, which might have been favourable to the development of early copepodite stages of *M. longa* in the wGSL despite warm water masses during summer and fall 2016 (Galbraith et al. 2017). On the eastern side, temperatures in the surface layer and CIL were generally near normal throughout the year (see Fig. 65 in Galbraith et al. 2017), and were possibly beneficial to the growth of cold/arctic species. However, these causal relationships between temperature and zooplankton community composition have not been addressed yet in the context of the AZMP program and they remained hypothetical.

In addition to their possible effect on the zooplankton assemblage, local environmental conditions might also have triggered a much earlier timing of *C. finmarchicus* development compared to previous years at Rimouski station, with potential consequences on upper trophic levels. Warm conditions in the CIL and deep layer probably caused an early arousal of CV stages from diapause and moulting into CVI stage. Moreover, the early onset of the phytoplankton bloom at Rimouski station due to the mild winter could have favoured early reproduction and improved offspring survival and development. Growth and development of *Pseudocalanus* spp. also depend on phytoplankton bloom phenology, and they could also have been earlier than normal at Rimouski station in 2016, as suggested by the strong contribution of early stages to total abundance in May compared to June in the climatology. This early production might allow the occurrence of two or more generations within a single year for *C. finmarchicus* and *Pseudocalanus* spp., as evidenced by the short periods of a higher proportion of adults and resulting peaks of early copepodite stages at Rimouski station for these two taxa. The development of these successive copepod cohorts was possibly facilitated by the occurrence of two phytoplankton blooms at Rimouski station in 2016. Overall, zooplankton communities in the GSL seem to be shaped by a combination of changing water-mass

properties and of bottom-up and top-down controls. However, the relative importance of these factors is not yet well understood.

SUMMARY

This document reports on the chemical and biological (plankton) conditions in the GSL in 2016 in the context of a strong warming event initiated in 2010. Data from 2016 are compared to time-series observations.

- Overall, surface nitrate inventories (0–50 m) averaged over sampling sections were below the long-term average in March and June over the GSL due to the mild winter. However, high positive deep-water (> 200 m) nutrient anomalies have been observed since 2012 in all areas but the Estuary region and are associated with intrusions of high temperature/high salinity water into the GSL through Cabot Strait.
- The spring bloom occurred earlier and lasted longer than normal in the Magdalen Shallows and Cabot Strait, while timing was normal and duration was shorter in the northern GSL. Overall, bloom magnitude and amplitude were higher than the climatology in the GSL. However, annually averaged chl *a* was generally lower than the historical mean in the GSL except in wGSL, where the spring phytoplankton biomass reached a new record high.
- The early stratification of the upper water column at Rimouski station, due to weak winter convection and a large spring freshet, resulted in an early bloom initiation (about two months earlier than the climatology). High annual phytoplankton biomass and the occurrence of a late summer/early fall bloom were associated with a positive annual diatom anomaly. At Shediac Valley station, the annual biomass was near normal while dinoflagellates and flagellates showed strong positive anomalies.
- Zooplankton biomass was below normal throughout the GSL during spring and fall due to the decreases of the large-bodied *C. finmarchicus* everywhere in the GSL and of *C. hyperboreus* in sGSL, that were likely beneficial to small calanoids, particularly *Pseudocalanus* spp., which exhibited widespread strong positive anomalies.
- The annual abundance of *C. hyperboreus* was above normal at Rimouski station and in wGSL during 2016, and the strong contribution of diatoms to the annual phytoplankton biomass combined with the reduction of predation pressure by redfish is a hypothesis that could partly explain this high abundance.
- Positive anomalies in the warm-water copepod index were measured throughout the GSL in 2016 and were particularly strong in wGSL due to the increased abundance of *M. lucens*. These extreme values represent the highest point of a trend initiated in 2008.
- Strong positive anomalies—among the strongest recorded since the beginning of the time series—for cold/arctic copepod species were observed in wGSL and eGSL and were associated with *M. longa*.
- Local conditions at Rimouski station triggered a much earlier timing of *C. finmarchicus* development compared to previous years, with potential consequences on upper trophic levels. In 2016, this keystone species showed the earliest development over a time series beginning in 1994.

ACKNOWLEDGEMENTS

We thank Jean-Yves Couture, Sylvie Lessard, Marie-France Beaulieu, Caroline Lebel, Isabelle St-Pierre, and Caroline Lafleur for preparation and standardization of the phytoplankton and zooplankton data. The data used in this report would not be available without the work of François Villeneuve and his AZMP team (Sylvain Chartrand, Rémi Desmarais, Marie-Lyne Dubé, Yves Gagnon, Line McLaughlin, Roger Pigeon, Michel Rousseau, Félix St-Pierre, Liliane St-Amand, Paul Nicot, David Leblanc, and Brian Boivin) in organizing and carrying out AZMP surveys and analyzing samples. We thank Jeff Spry and Kevin Pauley for providing data from the Shediac Valley station and BIO's remote sensing unit for the composite satellite images. We are grateful to Catherine Johnson and Pierre Pepin for their critical reviews.

REFERENCES

- Arun Kumar, S.V.V., Babu, K.N., and Shukla, A.K. 2015. Comparative analysis of chlorophyll-a distribution from SeaWiFS, MODIS-Aqua, MODIS-Terra and MERIS in the Arabian Sea. *Mar. Geod.* 38: 40–57.
- Barnes, B., and Hu, C. 2016. Dependence of satellite ocean color data products on viewing angles: A comparison between SeaWiFS, MODIS, and VIIRS. *Remote Sens. Environ.* 175:120–129.
- Bourdages, H., Brassard, C., Desgagnés, M., Galbraith, P., Gauthier, J., Légaré, B., Nozères, C. and Parent, E. 2017. [Preliminary results from the groundfish and shrimp multidisciplinary survey in August 2016 in the Estuary and northern Gulf of St. Lawrence](#). DFO Can. Sci. Advis. Sec. Res. Doc. 2017/002. v + 87 p.
- Brassard, C., Bourdages, H., Duplisea, D., Gauthier, J., and Valentin, A. 2017. [The status of the redfish stocks \(*Sebastes fasciatus* and *S. mentella*\) in Unit 1 \(Gulf of St. Lawrence\) in 2015](#). DFO Can. Sci. Advis. Sec. Res. Doc. 2017/023. ix + 53 p.
- Brickman, D., and Petrie, B. 2003. [Nitrate, silicate and phosphate atlas for the Gulf of St. Lawrence](#). Can. Tech. Rep. Hydrogr. Ocean Sci. 231: xi + 152 pp.
- Devine, L., Plourde, S., Starr, M., St-Pierre, J.-F., St-Amand, L., Joly, P., and Galbraith, P.S. 2015. [Chemical and biological oceanographic conditions in the Estuary and Gulf of St. Lawrence during 2014](#). DFO Can. Sci. Advis. Sec. Res. Doc. 2015/071. v + 46 pp.
- Devine, L., Scarratt, M., Plourde, S., Galbraith, P.S., Michaud, S., and Lehoux, C. 2017. [Chemical and biological oceanographic conditions in the Estuary and Gulf of St. Lawrence during 2015](#). DFO Can. Sci. Advis. Sec. Res. Doc. 2017/034. v + 48 pp.
- DFO. 2017. [Oceanographic conditions in the Atlantic zone in 2016](#). DFO Can. Sci. Advis. Sec. Sci. Advis. Rep. 2017/031.
- Ferland, J., Gosselin, M., and Starr, M. 2011. Environmental control of summer primary production in the Hudson Bay system: The role of stratification. *J. Mar. Syst.* 88(3): 385–400.
- Galbraith, P. S. 2006. Winter water masses in the Gulf of St. Lawrence. *J. Geophys. Res.* 111, C06022, doi:10.1029/2005JC003159.
- Galbraith, P. S., Desmarais, R., Pigeon, R., and Cantin, S. 2006. [Ten years of monitoring winter water masses in the Gulf of St. Lawrence by helicopter](#). AZMP Bulletin PMZA 5: 32–35.

-
- Galbraith, P.S., Chassé, J., Caverhill, C., Nicot, P., Gilbert, D., Pettigrew, B., Lefavre, D., Brickman, D., Devine, L., and Lafleur, C. 2017. [Physical oceanographic conditions in the Gulf of St. Lawrence in 2016](#). DFO Can. Sci. Advis. Sec. Res. Doc. 2017/044. v + 91 p.
- Gonzalez, C., Bruno, I., and Paz, X. 2000. Food and feeding of deep-sea redfish (*Sebastes mentella* Travin) in the North Atlantic. NAFO Sci. Coun. Studies 33: 89–101.
- Gregg, W. W., and Rousseaux, C. S. 2014. Decadal trends in global pelagic ocean chlorophyll: A new assessment integrating multiple satellites, in situ data, and models. J. Geophys. Res. Oceans, 119: 5921–5933, doi 10.1002/2014JC010158.
- Grønvik, S., and Hopkins, C. C. E. 1984. Ecological investigations of the zooplankton community of Balsfjorden, northern Norway: Generation cycle, seasonal vertical distribution, and seasonal variations in body weight and carbon and nitrogen content of the copepod *Metridia longa* (Lubbock). J. Exp. Mar. Biol. Ecol. 80: 93–107.
- Holm-Hansen, O., Lorenzen, C.J., Holmes, R.W., and Strickland, J.D. 1965. Fluorometric determination of chlorophyll. ICES J. Mar. Sci. 30: 3–15.
- Johnson, C., Casault, B., Head, E., and Spry, J. 2016. Optical, chemical, and biological oceanographic conditions on the Scotian Shelf and in the Eastern Gulf of Maine in 2014. DFO Can. Sci. Advis. Sec. Res. Doc. 2016/003. v + 51 p.
- Le Fouest, V., Zakardjian, B., Saucier, F., and Starr, M. 2005. Seasonal versus synoptic variability in planktonic production in a high-latitude marginal sea: the Gulf of St. Lawrence (Canada). J. Geophys. Res. 110, C09012, doi 10.1029/2004JC002423.
- Le Fouest, V., Zakardjian, B., and Saucier, F. J. 2010. Plankton ecosystem response to freshwater-associated bulk turbidity in the subarctic Gulf of St. Lawrence (Canada): A modelling study. J. Mar. Syst. 81(1-2): 75–85.
- Levasseur, M., Therriault, J.-C., and Legendre, L. 1984. Hierarchical control of phytoplankton succession by physical factors. Mar. Ecol. Prog. Ser. 19: 211–222.
- Li, W. K. W., and Harrison, W. G. 2008. Propagation of an atmospheric climate signal to phytoplankton in a small marine basin. Limnol. Oceanogr. 53(5): 1734–1745.
- Mei, Z.-P., Saucier, F., Le Fouest, V., Zakardjian, B., Sennville, S., Xie, H., and Starr, M. 2010. Modeling the timing of spring phytoplankton bloom and biological production of the Gulf of St. Lawrence (Canada): Effects of colored dissolved organic matter and temperature. Cont. Shelf Res. 30: 2027–2042.
- Mitchell, M. R., Harrison, G., Pauley, K., Gagné, A., Maillet, G., and Strain, P. 2002. [Atlantic Zonal Monitoring Program sampling protocol](#). Can. Tech. Rep. Hydrogr. Ocean Sci. 223: iv + 23 pp.
- Mucci, A., Starr, M., Gilbert, D., and Sundby, B. 2011. Acidification of lower St. Lawrence Estuary bottom waters. Atmos.-Ocean 49(3): 206–218.
- Pepin, P., Maillet, G., Fraser, S., Shears, T., and Redmond, G. 2013. [Optical, chemical, and biological oceanographic conditions on the Newfoundland and Labrador Shelf during 2011-12](#). DFO Can. Sci. Advis. Sec. Res. Doc. 2013/051. v + 38 p.
- Plourde, S., Dodson, J. J., Runge, J. A., and Therriault, J.-C. 2002. Spatial and temporal variations in copepod community structure in the lower St. Lawrence Estuary, Canada. Mar. Ecol. Prog. Ser. 230: 221–224.
-

-
- Plourde S., Joly, P., Runge, J. A., Dodson, J. J., and Zakardjian, B. 2003. Life cycle of *Calanus hyperboreus* in the lower St. Lawrence Estuary and its relationship to local environmental conditions. *Mar. Ecol. Prog. Ser.* 255: 219–233.
- Plourde, S., Maps, F., and Joly, P. 2009. Mortality and survival in early stages control recruitment in *Calanus finmarchicus*. *J. Plankton Res.* 31(4): 371–388.
- Runge, J. A., Castonguay, M., De Lafontaine, Y., Ringuette, M., and Beaulieu, J. L. 1999. Covariation of climate, zooplankton biomass and mackerel recruitment in the southern Gulf of St. Lawrence. *Fish. Oceanogr.* 8(2): 139–149.
- Therriault, J.-C., and Levasseur, M. 1985. Control of phytoplankton production in the Lower St. Lawrence Estuary: light and freshwater runoff. *Nat. Can.* 112: 77–96.
- Therriault, J.-C., Petrie, B., Pépin, P., Gagnon, J., Gregory, D., Helbig, J., Herman, A., Lefavre, D., Mitchell, M., Pelchat, B., Runge, J., and Sameoto, D. 1998. [Proposal for a Northwest Atlantic zonal monitoring program](#). *Can. Tech. Rep. Hydrogr. Ocean Sci.* 194: vii + 57 pp.
- Wang, M., Liu, X., Tan, L., Jiang, L., Son, S. H., Shi, W., Rausch, K., and Voss, K. 2013. Impacts of VIIRS SDR performance on ocean color products. *J. Geophys. Res. Atmos.* 118: 10,347–10,360, doi:10.1002/jgrd.50793.
- Welschmeyer, N. A. 1994. Fluorometric analysis of chlorophyll a in the presence of chlorophyll b and pheopigments. *Limnol. Oceanogr.* 39(8): 1985–1992.
- Zakardjian, B. A., Gratton, Y., and Vézina, A. F. 2000. Late spring phytoplankton bloom in the Lower St. Lawrence Estuary: the flushing hypothesis revisited. *Mar. Ecol. Prog. Ser.* 192: 31–48.
- Zhai, L., Platt, T., Tang, C., Sathyendranath, S., and Hernández Walls, R. 2011. Phytoplankton phenology on the Scotian Shelf. *ICES J. Mar. Sci.* 68: 781–791, doi:10.1093/icesjms/fsq175.
- Zibordi, G., Mélin, F., and Berthon, J.-F. 2006. Comparison of SeaWiFS, MODIS and MERIS radiometric products at a coastal site. *Geophys. Res. Letters* 33: L06617, doi:10.1029/2006GL0257.

TABLES

Table 1. List of AZMP surveys with locations, dates, and sampling activities for 2016. wGSL, eGSL, and sGSL denote the western, eastern, and southern subregions of the Gulf of St. Lawrence. See Figure 1 for station locations.

Sampling group	Name	Location	Dates (2016)	Vessel	CTD/bottle	Net
Fixed	Rimouski	48°40.0'N 068°35.0'W	23 Jan–12 Dec	Beluga II (+ others)	43	34
	Shediac Valley	47°46.8'N 064°01.8'W	01 Mar–02 Nov	Multiple	10	9
	-	Estuary and Gulf	29 Feb – 14 March	Martha Black & Cornwallis	74	30
Spring Sections	TESL	wGSL	1–11 Jun	Coriolis II	7	7
	TSI	wGSL	1–11 Jun	Coriolis II	6	6
	TASO	wGSL	1–11 Jun	Coriolis II	5	5
	TIDM	sGSL	1–11 Jun	Coriolis II	10	10
	TDC	eGSL	1–11 Jun	Coriolis II	6	6
	TCEN	eGSL	1–11 Jun	Coriolis II	5	4
	TBB	eGSL	1–11 Jun	Coriolis II	7	7
Total					46	45
Fall Sections	TESL	wGSL	24 Oct–02 Nov	Hudson	7	7
	TSI	wGSL	24 Oct–02 Nov	Hudson	6	6
	TASO	wGSL	24 Oct–02 Nov	Hudson	5	5
	TIDM	sGSL	24 Oct–02 Nov	Hudson	10	10
	TDC	eGSL	24 Oct–02 Nov	Hudson	6	6
	TCEN	eGSL	24 Oct–02 Nov	Hudson	5	5
	TBB	eGSL	24 Oct–02 Nov	Hudson	7	7
Total					46	46

FIGURES

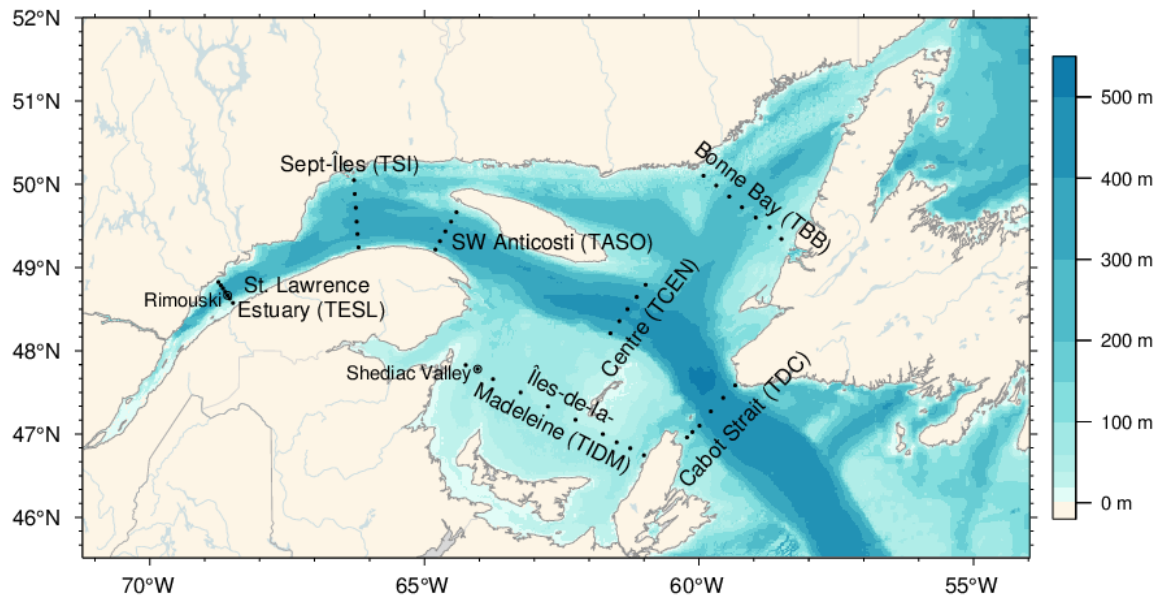


Figure 1. Bathymetric map of the Estuary and Gulf of St. Lawrence showing sampling stations on the different sections (dots) and at Rimouski and Shediac Valley stations (circles). Sections were grouped to form subregions within the western GSL: TESL, TSI, TASO; southern GSL: TIDM; and eastern GSL: TBB, TCEN, TDC.

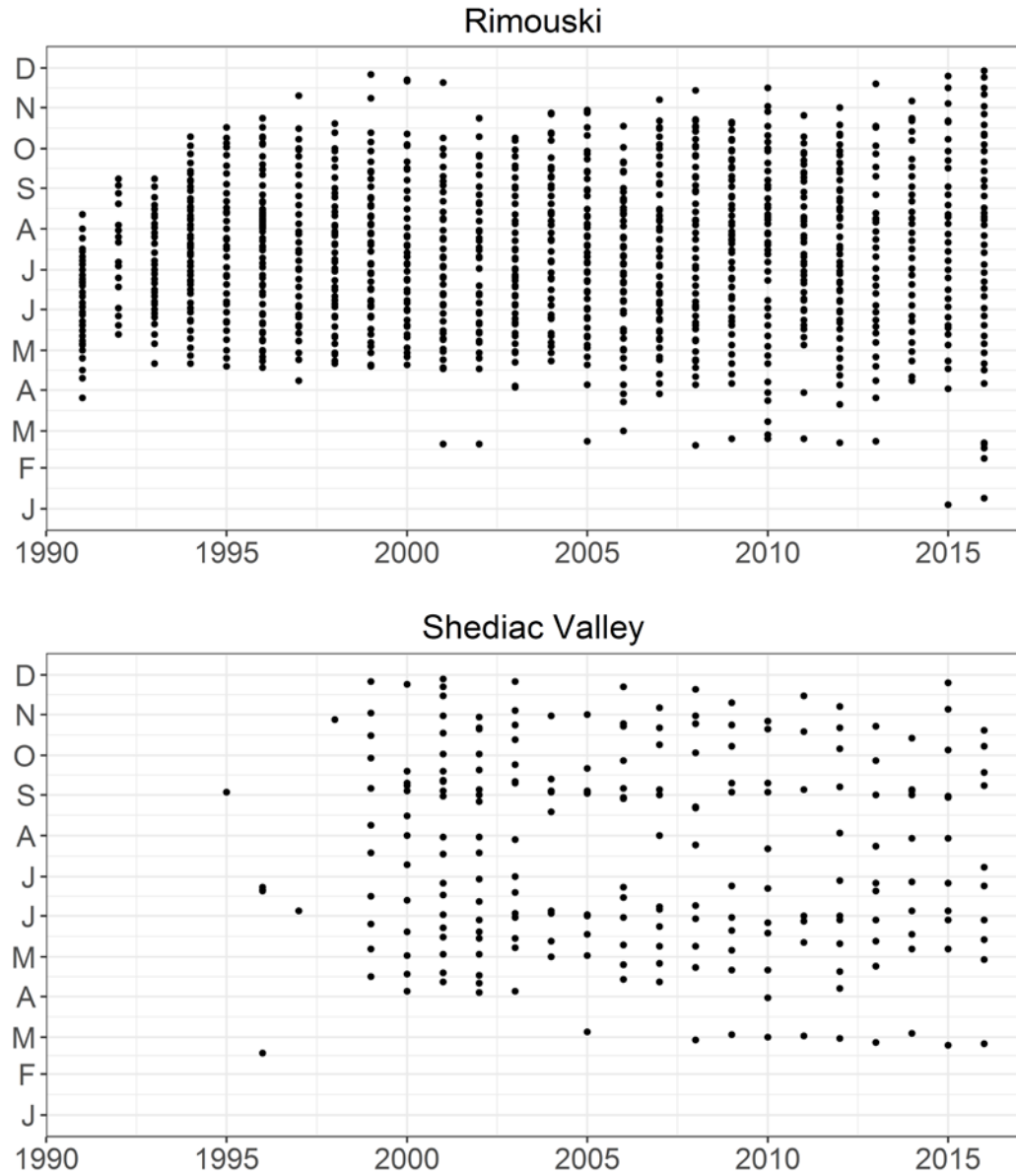


Figure 2. Sampling frequencies at Rimouski and Shediac Valley stations through 2016. Sampling included CTD/bottle as well as plankton net tows most of the time (weather permitting).

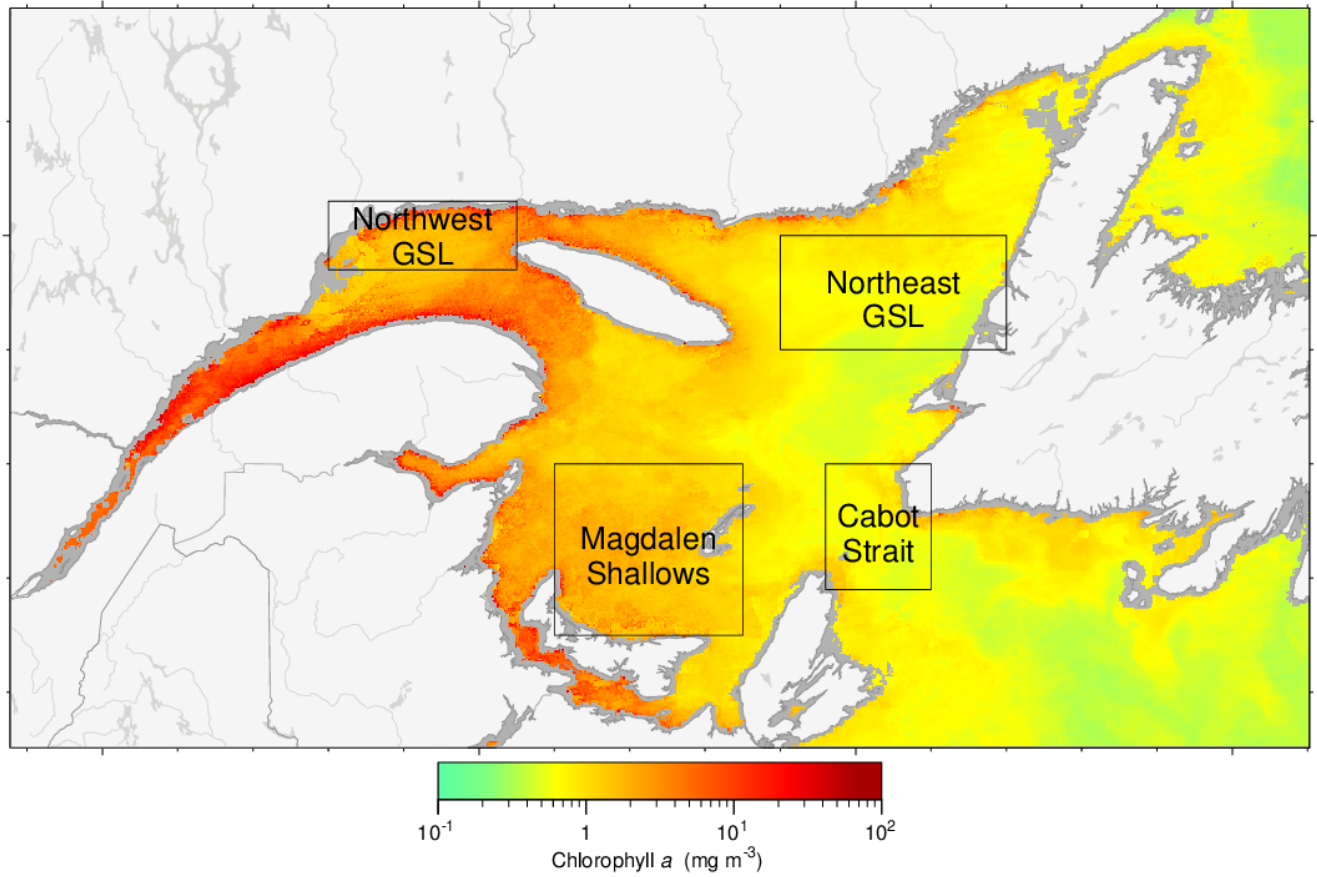


Figure 3. Statistical subregions in the Gulf of St. Lawrence (GSL) identified for the spatial/temporal analysis of satellite ocean colour data. The figure is a VIIRS composite image showing chlorophyll a from 16–31 July 2016. Gray areas indicate no data (in this case near-shore regions).

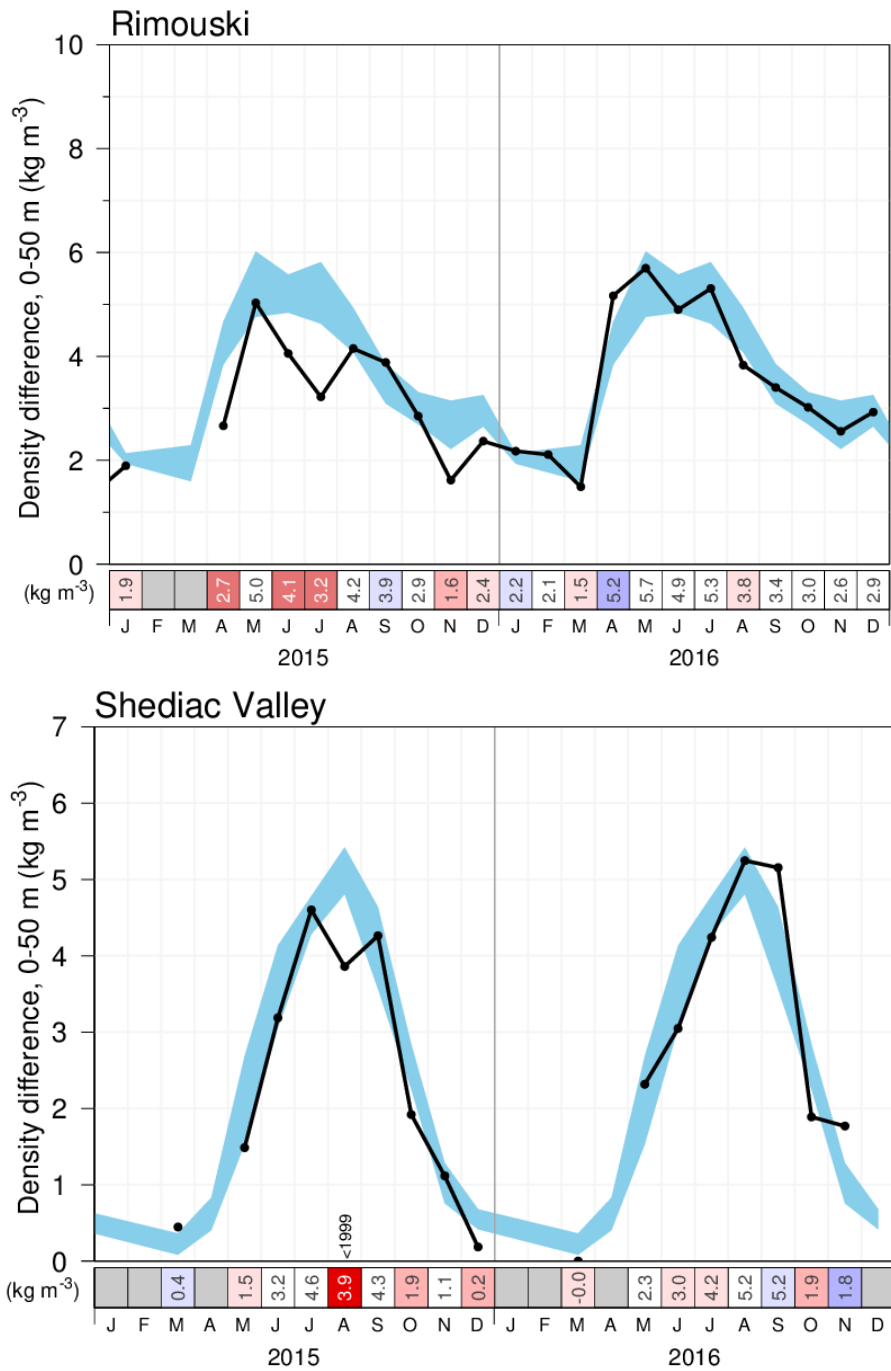
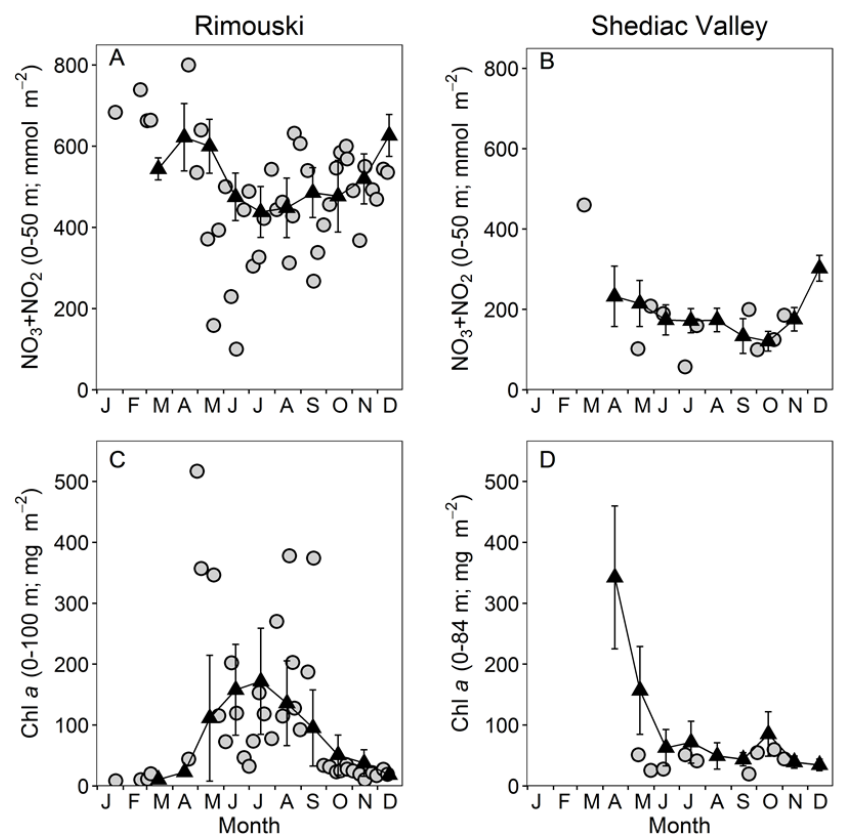


Figure 4. Seasonal stratification index (calculated as the density difference between 50 m and the surface) during 2015 and 2016 at Rimouski station (upper panel) and at Shediac Valley station (lower panel). The blue area represents the climatological monthly mean \pm 0.5 SD (1991–2010 for Rimouski and 1981–2016 for Shediac Valley). The bottom scorecards have reverse colour codes; positive anomalies are shown in blue and correspond to low salinity and strong stratification. Numbers in the scorecard are the monthly density difference in kg m^{-3} . For anomalies greater than 2 SD from normal, the prior year with a greater anomaly is indicated.



E

Mean concentration (mmol m ⁻²):	depth (m):	Stn	1999	2000	2001	2002	2003	2004	2005	2006	2007	2008	2009	2010	2011	2012	2013	2014	2015	2016	mean	S.D.	% 2016
Nitrate April–October	0-50	R	-0.3	0.6	0.1	1.1	-0.3	0.8	-0.3	0.0	-0.1	0.4	-0.4	-1.3	-0.6	-0.3	0.1	0.3	0.5	-0.8	554.5	116.2	-14.5
Nitrate April–December	0-50	SV	0.2	0.7	-0.3	0.2	0.2	0.6	-0.2	0.7	-1.1	-0.1	0.7	-1.2	-0.9	0.2	-0.4	0.1	-0.6	-0.4	187.9	70.6	-21.9
Nitrate April–October	50-150	R	N.A.	-0.4	0.7	1.0	-0.7	-0.1	-0.2	0.6	0.5	-0.2	0.1	-1.2	-1.0	0.2	-0.7	1.1	0.6	0.6	1466.4	146.3	7.7
Nitrate April–December	50-84	SV	-0.2	1.0	0.2	0.7	-0.1	0.5	-0.2	0.6	-1.2	0.1	-0.1	-1.4	-1.5	-0.4	-1.0	-0.4	-0.7	-1.1	274.7	65.3	-18.4
Chl a April–October	0-100	R	1.7	-0.2	0.0	-0.3	0.5	-0.8	-0.4	-0.5	0.5	-0.9	0.2	0.0	-0.3	0.6	0.1	1.4	0.4	4.3	109.3	58.2	59.9
Chl a April–December	0-84	SV	-0.4	-0.7	-0.3	1.1	0.2	-0.5	-0.6	-0.1	0.5	0.6	0.1	-0.3	-0.7	-0.1	0.7	-0.2	-0.5	-0.4	96.9	72.7	-53.5

Figure 5. Nitrate inventories (0–50 m; top panels) and chlorophyll a levels (0–100 m Rimouski and 0–84 m Shediac Valley; bottom panels) in 2016 (gray circles) with mean conditions (± 0.5 SD) from 1999–2010 (black triangles) at Rimouski and Shediac Valley stations. Normalized annual anomalies (scorecard) for chlorophyll a levels (mg m⁻²) and nutrient inventories (mmol m⁻²) are also presented with the variables' means and standard deviations. Blue colours indicate anomalies below the mean and reds are anomalies above the mean.

Shediac Valley - $\text{NO}_3^- + \text{NO}_2^-$

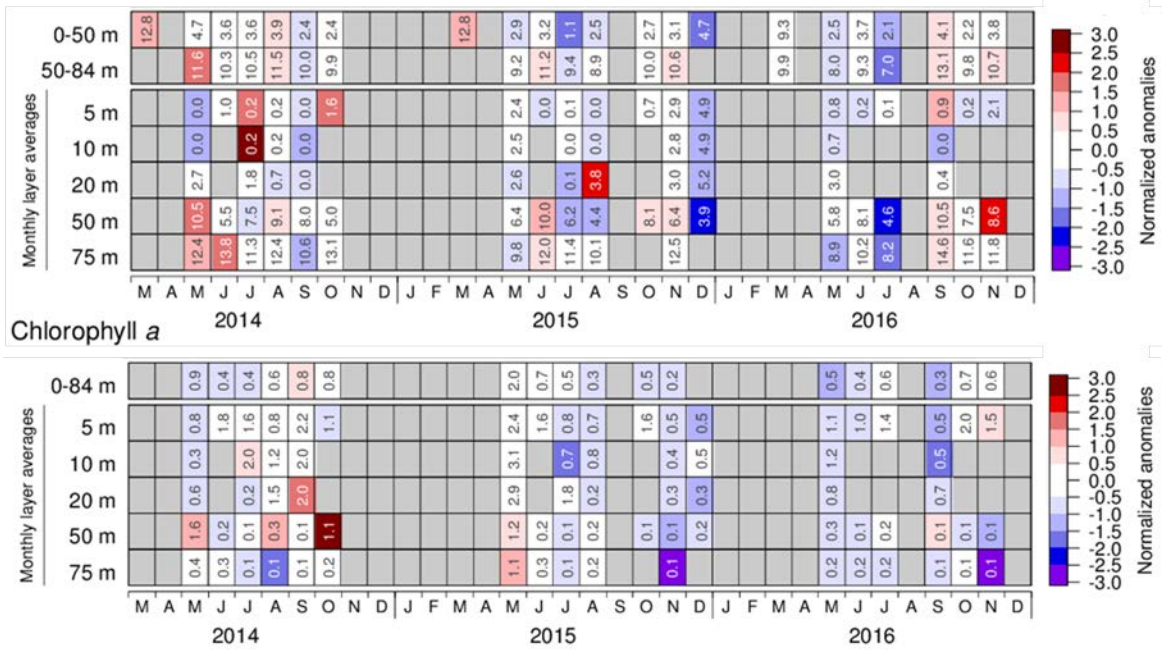


Figure 7. Nitrate (top) and chlorophyll a (bottom) concentrations at Shediac Valley station during the 2014 to 2016 sampling seasons. Nitrate values in March are from the winter survey across the Gulf. Cell colours indicate normalized anomalies based on the 1991–2010 climatology: blue colours indicate anomalies below the mean and reds are anomalies above the mean.

Rimouski

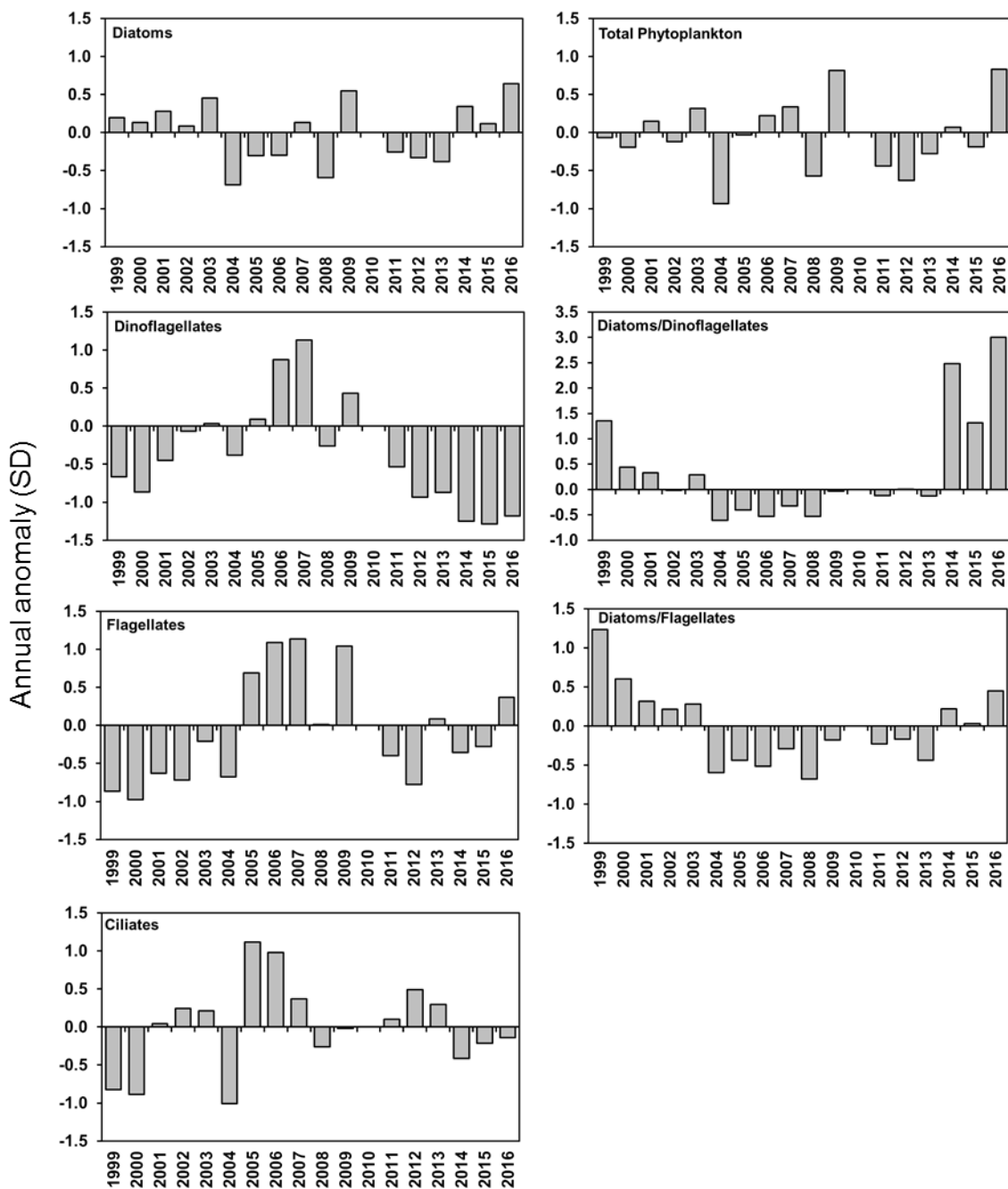


Figure 8. Time series of annual (May–October) averaged microphytoplankton abundance normalized anomalies (relative to the 1999–2009 climatology; no data in 2010) for total phytoplankton and by groups (diatoms, dinoflagellates, flagellates, ciliates) and for the diatom/dinoflagellate and diatom/dinoflagellate ratios at Rimouski station. Note the change in the y-axis scale for the diatom/dinoflagellate ratio.

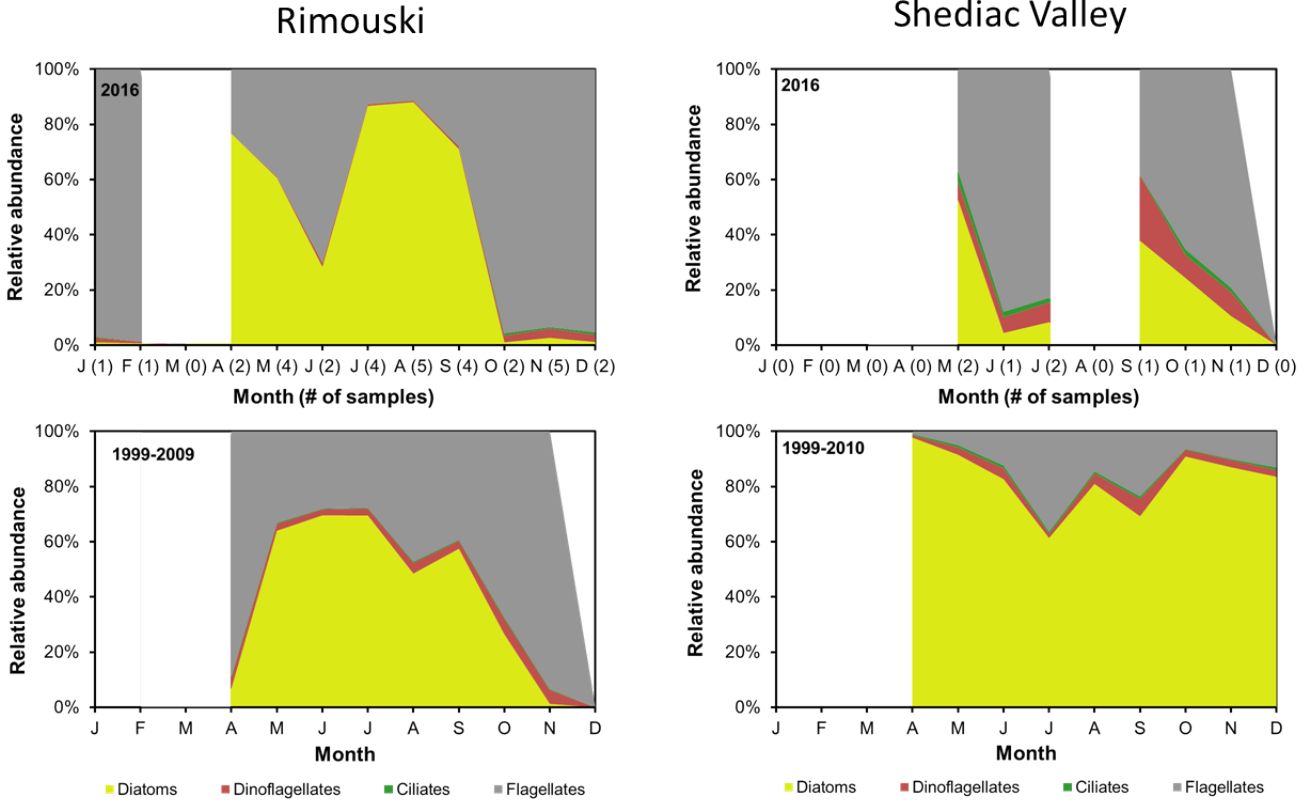


Figure 9. Phytoplankton community composition at Rimouski and Shediac Valley stations for 2016 (top panels) and for the 1999–2009 (Rimouski; no data available in 2010) or 1999–2010 (Shediac Valley) average (bottom panels). The ciliate group is shown between the dinoflagellate and flagellate groups on the figures; it is usually so scarce that it is barely visible.

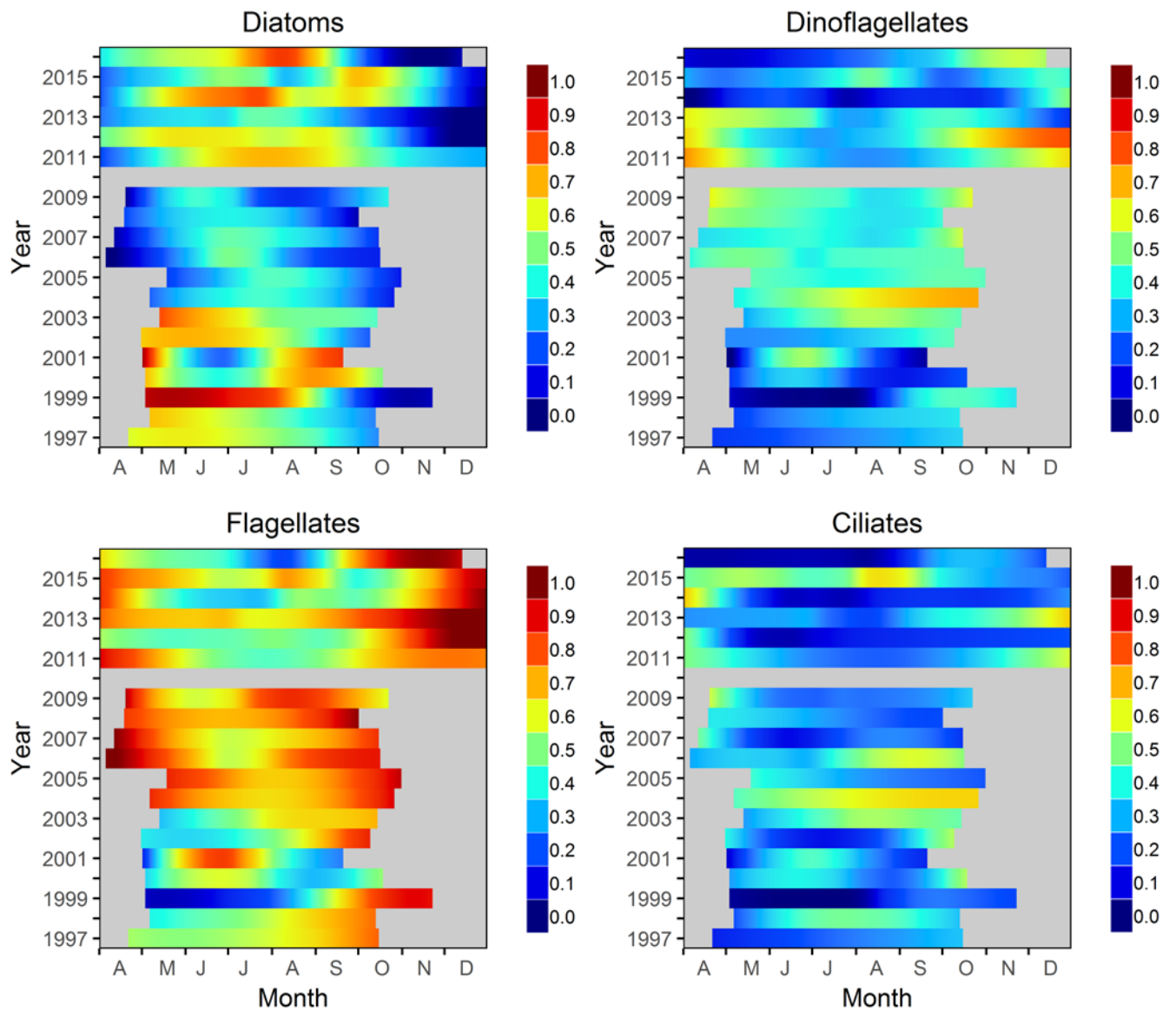


Figure 10. Seasonal cycle in relative abundance of diatoms, dinoflagellates, flagellates, and ciliates from 1997 to 2016 (no data in 2010) at Rimouski station. Proportions are normalized by the annual maximum and smoothed using a Loess.

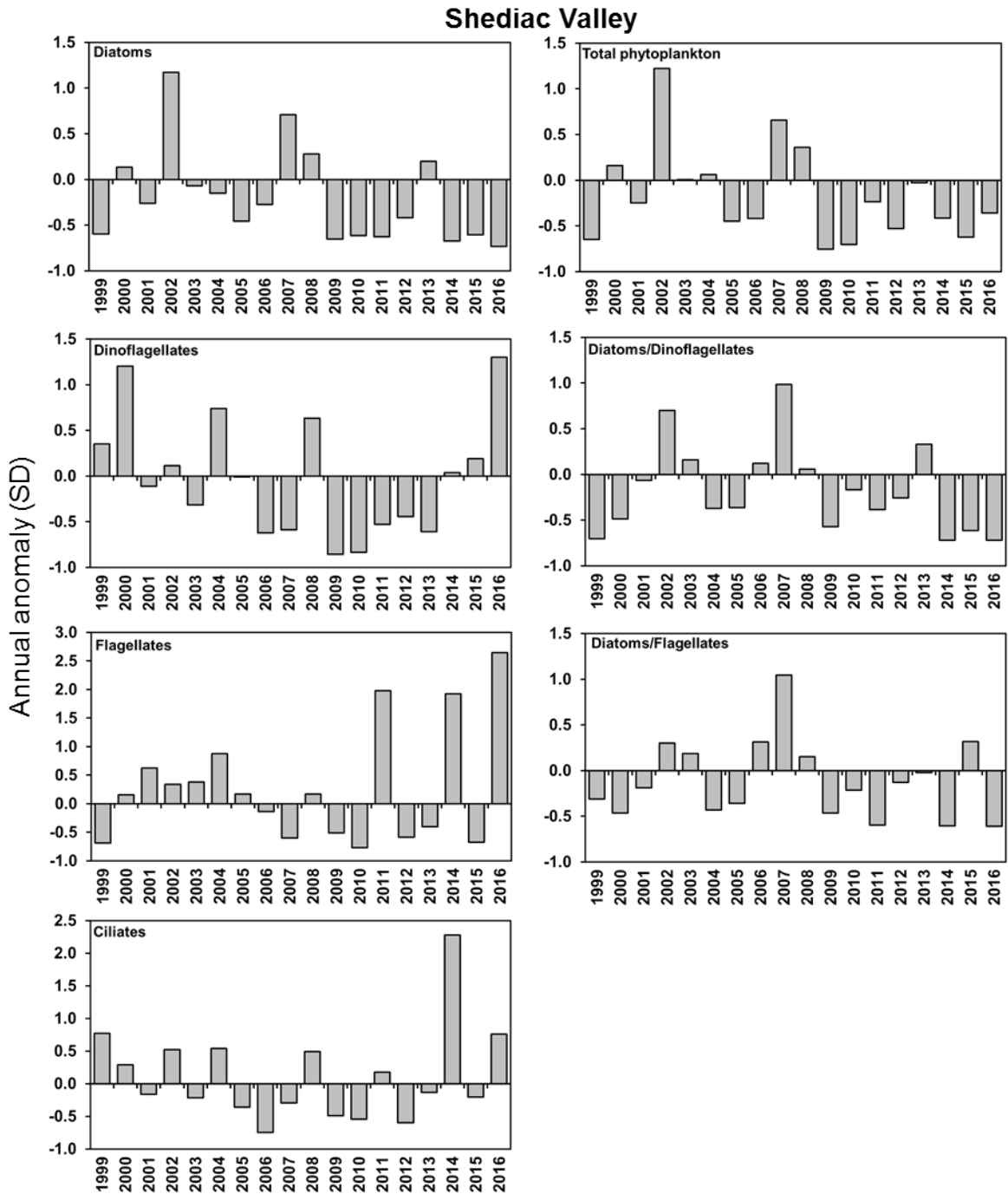
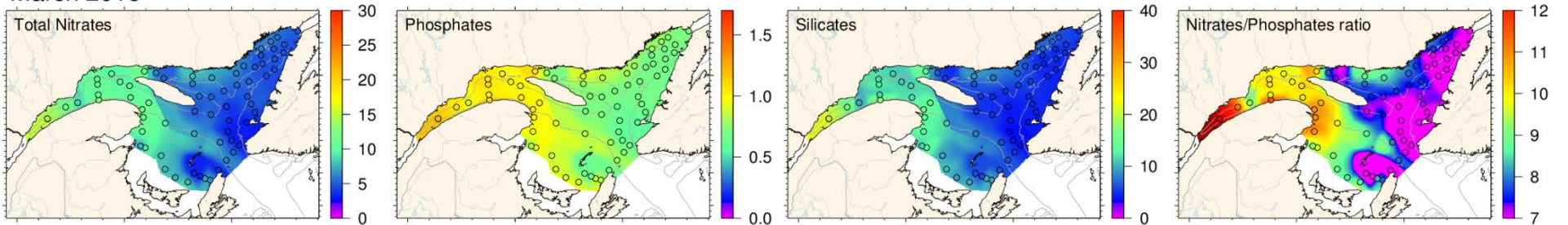


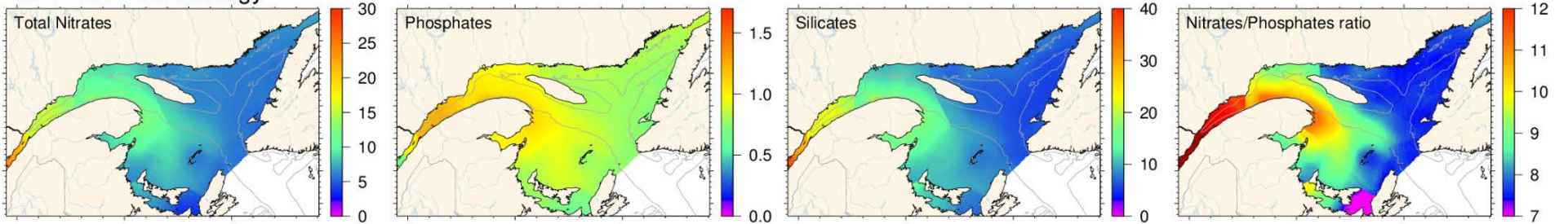
Figure 11. Time series of annual (April–October) averaged microphytoplankton abundance normalized anomalies (relative to the 1999–2010 climatology) for total phytoplankton and by groups (diatoms, dinoflagellates, flagellates, ciliates), and for the diatom/dinoflagellate and diatom/dinoflagellate ratios at Shediac Valley station. Note the change in the y-axis scale for flagellates and ciliates.

Index	Sub-region	Trans- sect	Year														Climatology 99–10											
			99	00	01	02	03	04	05	06	07	08	09	10	11	12	13	14	15	16	Mean	S.D.	%16					
NO ₂ + NO ₃ inventory	W	0–50 m mmol m ⁻²	wGSL	TESL			-0.3	-0.6	0.9	0.6			1.5	0.7	-1.5	0.2	-1.5	-1.7	-0.2	0.4			-1.3	770	85	-15		
			wGSL	TSI			-0.1	0.4	1.2	0.5	-0.8	0.0	1.3	-0.7	0.3	-2.1	-1.2	-0.4	0.5	-0.1	-0.7	0.1		528	125	-2		
			wGSL	TASO			-0.2	0.0	1.2	0.1	1.2	0.1	0.3	1.0	-0.1	0.2	-2.5	-1.8	-0.4	-0.4	0.9	-0.3	-0.1		522	89	-2	
			sGSL	TIDM			0.0	0.4	0.6	0.9	-0.5	0.8	0.5	-0.8	0.4	-2.4	-0.9	-1.3	-0.8	0.5	0.7	-0.6			384	99	-16	
			eGSL	TCEN			-0.6	-0.3	1.9	0.8	-0.9	-0.1	1.3	-0.6	-0.6	-0.9	-1.5	0.3	0.4	0.3	-0.2	-1.5			344	51	-23	
			eGSL	TBB			-0.3	0.3	1.9	0.9	-0.7	-0.2	0.5	-0.7	0.0	-1.7	-0.5	0.6	0.5	-0.1	0.2	-1.2			299	38	-15	
	eGSL	TDC			0.4	0.2	1.3	0.8	-1.0	-0.4	0.7	0.2	0.0	-2.2	-0.4	-1.0	0.2	0.1	0.3	-0.3			293	80	-8			
	S	0–50 m mmol m ⁻²	wGSL	TESL			0.0	1.7	-0.2	0.4			1.3	-0.8	0.0	-0.9	-1.4	-0.6	0.2	1.6	1.6	1.6	-0.2		437	92	-5	
			wGSL	TSI	-1.2	-0.1	1.0	1.4	1.2	-0.7	-0.6	0.0	-0.9	1.5	-0.6	-1.0	-1.0	-0.7	1.3	2.7	0.8	1.9			203	46	43	
			wGSL	TASO	-1.5	-0.6	-0.2	1.2	1.7	0.5	-0.7	-0.8	0.8	0.6	0.2	-1.2	-1.0	-1.3	1.5	2.9	1.3	-0.9			186	59	-28	
			sGSL	TIDM	-0.8	1.0	-0.8	-0.2	0.3	-0.6	-0.2	1.7	0.0	1.1	0.6	-1.9	-0.5	-1.0	0.9	0.4	-0.2	-1.0			109	38	-37	
			eGSL	TCEN								-1.5	0.0	1.0	0.0	1.3	0.2	-0.9	-0.9	-1.6	2.6	4.4	0.8	-1.6		68	20	-46
			eGSL	TBB	-0.3	0.3	-0.3	-0.3	2.5	-1.4	-1.0	-0.1	0.7	0.8	-0.6	-0.3	-1.1	-0.8	-1.3	2.1	1.0	-1.4			63	24	-54	
	eGSL	TDC	-1.2	1.0	-0.2	-1.5	0.8	-0.1	-1.0	0.0	0.6	2.1	0.0	-0.4	-1.5	-0.7	-0.1	0.5	1.0	-2.1			71	21	-62			
	Δ W - S	0–50 m mmol m ⁻²	wGSL	TESL			-0.3	-1.9	0.9	0.1			0.1	1.2	-1.1	1.0	0.0	-0.8	-0.3	-1.1				332	111	-28		
			wGSL	TSI			-0.4	-0.1	0.9	0.8	-0.5	0.1	1.6	-1.2	0.5	-1.6	-0.8	-0.1	0.1	-1.0	-0.9	-0.6			319	126	-22	
			wGSL	TASO			0.1	-0.8	0.3	-0.3	0.9	1.4	0.9	-0.5	0.3	-2.1	-1.4	0.8	-1.7	-1.2	-1.3	0.8			323	65	17	
			sGSL	TIDM			0.3	0.6	0.6	1.3	-0.5	0.2	0.6	-1.4	0.1	-1.9	-0.9	-1.1	-1.4	0.5	0.9	-0.3			275	84	-8	
eGSL			TCEN							1.4	-0.7	-0.3	1.4	-0.9	-0.5	-0.4	-0.9	1.0	-0.4	-1.2	-0.3	-0.7			269	54	-15	
eGSL			TBB			-0.1	0.5	0.4	2.0	-0.1	-0.1	0.1	-1.3	0.4	-1.7	0.2	-0.1	1.5	-1.5	-0.5	-0.3			236	35	-5		
eGSL	TDC			0.5	0.6	1.2	0.9	-0.8	-0.4	0.6	-0.4	0.0	-2.2	0.0	-0.9	0.2	0.0	0.1	0.3			221	75	10				
F	0–50 m mmol m ⁻²	wGSL	TESL	2.5	-0.1	0.5	1.1	-0.6	-1.1	0.3	-0.8	-0.8	-0.1	-0.6	-0.3	-0.1	0.7	-0.4	-0.1	1.0	-0.1			534	116	-3		
		wGSL	TSI	1.9	-0.7	1.1	1.2	0.5	-1.3	-1.2	-0.3	-0.7	-0.5	-0.3	0.3	-0.5	1.6	0.7	-0.1	1.7	0.9			268	102	36		
		wGSL	TASO	1.9	-0.3	0.9	1.2	-1.2	-1.0	-0.6	-0.3	-0.6	-0.4	-1.0	0.8	-1.0	1.3	0.0	0.7	1.3	0.6			278	74	17		
		sGSL	TIDM			1.2	0.6	0.0	-1.2	1.3	0.1	1.3	-0.9	-0.2	-0.9	-1.2	-2.2	-1.3	-0.2	-0.6	-2.1	-1.3			183	36	-26	
		eGSL	TCEN						-0.1	-0.9	-0.4	-0.3	2.1	0.2	0.5	-1.2	-2.8	-1.9	-1.1	-0.8	-0.9	-1.6			136	28	-33	
		eGSL	TBB	0.9	0.3	1.3	0.1	0.8	-1.9	-0.3	-1.6	1.0	-0.4	0.2	-0.5	-0.5	-1.5	-1.0	-1.4	-0.1	-1.1	-1.1			125	31	-26	
eGSL	TDC	1.4	0.7	-0.2	2.2	-0.6	-1.3	0.1	-0.1	-0.5	-0.6	-0.2	-0.9	-1.0	-0.5	0.1	-1.2	-0.8	-1.5			135	45	-51				
Mean S + F	0–50 m mmol m ⁻²	wGSL	TESL	2.6	0.1	0.0	1.0	-0.6	-0.6	0.5	-0.1	-0.9	-0.3	-0.9	-0.9	-0.5	0.2	0.2	0.4	0.9	-0.4			511	120	-9		
		wGSL	TSI	1.2	-0.6	1.3	1.6	0.9	-1.3	-1.2	-0.3	-0.9	0.2	-0.5	-0.2	-0.8	1.1	1.1	0.9	1.7	1.5			235	60	39		
		wGSL	TASO	0.7	-0.8	0.7	2.2	0.2	-0.7	-1.2	-1.0	0.1	0.8	-0.9	-0.2	-1.8	0.3	1.2	3.1	2.3	-0.1			232	36	-1		
		sGSL	TIDM	-1.8	1.3	0.0	0.0	-0.4	0.5	0.1	1.7	-0.4	0.6	0.0	-1.5	-1.3	-1.1	0.5	0.0	-1.1	-1.1			142	36	-28		
		eGSL	TCEN					1.2	-1.4	-0.4	0.1	1.1	0.5	0.2	-1.3	-2.3	-2.1	0.2	1.2	-0.4	-1.9			106	23	-40		
		eGSL	TBB	0.4	0.4	0.7	-0.1	1.8	-2.0	-0.7	-1.1	1.0	0.1	-0.1	-0.5	-0.9	-1.4	-1.3	0.2	0.5	-1.4			94	23	-35		
eGSL	TDC	1.0	1.4	-0.3	1.8	-0.3	-1.6	-0.4	-0.1	-0.3	0.4	-0.3	-1.3	-2.0	-1.0	0.1	-1.1	-0.4	-2.9			103	19	-55				
Mean S + F	50–150 m mmol m ⁻²	wGSL	TESL			1.0	1.6	0.2	-1.3			0.5	0.0	-0.5	0.1	-1.5	-1.2	1.0	0.5	0.8	2.9	0.9		1336	110	7		
		wGSL	TSI	0.0	-1.4	0.7	1.2	0.9	-1.4	-0.9	0.7	-0.2	1.3	-1.1	-0.1	-0.5	1.1	0.6	0.2	2.4	1.7			1354	144	18		
		wGSL	TASO	-0.1	-1.5	0.2	1.4	0.9	-1.0	-1.0	1.0	-0.1	1.1	0.4	-1.3	-0.5	2.2	0.4	2.5	3.1	0.4			1256	100	4		
		eGSL	TCEN						-1.5	-0.3	1.2	0.7	0.3	0.7	-1.1	-0.9	-0.3	1.0	0.2	1.6	-1.3			1093	106	-12		
		eGSL	TBB	-2.6	-0.2	0.0	0.5	1.1	-1.0	-0.1	0.9	0.7	0.1	-0.1	0.7	0.4	0.4	0.6	0.5	2.5	0.2			898	99	2		
		eGSL	TDC	-1.1	1.9	-1.3	0.0	0.3	-1.1	-0.6	1.5	-0.3	0.5	0.4	-0.1	-0.5	1.8	0.6	1.0	2.2	-1.0			867	86	-10		
Mean S + F	300 m mmol m ⁻³	wGSL	TESL	2.5	-0.7	-0.3	0.1	-0.4	-0.2	0.5	0.8	-0.7	0.0	-1.6	0.1	-0.6	0.2	0.3	0.4	0.2	-0.4	2.4	1.1		24	1	-2	
		wGSL	TSI	-2.2	-1.3	-0.2	0.8	1.1	-0.5	-0.4	1.2	0.5	0.7	0.2	0.0	0.4	1.5	2.6	2.1	2.1	1.3			24	1	4		
		wGSL	TASO	-0.5	-0.4	-2.2	0.5	0.0	0.8	0.8	0.2	-1.6	0.8	0.8	0.8	-0.9	1.4	2.3	2.7	2.6	1.2			23	1	3		
		eGSL	TCEN						-0.7	0.0	0.8	0.1	1.4	0.2	-1.7	0.3	2.3	3.8	3.8	4.0	4.6			22	0	9		
		eGSL	TBB	-1.4	0.8	-0.2	-1.3	1.6	-0.1	-0.6	0.9	-0.3	0.1	-0.3	1.3	-2.0	1.4	1.9	2.3	2.9	2.8			21	1	9		
		eGSL	TDC																									
Chl <i>a</i> concentration	S	0–100m mg m ⁻²	wGSL	TESL			0.0	1.0	-0.9	1.7	-0.9	0.0	-1.0	1.1	-0.7	-0.1	-0.2	-0.4	-0.1	-1.2	0.1	-1.1	-0.7		148	97	-49	
			wGSL	TSI	-0.2	-1.4	0.1	2.3	-0.3	1.3	-0.8	0.3	0.2	-0.9	-0.7	0.1	-0.3	0.5	-1.2	-0.2	1.1	-0.8			69	38	-46	
			wGSL	TASO	-0.4	-0.7	-0.7	2.8	-0.4	0.5	0.5	0.4	-0.7	-0.6	-0.6	-0.1	-0.6	-0.1	-1.0	-0.4	0.0	-0.8			94	67	-57	
			sGSL	TIDM	-0.2	-1.6	-0.5	2.4	0.3	0.1	0.7	0.0	-0.2	-0.4	-0.2	1.2	-0.2	-0.3	0.6	0.0	0.3	0.9			36	14	37	
			eGSL	TCEN							-0.8	-0.6	-0.7	0.6	1.7	0.6	-0.8	-0.8	-0.9	0.0	-0.8	3.1	1.2			38	12	37
			eGSL	TBB	-1.0	0.5	-1.2	1.6	-0.8	1.7	-0.7	-0.8	-0.1	0.8	-0.5	0.4	-1.1	-0.4	1.6	-0.4	1.8	-0.7			29	11	-25	
	eGSL	TDC	2.0	-0.6	0.0	2.1	-0.7	-0.7	-0.7	-0.1	-0.4	-0.5	-0.4	0.1	-0.5	-0.4	-0.4	0.2	-0.2	0.0			47	32	2			
	F	0–100m mg m ⁻²	wGSL	TESL	-0.7	-1.6	-0.6	-0.1	1.2	0.2	-0.3	-0.1	0.0	2.4	-0.2	-0.1	-0.4	0.7	-1.0	0.7	1.2	0.5			23	9	19	
			wGSL	TSI	-0.5	-0.9	-0.6	-0.2	0.3	-0.3	0.4	-0.3	-0.2	3.0	-0.5	-0.3	-0.5	-0.3	-0.5	-0.2	0.6	-0.5			46	34	-34	
			wGSL	TASO	-0.6	-1.0	-0.5	-0.2	0.6	-0.5	0.2	-0.1	-0.2	2.9	-0.1	-0.5	-0.3	0.1	0.0	-0.2	1.4	-0.5			45	32	-34	
			sGSL	TIDM			-1.6	0.6	1.7	0.8	-0.9	-0.9	-0.4	1.2	-0.5	-0.1	0.1	0.5	1.7	2.1	1.0	1.4	0.5			38	13	19
			eGSL	TCEN						1.3	-1.4			-0.9	-0.6	0.2	0.3	1.1	-1.5	0.0	-0.2	1.8	1.1	0.2		42	8	4
			eGSL	TBB	-0.6	-1.4	-0.3	1.4	1.0	2.1	-0.6	-0.7	0.3	-0.6	-0.2	-0.4	1.0	0.8	0.4	1.2	0.3	0.1			35	11	4	
	eGSL	TDC	-0.9	-1.7	-0.2	1.5	0.4	-0.3	-0.8	0.8	1.1	-0.4	1.3	-0.6	-0.8	-0.7	1.1	1.5	3.0	3.3			41	11	91			
	Mean S + F	0–100m mg m ⁻²	wGSL	TESL	-1.0	-1.2	1.2	-0.5	1.9	-0.5	-0.9	-0.6	1.3	-0.1	0.2	0.1	-0.1	0.3	-0.9	0.5	-0.6							

March 2016



2001-2016 Climatology



March 2016 anomalies

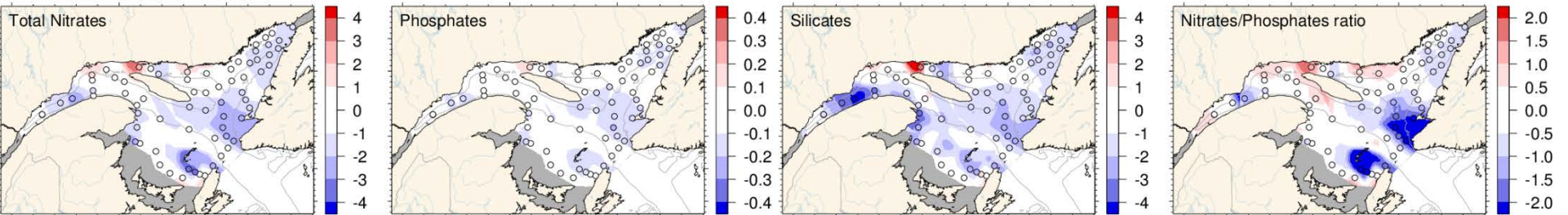
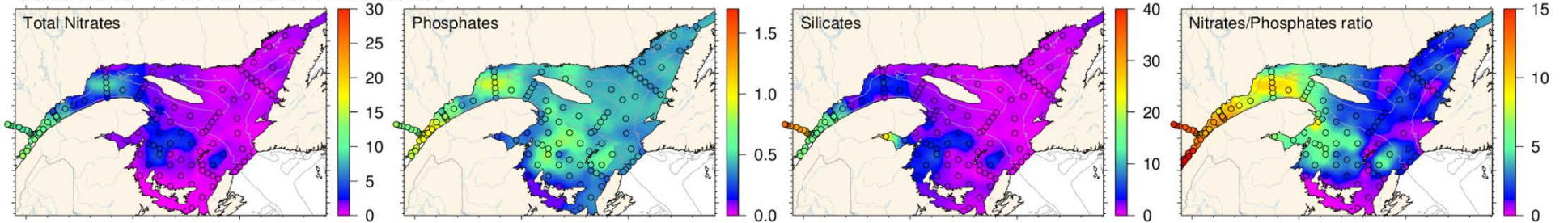
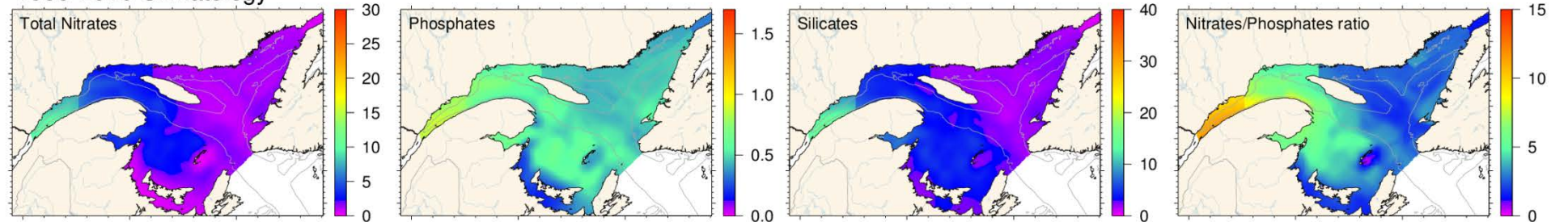


Figure 13. Total nitrate ($\text{NO}_3^- + \text{NO}_2^-$), phosphate, and silicate concentrations (mmol m^{-3}) and N:P ratio at 2 m in the Estuary and Gulf of St. Lawrence during early March 2016 (upper panels). The climatology (2001–2016; middle panels) and anomalies (lower panels) are shown for each nutrient. Blue colours indicate anomalies below the mean and reds are anomalies above the mean.

June 2016 - 0-50 m nutrient inventories



1999-2010 Climatology



June 2016 anomalies

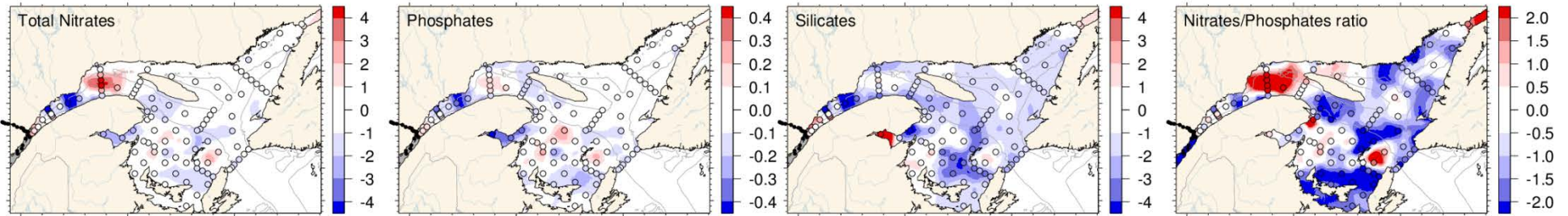
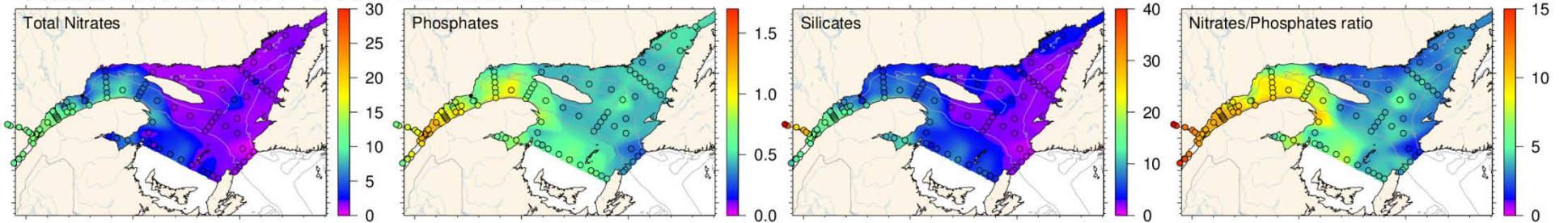
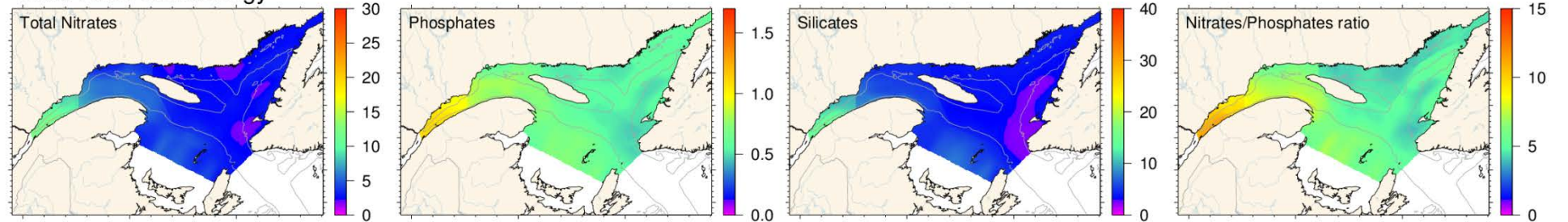


Figure 14. Total nitrate ($\text{NO}_3^- + \text{NO}_2^-$), phosphate, and silicate concentrations (mmol m^{-3}) and N:P ratio averaged in the surface layer (0–50 m) in the Estuary and Gulf of St. Lawrence during early June 2016 (upper panels). The climatology (1999–2010; middle panels) and anomalies (lower panels) are shown for each nutrient. Blue colours indicate anomalies below the mean and reds are anomalies above the mean.

October-November 2016 - 0-50 m nutrient inventories



1999-2010 Climatology



October-November 2016 anomalies

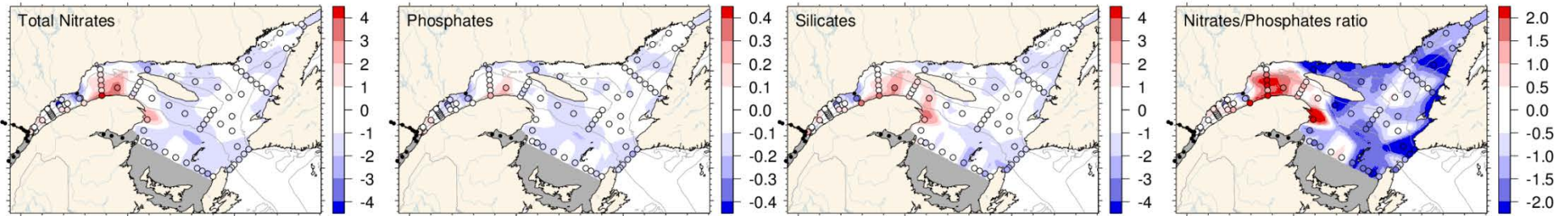
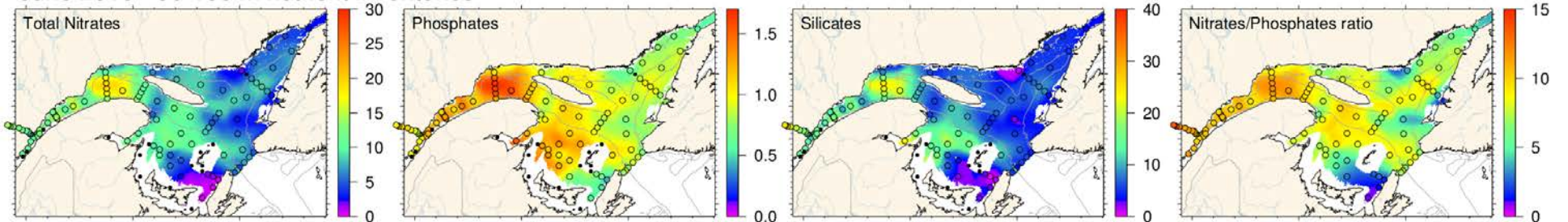
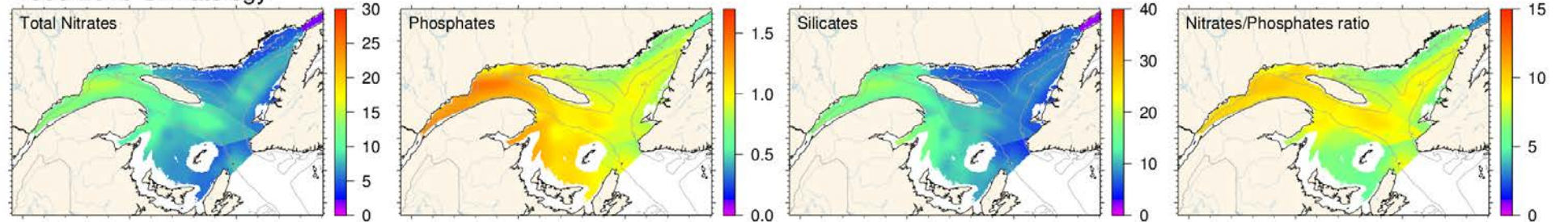


Figure 15. Total nitrate ($\text{NO}_3^- + \text{NO}_2^-$), phosphate, and silicate concentrations (mmol m^{-3}) and N:P ratio averaged in the surface layer (0–50 m) in the Estuary and Gulf of St. Lawrence during late October – early November 2016 (upper panels). The climatology (1999–2010; middle panels) and anomalies (lower panels) are shown for each nutrient. Blue colours indicate anomalies below the mean and reds are anomalies above the mean.

June 2016 - 50-150 m nutrient inventories



1999-2010 Climatology



June 2016 anomalies

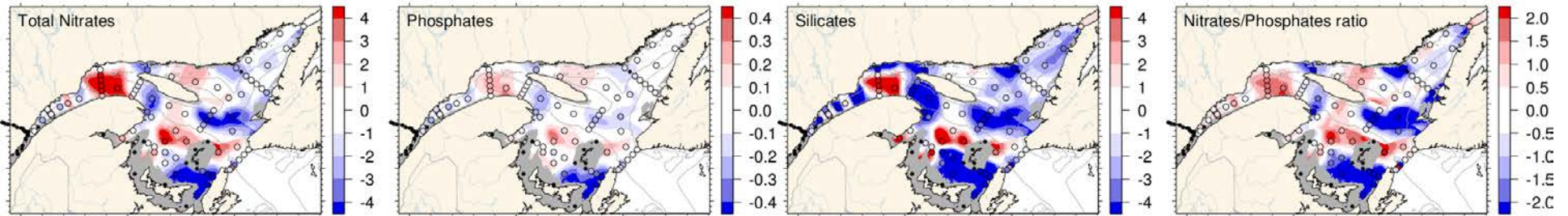
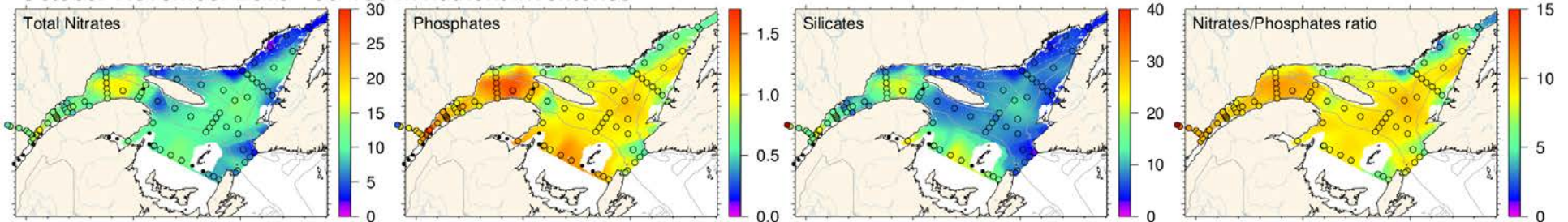
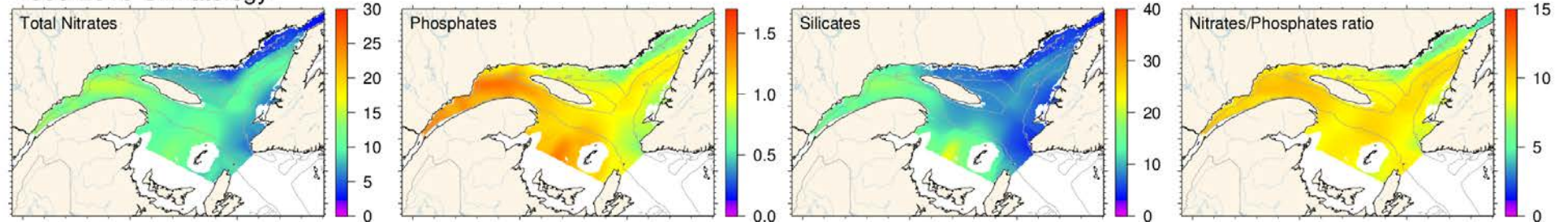


Figure 16. Total nitrate ($\text{NO}_3^- + \text{NO}_2^-$), phosphate, and silicate concentrations (mmol m^{-3}) and N:P ratio averaged in the mid-layer (50–150 m) in the Estuary and Gulf of St. Lawrence during early June 2016 (upper panels). The climatology (1999–2010; middle panels) and anomalies (lower panels) are shown for each nutrient. Blue colours indicate anomalies below the mean and reds are anomalies above the mean.

October-November 2016 - 50-150 m nutrient inventories



1999-2010 Climatology



October-November 2016 anomalies

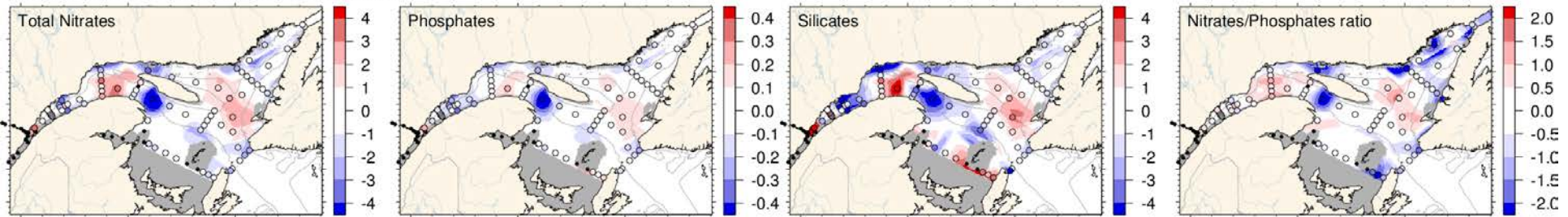


Figure 17. Total nitrate ($\text{NO}_3^- + \text{NO}_2^-$), phosphate, and silicate concentrations (mmol m^{-3}) and N:P ratio averaged in the mid-layer (50–150 m) in the Estuary and Gulf of St. Lawrence during late October – early November 2016 (upper panels). The climatology (1999–2010; middle panels) and anomalies (lower panels) are shown for each nutrient. Blue colours indicate anomalies below the mean and reds are anomalies above the mean.

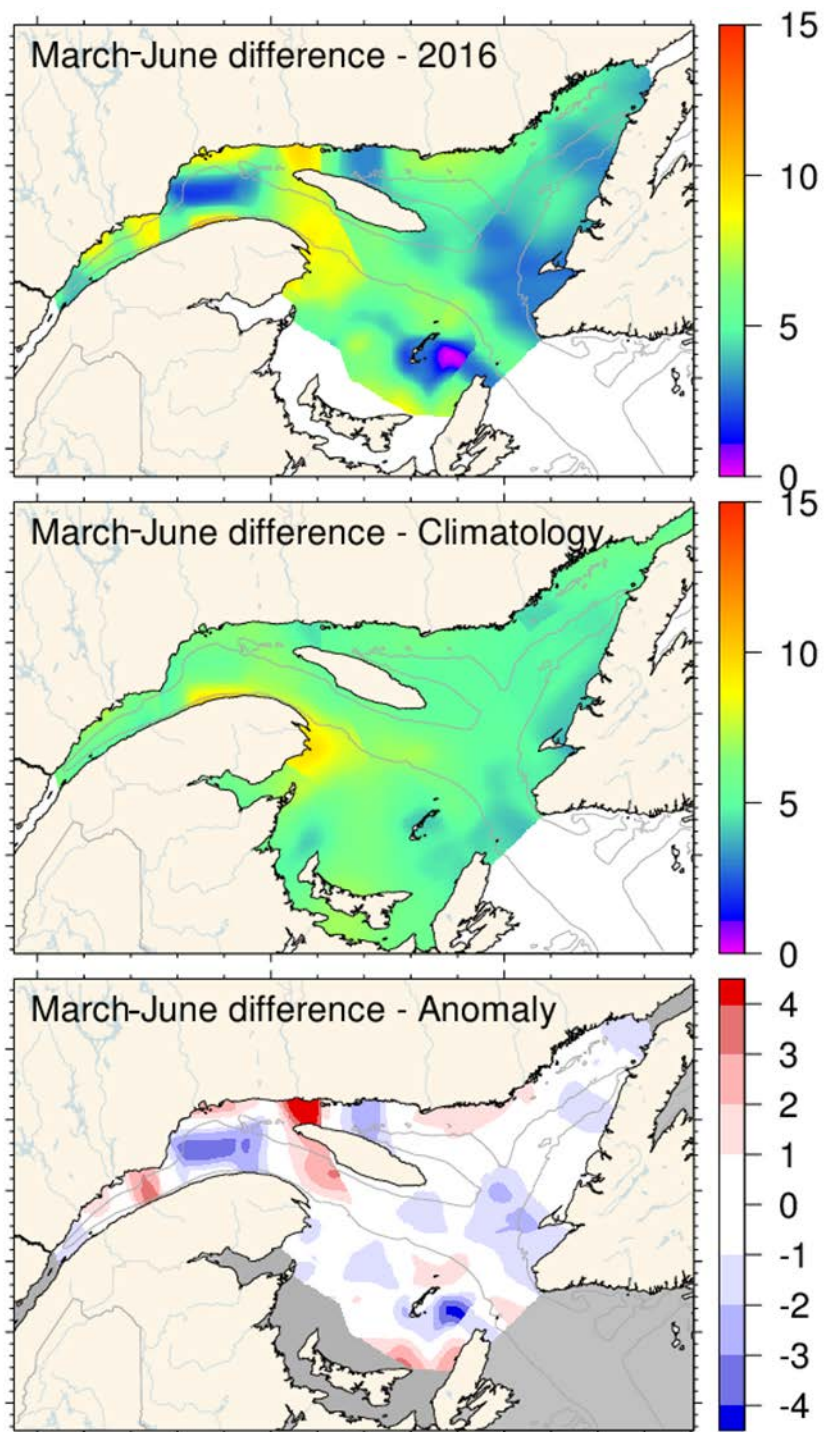


Figure 18. Difference in total nitrate ($\text{NO}_3^- + \text{NO}_2^-$) concentrations (mmol m^{-3}) at 2 m in the Estuary and Gulf of St. Lawrence between March and June. Top: March–June 2016 difference; middle: March–June difference climatology (2001–2016); bottom: March–June 2016 difference anomalies. Negative anomalies (blue) suggest weak nitrate drawdowns and positive anomalies (red) suggest strong nitrate drawdowns.

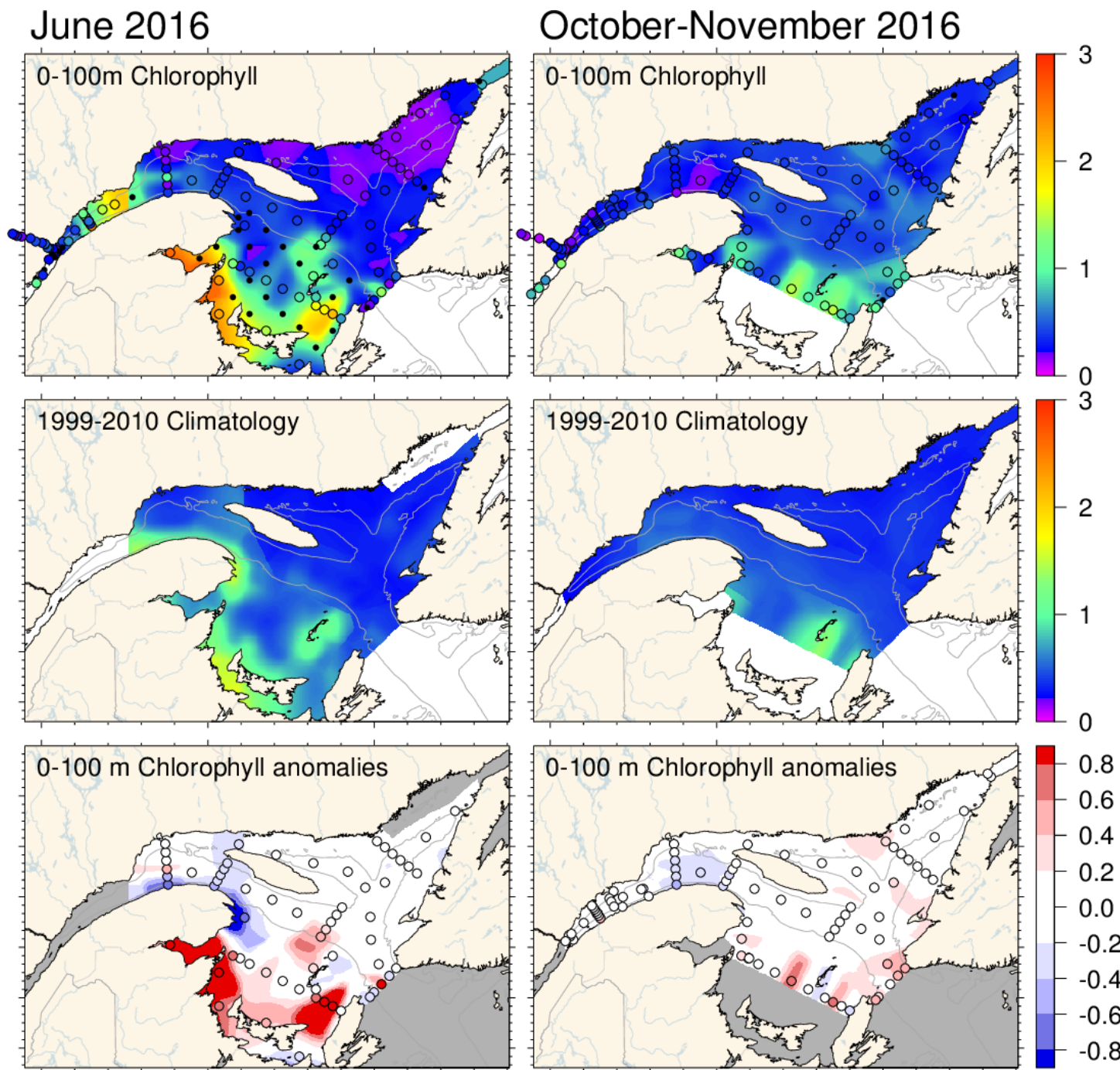


Figure 19. Vertically averaged (0–100 m) chlorophyll a concentrations (mg m^{-3}) in the Estuary and Gulf of St. Lawrence during early June (left panels) and late October – early November 2016 (right panels). The climatology (1999–2010; middle panels) and anomalies (lower panels) are shown for both periods. Blue colours indicate anomalies below the mean and reds are anomalies above the mean.

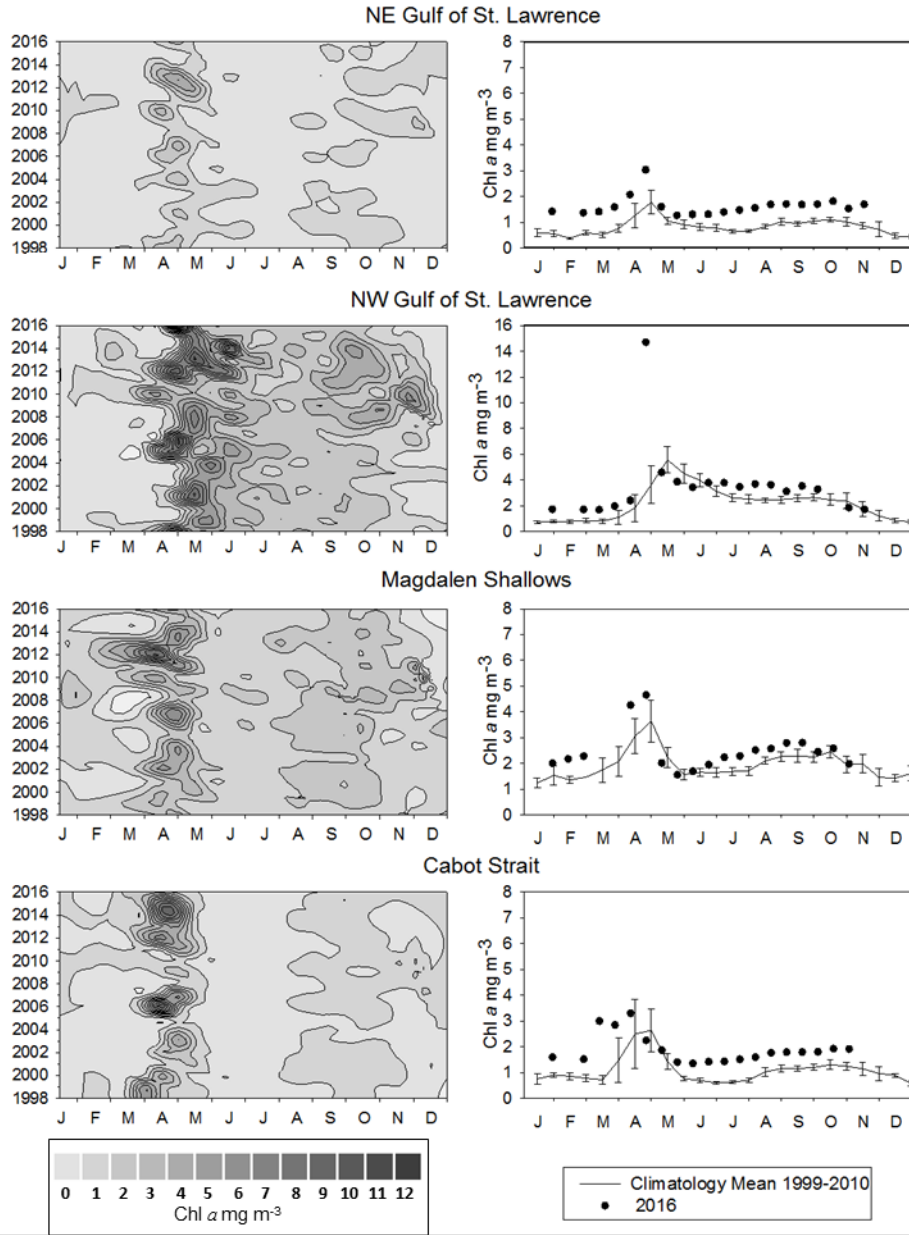


Figure 20. Left panels: Time series of surface chlorophyll a concentrations from twice-monthly SeaWiFS (1998–2007), MODIS (2008–2011), and VIIRS (since 2012) ocean colour data in the northeast Gulf of St. Lawrence, northwest Gulf of St. Lawrence, Magdalen Shallows, and Cabot Strait statistical subregions (see Fig. 3). Right panels: comparison of 2016 (black circles) surface chlorophyll estimates using satellite ocean colour with mean conditions from 1999–2010 (solid line \pm 0.5 SD) for the same statistical subregions.

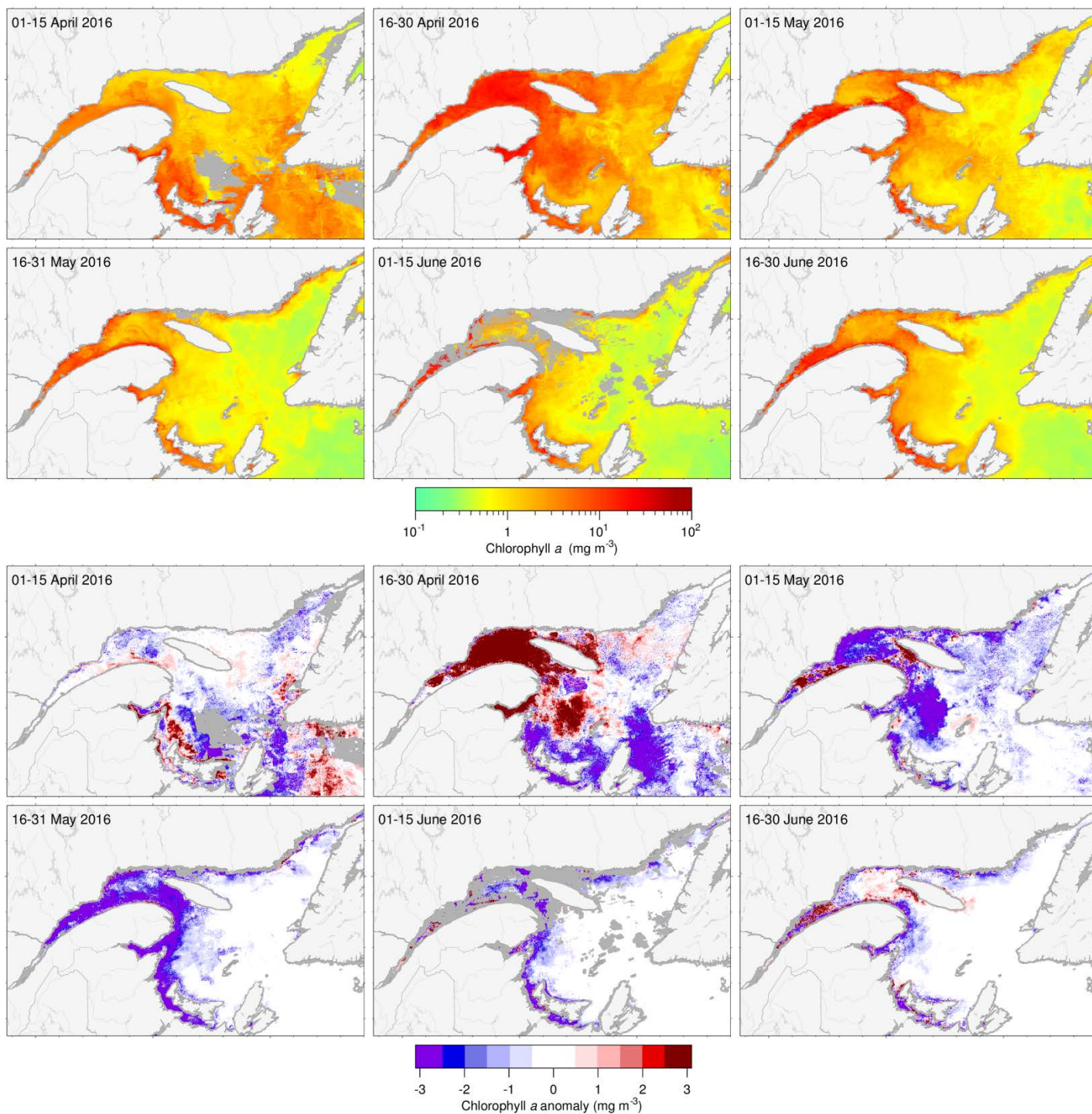


Figure 21. VIIRS twice-monthly composite images of surface chlorophyll a (upper panels) and anomaly based on the 1999–2010 climatology (lower panels) in the Gulf of St. Lawrence during spring 2016.

Indices of change in spring bloom properties based on SeaWiFS (1998-2007), MODIS (2008-2011) and VIIRS (2012-present)

Index	Subregion	1998	1999	2000	2001	2002	2003	2004	2005	2006	2007	2008	2009	2010	2011	2012	2013	2014	2015	2016	Mean	S.D.
Start of spring bloom (day of the year)	Northwest GSL	-0.74	0.59	0.21	-0.46	1.39	0.10	0.76	-0.87	-0.42	0.32	0.53	0.36	-2.53	-0.74	-0.70	-0.09	0.36	0.82	0.10	107	13
	Northeast GSL	-0.70	-0.03	2.08	0.02	0.24	1.01	-1.10	0.35	-1.11	0.55	0.21	-0.74	-1.47	1.88	1.52	-1.06	1.38	2.51	0.03	99	9
	Magdalen Shallows	0.29	-0.95	-0.58	0.59	-0.50	0.28	0.91	n.d.	1.19	-0.35	0.89	0.65	-2.12	0.35	-1.35	-0.98	1.01	1.32	-1.64	91	13
	Cabot Strait	-0.64	-0.83	-0.19	0.60	0.21	0.78	0.63	0.04	-0.54	0.12	1.67	-0.09	-2.40	0.54	-1.71	-0.82	0.85	1.83	-3.06	92	14
Spring bloom duration (days)	Northwest GSL	-0.12	0.48	2.08	0.43	-1.24	1.35	0.46	-0.85	-0.74	-0.01	-0.60	-0.95	-0.41	0.16	-0.97	0.03	1.49	-0.60	-1.21	42	22
	Northeast GSL	-0.39	-0.37	-0.79	-0.28	0.51	2.90	0.23	-0.82	-0.06	-0.53	0.12	-0.32	-0.60	-0.99	-0.78	0.03	-0.19	-0.70	-0.51	35	22
	Magdalen Shallows	-0.05	-0.44	2.03	-0.66	0.31	0.12	-1.29	n.d.	1.21	0.81	-0.66	0.04	0.96	-0.06	0.11	1.17	-0.38	-0.66	1.14	36	16
	Cabot Strait	0.09	-0.55	-1.23	0.93	-1.24	-1.34	0.13	0.54	0.28	0.57	-0.70	0.88	1.74	-0.49	3.00	1.29	-1.27	-0.84	4.36	30	12
Spring bloom magnitude (mg Chl m ⁻²)	Northwest GSL	0.80	0.22	1.34	0.69	-1.49	1.13	1.35	-0.73	-0.27	0.45	-0.61	-0.91	-1.16	-1.11	0.92	1.47	3.96	-0.23	0.67	156	51
	Northeast GSL	1.79	-0.56	-1.23	0.29	-0.30	1.37	0.71	-1.43	0.75	1.17	-0.70	-1.08	1.00	-0.98	0.87	4.27	-0.98	-1.63	-0.17	39	18
	Magdalen Shallows	-0.04	-0.87	-0.20	-0.61	0.67	0.84	-1.01	n.d.	-0.83	2.11	-0.67	-0.39	0.96	0.70	3.70	1.76	0.95	-0.62	1.83	78	48
	Cabot Strait	2.57	0.41	-0.37	-0.34	0.06	-0.18	-0.45	-0.98	2.42	1.31	-1.24	-0.11	-0.52	-0.03	3.12	1.51	1.21	-1.08	1.21	67	42
Spring bloom amplitude (mg Chl m ⁻³)	Northwest GSL	0.82	-0.90	-1.50	-0.39	1.23	-1.10	0.19	0.91	1.37	0.14	0.18	1.01	-1.13	-1.84	5.38	1.24	0.63	0.84	7.78	5.94	1.50
	Northeast GSL	2.04	-0.27	-0.41	0.39	-0.78	-0.91	0.03	-0.65	0.40	1.87	-0.81	-0.81	1.94	0.55	2.59	2.80	-0.81	-1.08	0.36	1.79	0.97
	Magdalen Shallows	0.01	-1.15	-1.46	-0.30	0.68	1.22	-0.29	n.d.	0.22	1.89	-0.44	-0.69	0.32	1.30	5.84	1.02	2.51	-0.34	1.13	3.11	1.15
	Cabot Strait	1.93	0.65	0.46	-0.79	1.24	1.00	-0.64	-1.15	1.57	0.48	-1.16	-0.63	-1.03	0.10	0.30	0.21	3.28	-0.93	-0.68	3.65	2.32

Indices of change in productivity based on SeaWiFS (1998-2007), MODIS (2008-2011) and VIIRS (2012-present; recalculated Feb 2017)

Index	Subregion	1998	1999	2000	2001	2002	2003	2004	2005	2006	2007	2008	2009	2010	2011	2012	2013	2014	2015	2016	Mean	S.D.
Annual mean surface Chl March to November (mg m ⁻³)	Northwest GSL	0.82	-0.63	-0.75	0.05	-0.96	-0.92	-0.70	1.33	0.01	-0.91	1.98	1.00	0.50	0.01	3.08	2.14	2.34	-0.84	0.66	2.75	0.40
	Northeast GSL	0.22	0.74	1.12	0.08	-0.75	0.24	0.16	-1.92	0.07	-0.29	-1.57	0.87	1.26	-0.85	2.16	4.15	-1.32	-1.33	-0.64	0.95	0.10
	Magdalen Shallows	-2.10	-1.06	0.38	-1.35	1.59	-0.80	-0.03	-1.46	0.58	0.82	0.32	1.20	-0.19	1.25	2.22	2.57	1.71	-1.39	-1.23	2.12	0.20
	Cabot Strait	0.71	0.46	0.57	-0.60	0.26	0.05	-0.97	-1.41	2.49	0.35	-0.86	-0.20	-0.14	-0.28	1.23	1.20	1.04	-0.78	-0.05	1.19	0.31
Mean surface Chl - March to May (mg m ⁻³)	Northwest GSL	2.45	-0.26	-1.66	0.86	-0.62	-1.31	0.08	2.05	0.74	-0.62	0.27	0.25	0.22	-0.85	3.29	2.23	0.47	-0.28	1.68	3.10	0.63
	Northeast GSL	1.36	-0.06	-0.92	0.04	-0.39	-0.81	1.69	-1.34	0.48	0.92	-0.61	-0.67	1.66	0.32	3.54	4.58	-0.26	-1.91	-0.11	1.10	0.20
	Magdalen Shallows	-0.74	-0.48	-0.15	-1.07	1.04	0.79	0.86	-1.45	0.07	1.86	-1.19	-0.40	0.12	0.69	3.65	2.02	2.28	-0.71	0.05	2.48	0.57
	Cabot Strait	1.20	0.86	-0.01	-0.78	-0.03	0.85	-0.71	-1.13	2.20	0.78	-1.12	-0.35	-0.56	-0.01	1.82	1.23	2.22	-0.53	0.16	1.63	0.75
Mean surface Chl - June to August (mg m ⁻³)	Northwest GSL	0.50	-0.55	0.09	-0.61	0.36	-0.51	-0.18	2.18	-0.07	-1.55	1.55	-0.19	-0.51	-1.64	1.00	0.41	3.14	-1.89	-0.11	2.87	0.36
	Northeast GSL	-1.02	0.59	1.53	0.25	-0.46	1.84	0.25	-0.43	-0.41	-1.14	-1.54	0.24	-0.73	-1.01	-1.17	0.51	-1.15	-0.17	-0.94	0.80	0.15
	Magdalen Shallows	-1.44	-0.06	0.42	-0.62	0.61	-1.53	0.42	0.10	2.09	-0.70	0.62	0.14	-1.51	-1.36	-1.88	1.23	0.24	-1.99	-1.91	1.84	0.19
	Cabot Strait	-0.84	-0.78	2.06	0.55	0.54	-0.69	-0.98	-1.68	0.97	-0.07	-0.47	0.18	0.37	-0.85	-1.52	0.44	-0.14	-0.33	-0.78	0.80	0.13
Mean surface Chl - September to November (mg m ⁻³)	Northwest GSL	-0.70	-0.60	0.09	-0.41	-1.07	-0.17	-0.98	-0.46	-0.61	-0.24	2.23	1.46	0.76	1.59	1.54	1.01	1.64	-0.20	-0.61	2.32	0.76
	Northeast GSL	-0.02	0.69	1.47	-0.07	-0.35	-0.37	-1.43	-1.36	-0.19	-0.64	-0.26	1.77	0.74	-0.98	0.50	1.21	-0.17	0.02	-0.24	0.97	0.19
	Magdalen Shallows	-1.48	-0.90	0.50	-0.35	0.35	-1.07	-0.90	-0.42	-0.26	-0.73	1.63	2.07	0.08	1.34	-0.35	0.61	0.63	-0.17	-0.65	2.10	0.40
	Cabot Strait	-0.37	-0.70	1.15	-0.40	0.77	-1.03	-1.23	-0.56	1.64	-1.31	0.56	0.21	0.90	-0.42	-0.31	-0.16	0.10	-0.54	-0.57	1.20	0.22

Figure 22. Normalized annual anomalies (scorecard) of indices of change of spring bloom properties (upper section) and productivity indices (lower section; mean surface chlorophyll for various time periods; mg m⁻³) across the Gulf of St. Lawrence statistical subregions (see Fig. 3) from 1998 to 2016. The spring bloom indices are start (day of the year), duration (days), magnitude (mg chl m⁻²), and amplitude (mg chl m⁻³). The reference period used to compute annual anomalies was 1999–2010. Blue colours indicate anomalies below the mean and reds are anomalies above the mean. The climatological means and standard deviations are shown to the right of the table.

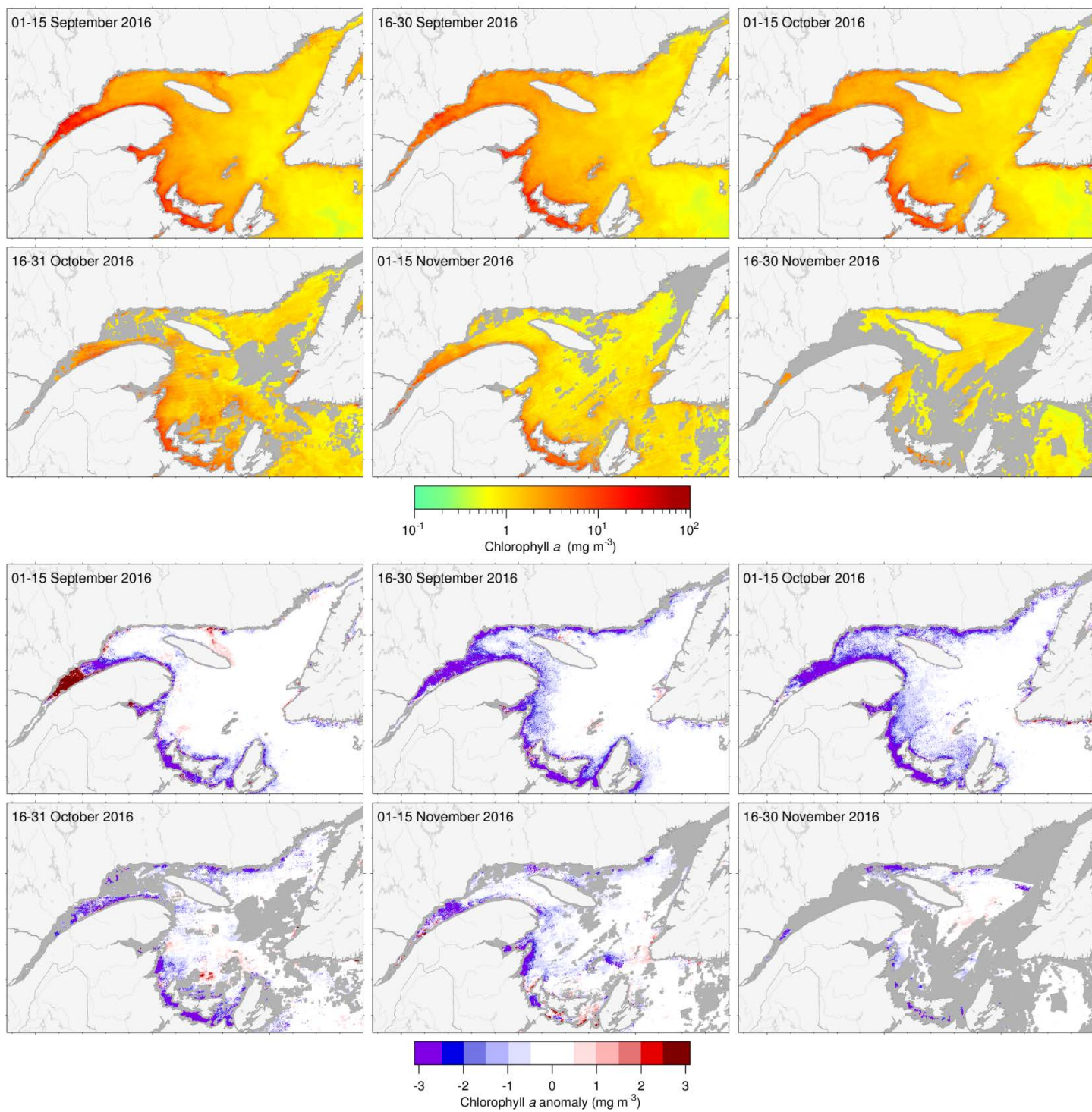


Figure 23. VIIRS twice-monthly composite images of surface chlorophyll a (upper panels) and anomaly based on the 1999–2010 climatology (lower panels) in the Gulf of St. Lawrence during fall 2016.

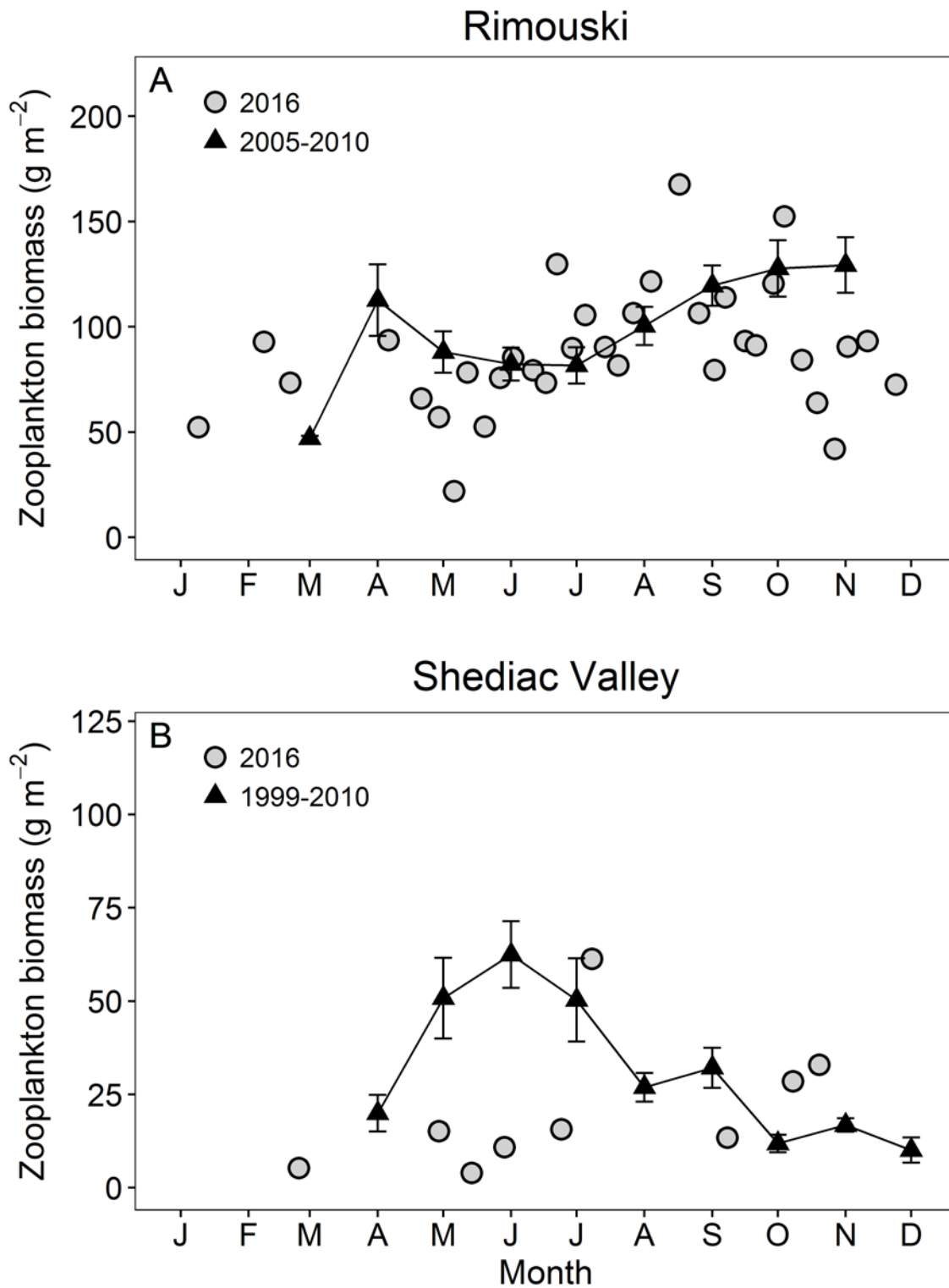


Figure 24. Comparison of total zooplankton biomass in 2016 (circles) with the monthly climatology from (A) Rimouski (2005–2010) and (B) Shediac Valley (1999–2010) stations (triangles with solid line). Vertical lines are standard errors of the monthly means.

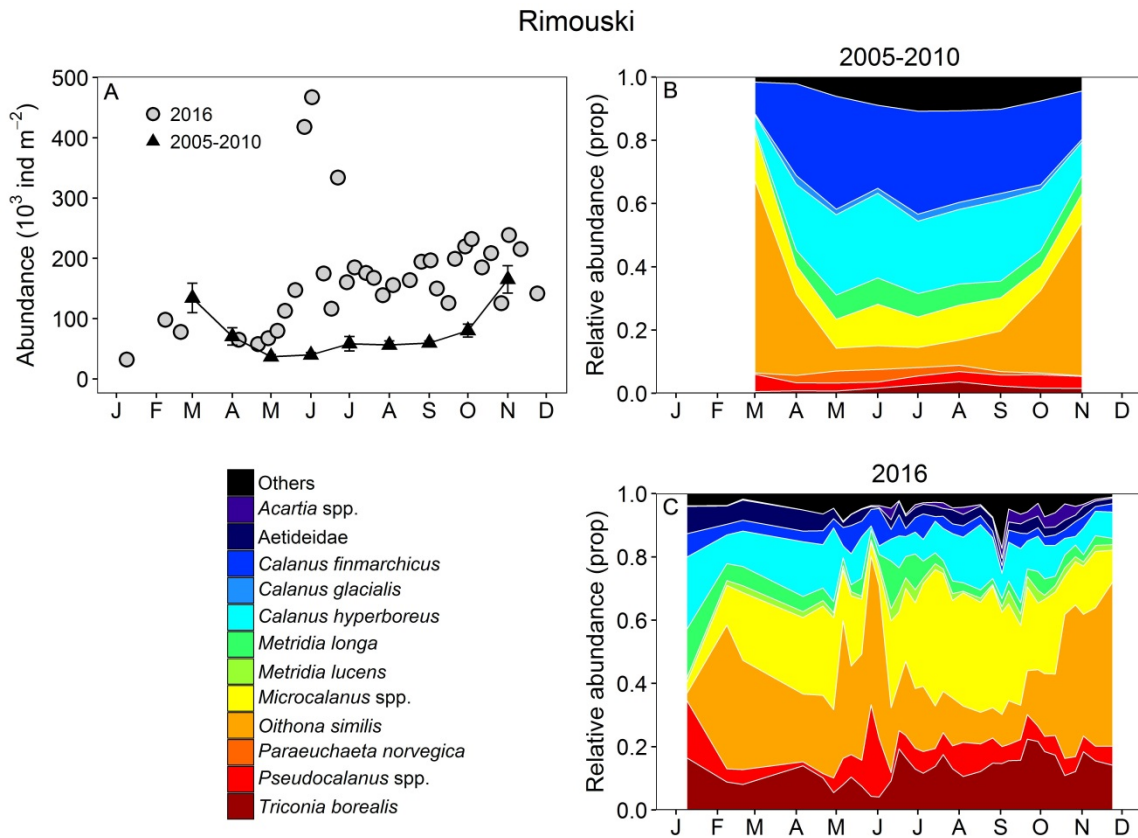


Figure 25. Seasonal variability of dominant copepods at Rimouski station. Copepod abundance (excluding nauplii) during the reference period (triangles and solid line with standard errors) and 2016 (circles) (A); Climatology of the relative abundance of the top 95% of identified copepod taxa during the 2005–2010 period (B) and in 2016 (C).

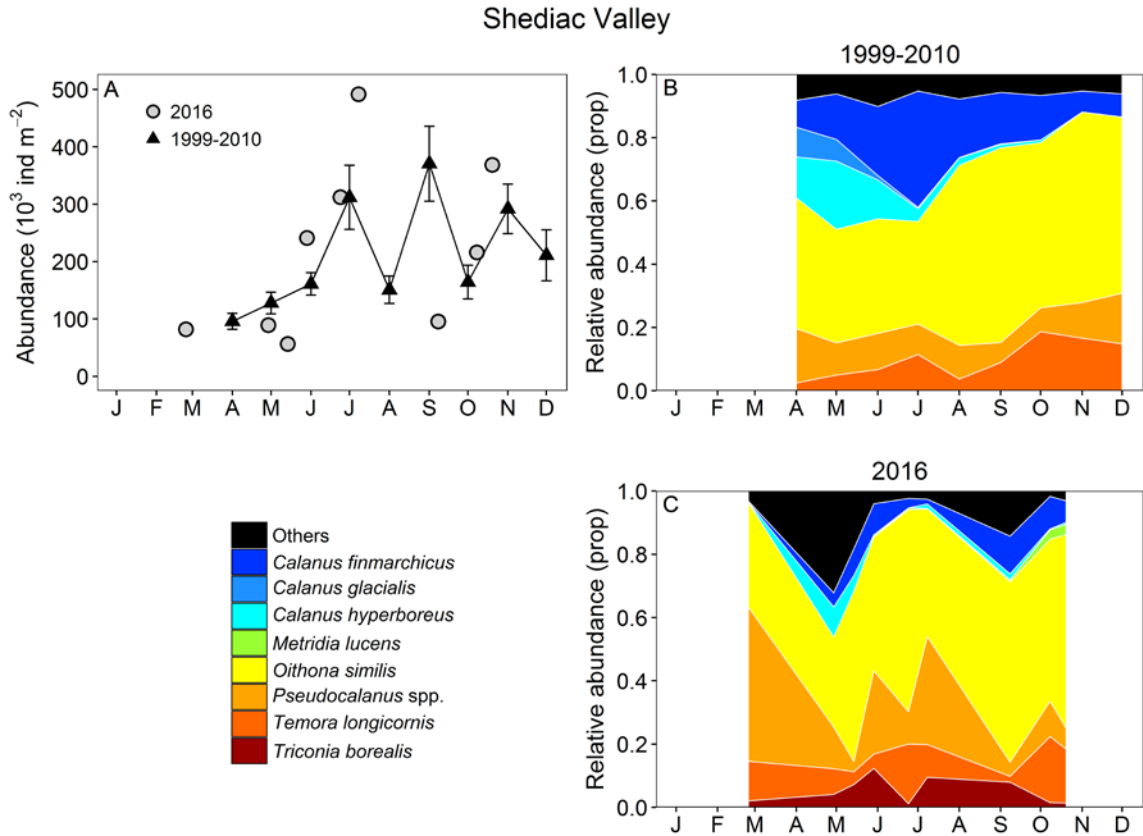


Figure 26. Seasonal variability of dominant copepods at Shediac Valley station. Copepod abundance (excluding nauplii) during the reference period (triangles and solid line with standard errors) and 2016 (circles) (A); Climatology of the relative abundance of the top 95% of identified copepod taxa during the 1999–2010 period (B) and in 2016 (C).

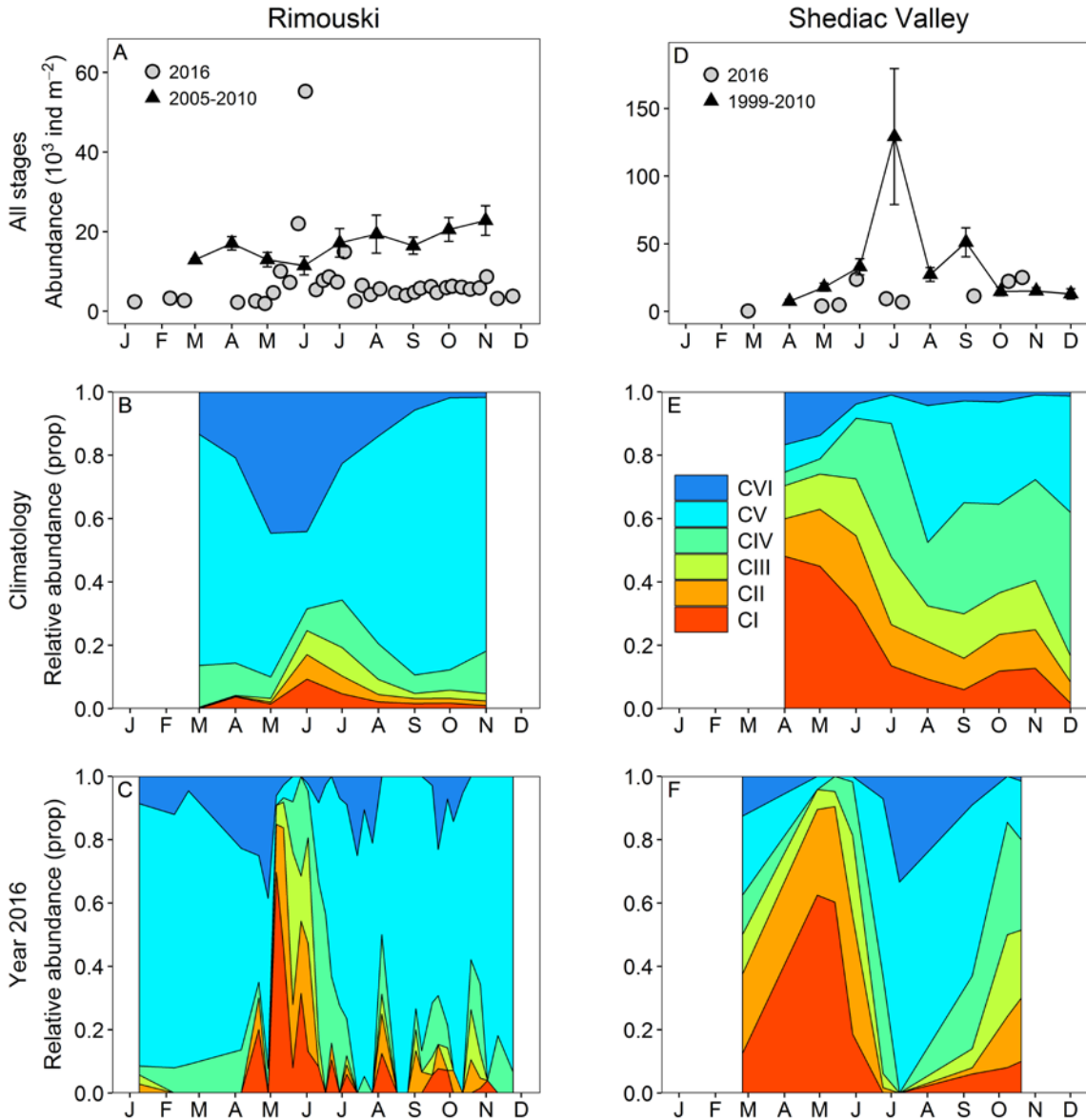


Figure 27. Seasonal variability in *Calanus finmarchicus* copepodite abundance at Rimouski (A–C) and Shediac Valley (D–F) stations. The climatologies of the combined counts for the reference periods (triangles and solid lines with standard errors; 2005–2010 for Rimouski and 1999–2010 for Shediac Valley) are plotted with data from 2016 (circles) (A, D). The seasonal variabilities for the individual copepodite stages for the reference periods (B, E) and for 2016 (C, F) are also shown.

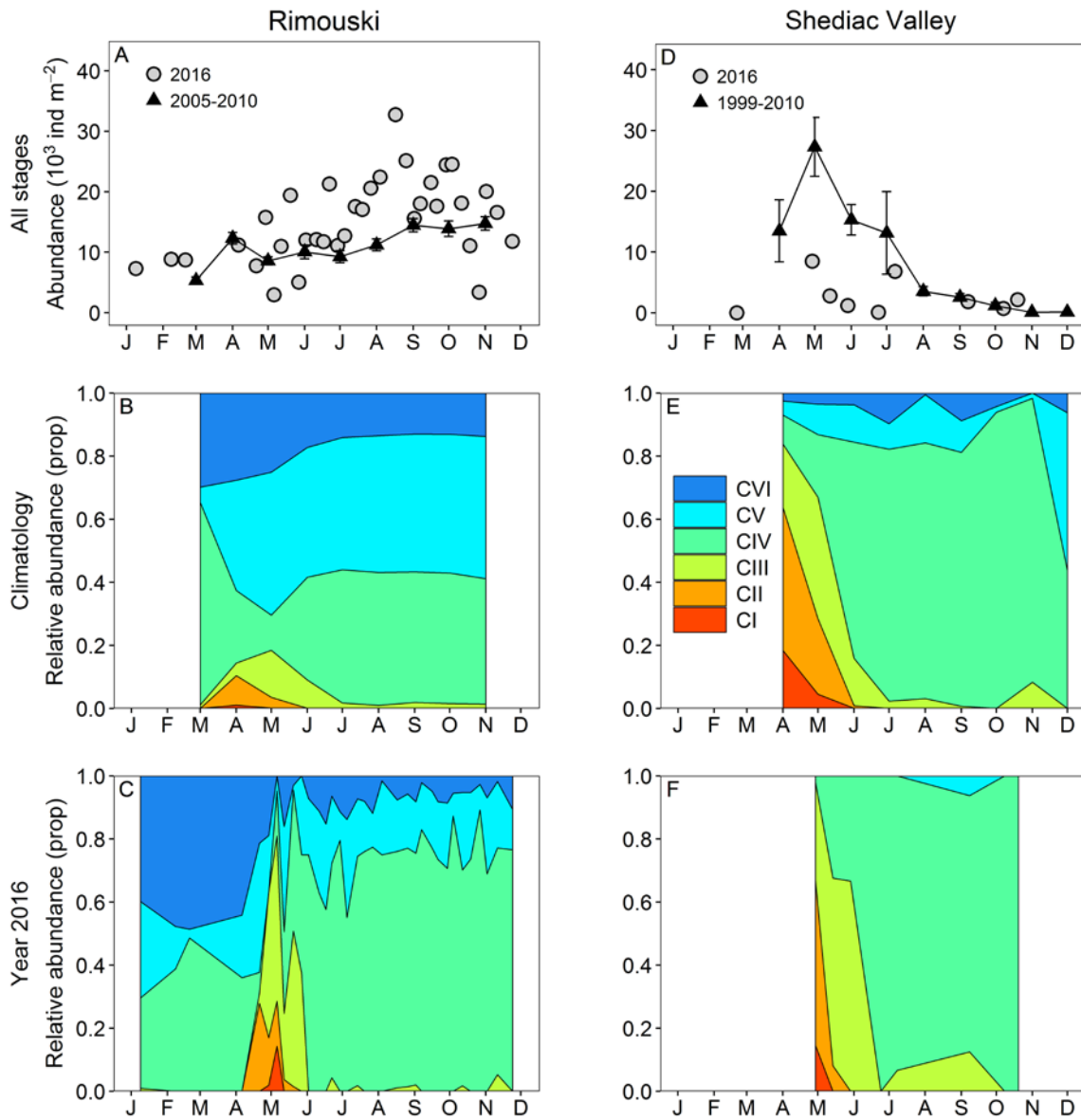


Figure 28. Seasonal variability in *Calanus hyperboreus* copepodite abundance at Rimouski (A–C) and Shediac Valley (D–F) stations. The climatologies of the combined counts for the reference periods (triangles and solid lines with standard errors; 2005–2010 for Rimouski and 1999–2010 for Shediac Valley) are plotted with data from 2016 (circles) (A, D). The seasonal variabilities for the individual copepodite stages for the reference periods (B, E) and for 2016 (C, F) are also shown.

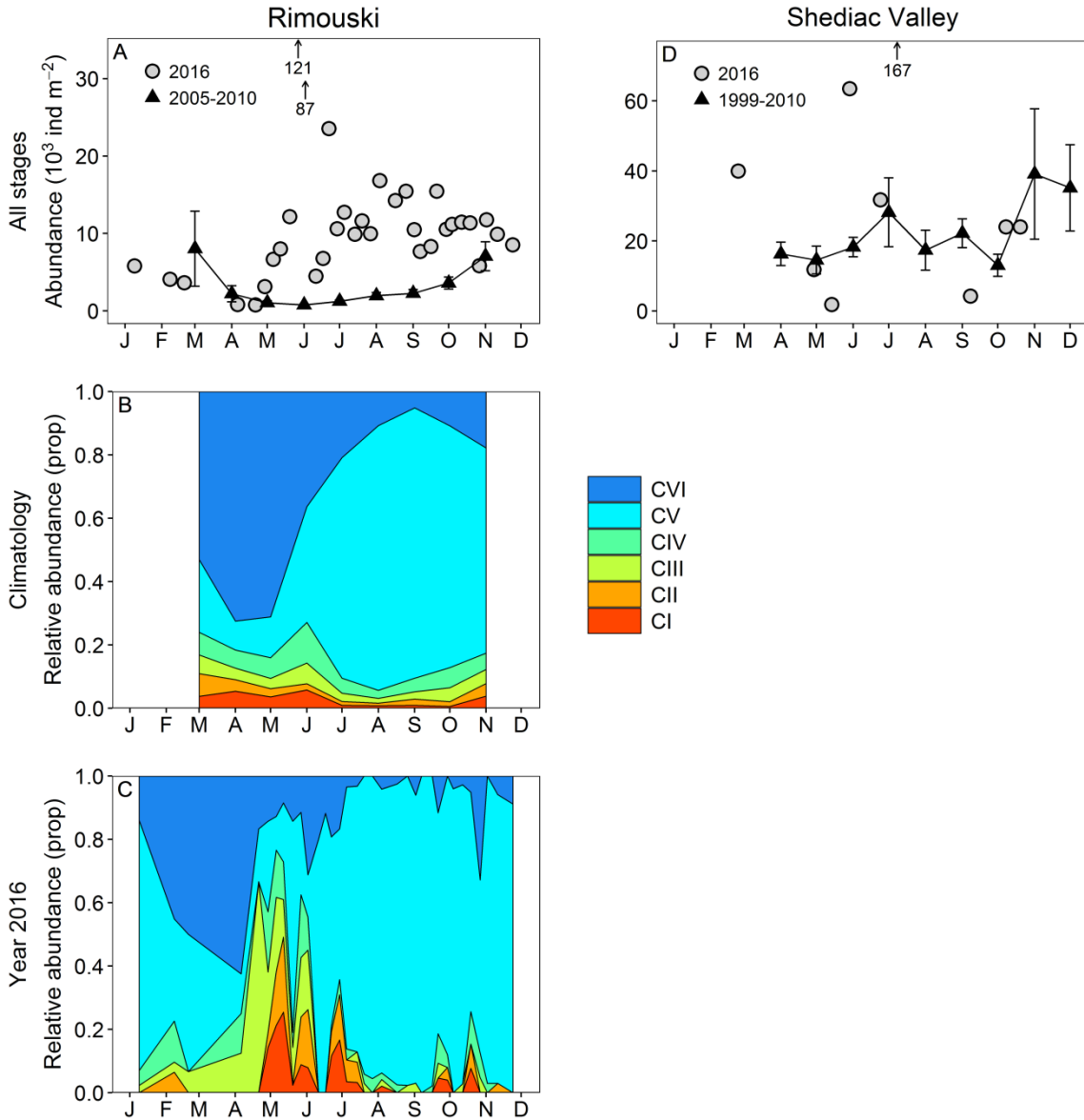


Figure 29. Seasonal variability in *Pseudocalanus* spp. copepodite abundance at Rimouski (A–C) and Shediac Valley (D) stations. The climatologies of the combined counts for the reference periods (triangles and solid lines with standard errors; 2005–2010 for Rimouski and 1999–2010 for Shediac Valley) are plotted with data from 2016 (circles) (A, D). Seasonal variability for the individual copepodite stages for the reference period (B) and for 2016 (C) are also shown. No stage information is available for Shediac Valley. The off-scale values for Rimouski station were sampled on 9 June (120,500 ind. m⁻²) and 15 June (86,500 ind. m⁻²), and that for Shediac Valley on 21 July (167,500 ind. m⁻²).

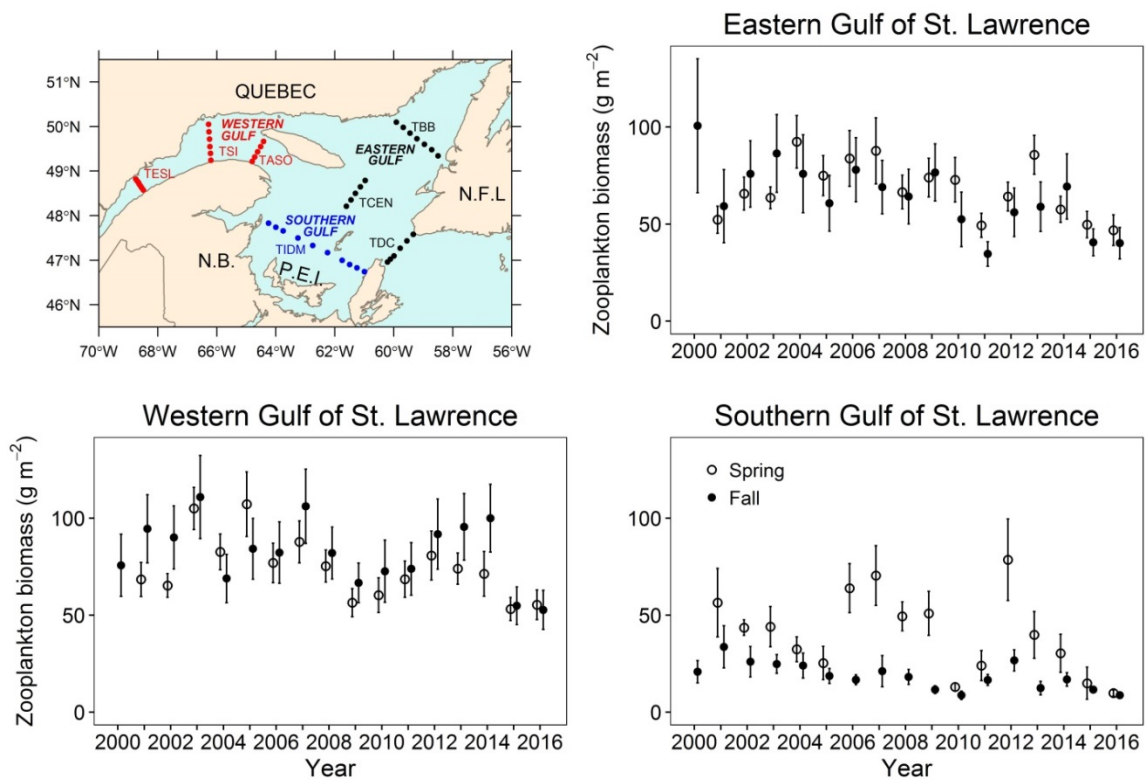


Figure 30. Mean total zooplankton biomass during spring (open circles) and fall (filled circles) for the three subregions of the Estuary and Gulf of St. Lawrence from 2000 to 2016. Vertical lines represent standard errors.

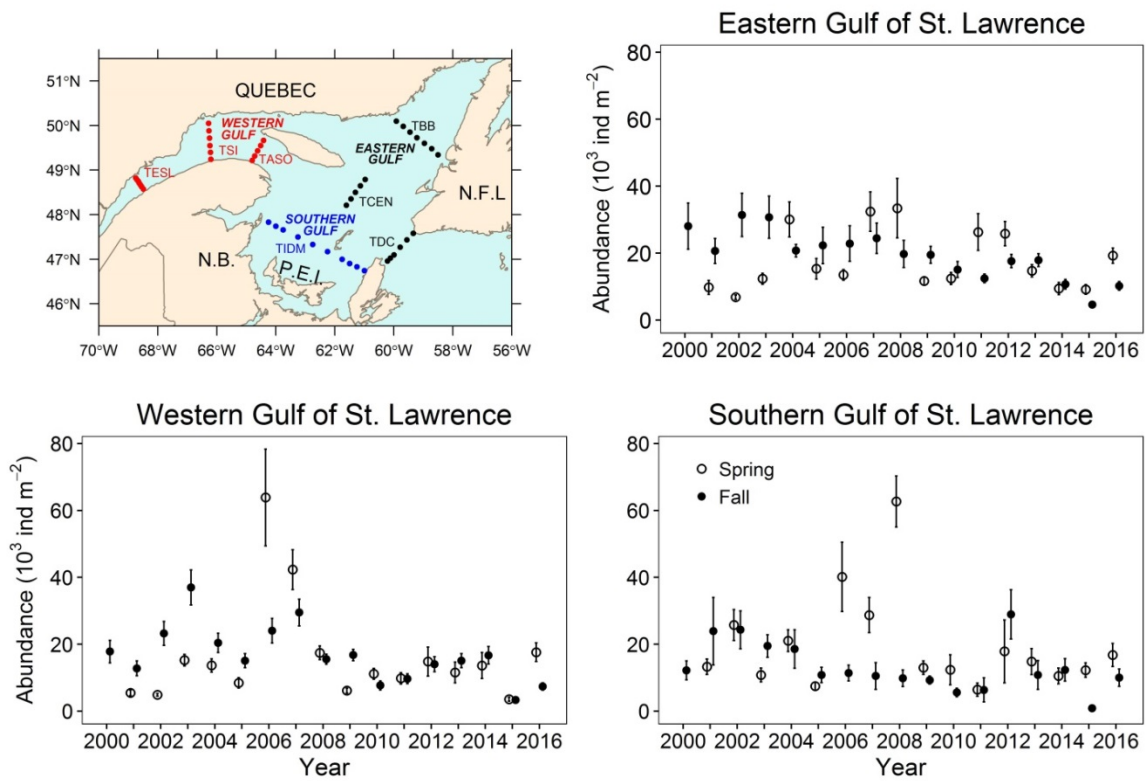


Figure 31. Mean total abundance of *Calanus finmarchicus* during spring (open circles) and fall (filled circles) for the three subregions of the Estuary and Gulf of St. Lawrence from 2000 to 2016. Vertical lines represent standard errors.

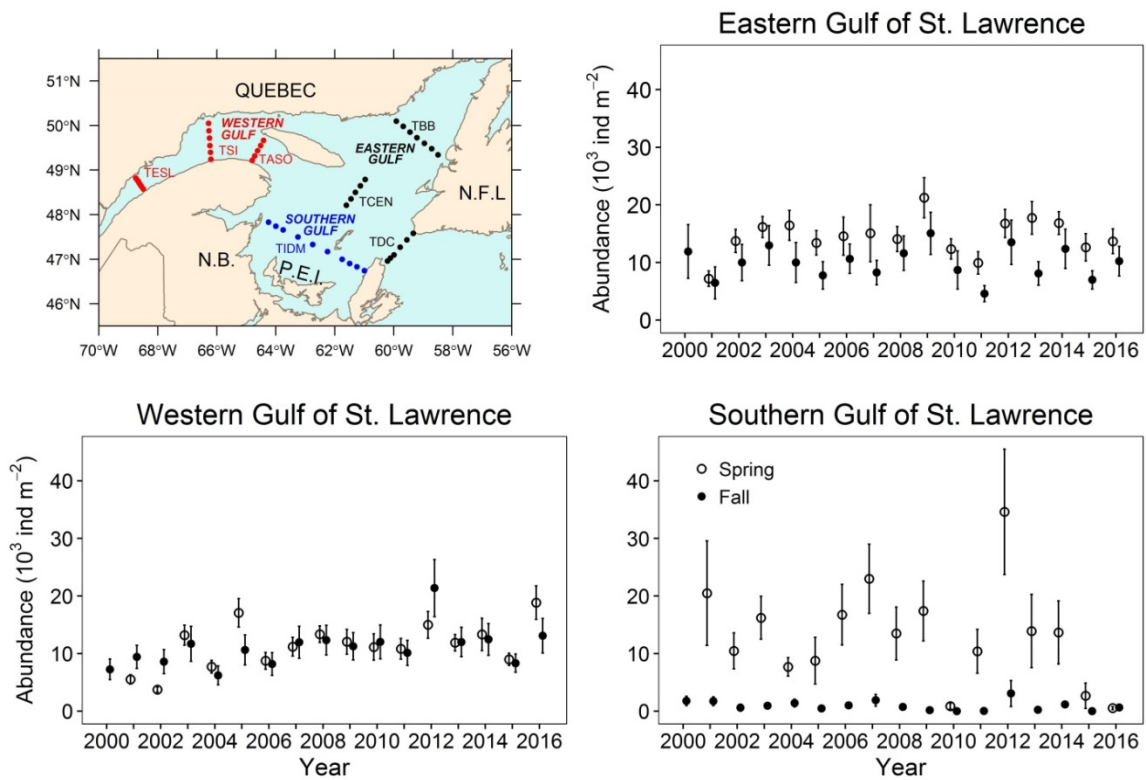


Figure 32. Mean total abundance of *Calanus hyperboreus* during spring (open circles) and fall (filled circles) for the three subregions of the Estuary and Gulf of St. Lawrence from 2000 to 2016. Vertical lines represent standard errors.

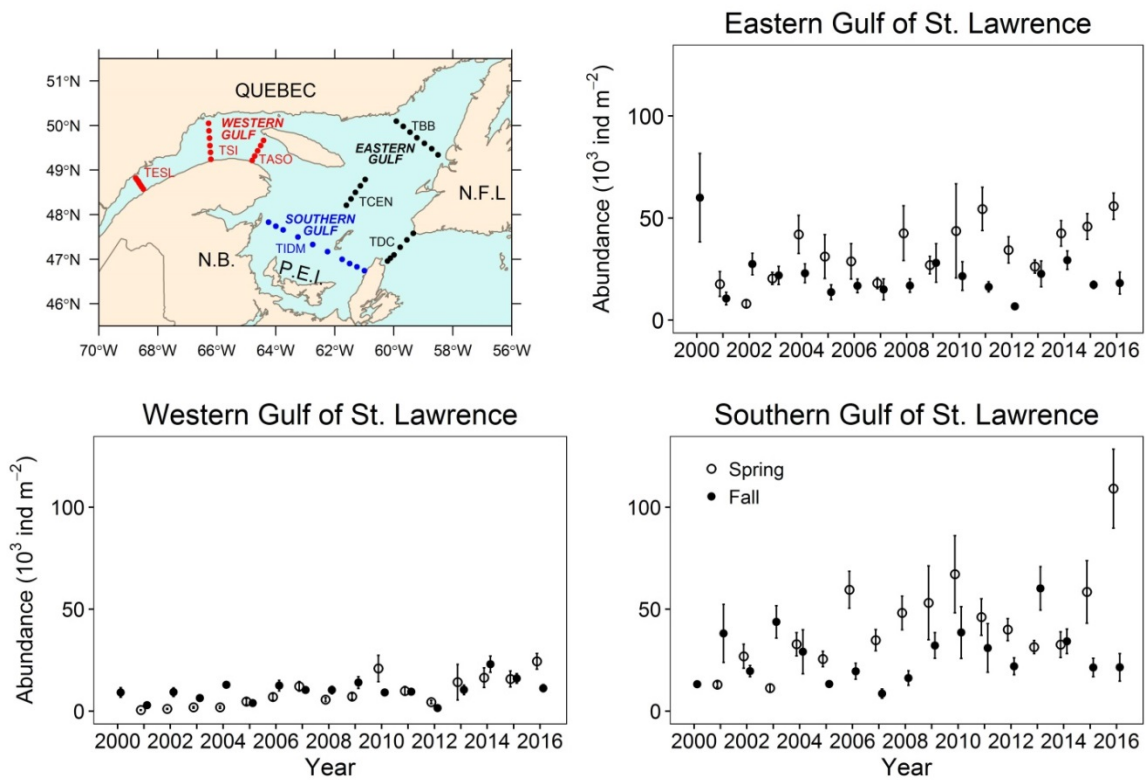


Figure 33. Mean total abundance of *Pseudocalanus* spp. during spring (open circles) and fall (filled circles) for the three subregions of the Estuary and Gulf of St. Lawrence from 2000 to 2016. Vertical lines represent standard errors.

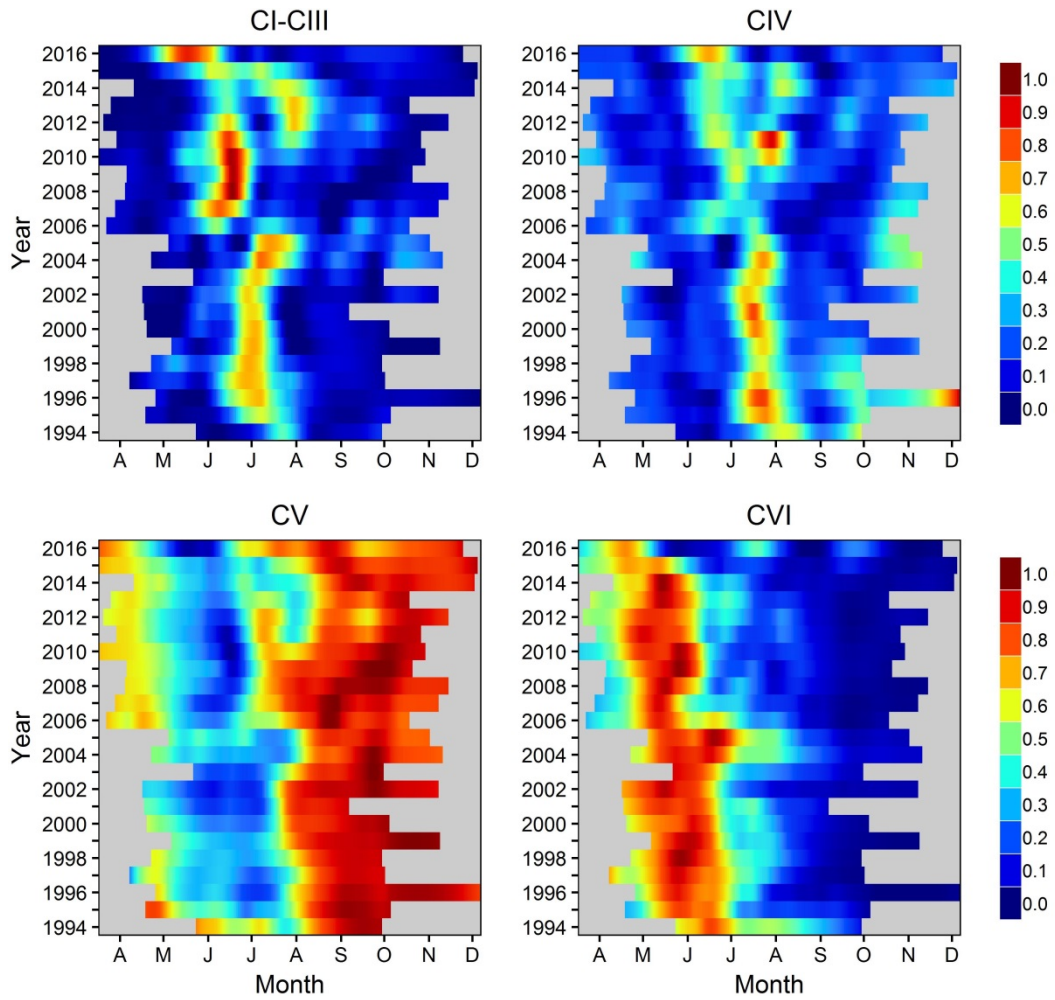


Figure 34. Seasonal cycle in relative proportions of total abundance for stages CI–CIII, CIV, CV, and CVI (male+female) *Calanus finmarchicus* copepodites from 1994 to 2016 at Rimouski station. Proportions are normalized by the annual maximum and smoothed using a Loess.

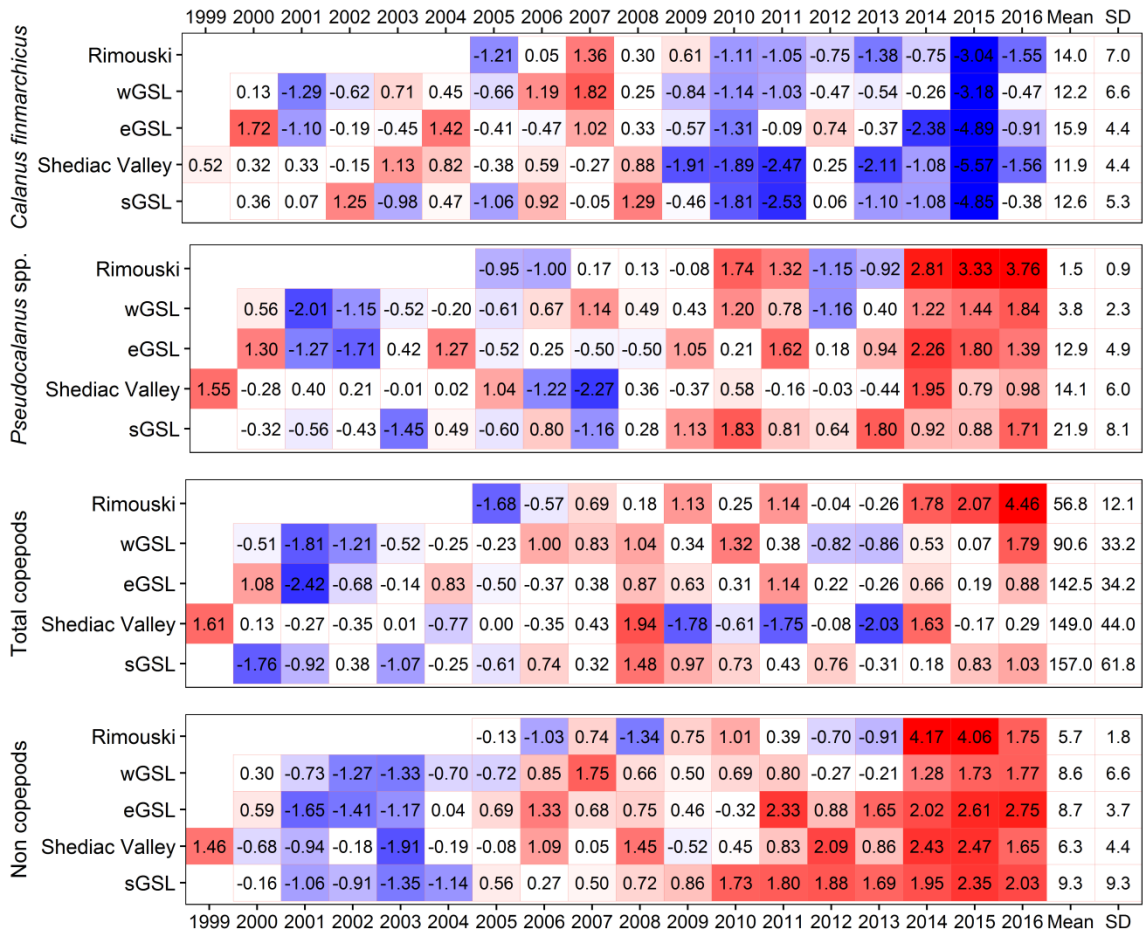


Figure 35. Normalized annual anomalies (scorecard) for four zooplankton categories at the high-frequency monitoring sites and the three subregions of the Estuary and Gulf of St. Lawrence (reference period 1999–2010 [2005–2010 for Rimouski]). Blue colours indicate anomalies below the mean and reds are anomalies above the mean. The climatological means and standard deviations are also given (abundance; $\times 10^3 \text{ ind. m}^{-2}$).

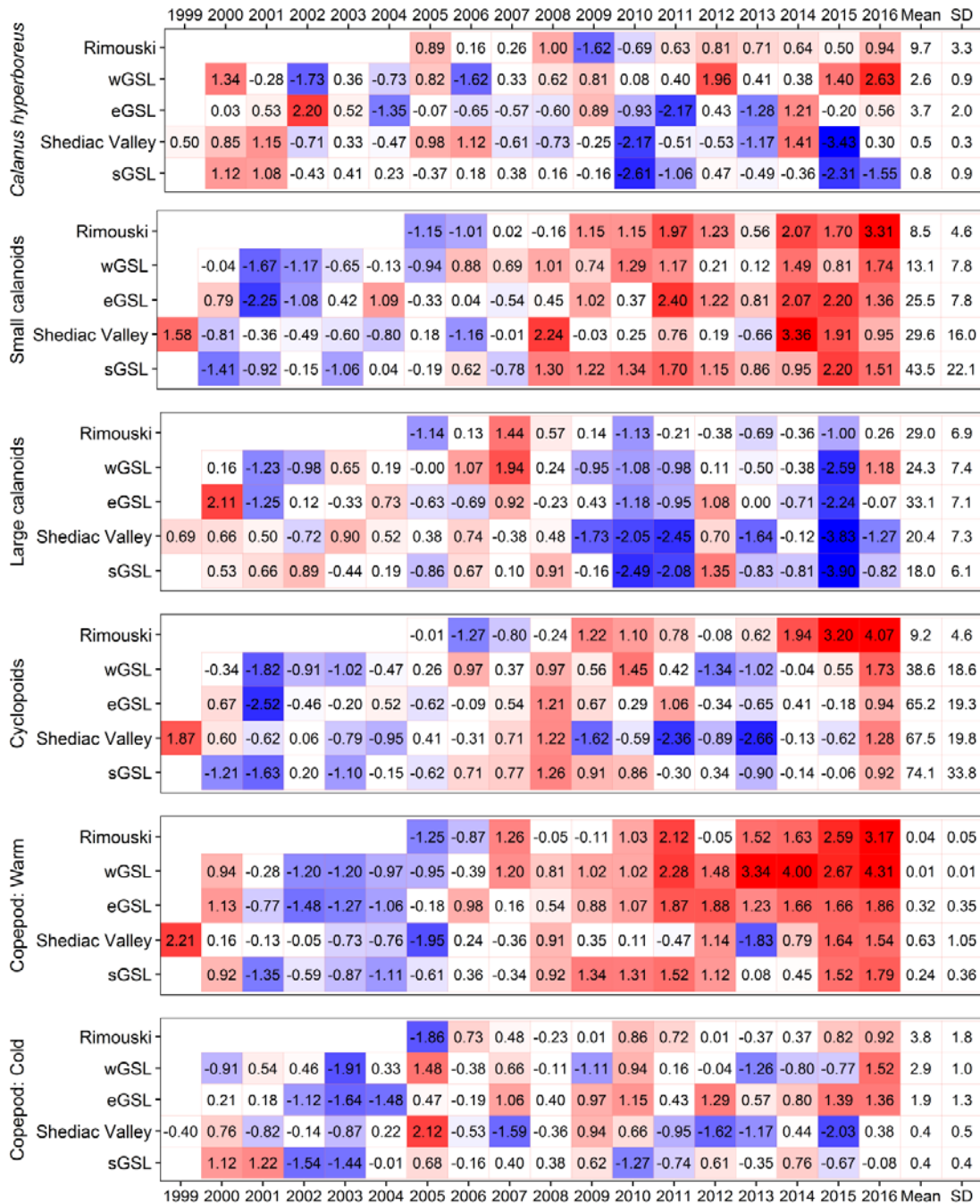


Figure 36. Normalized annual anomalies (scorecard) for six categories of zooplankton assemblages at the high-frequency monitoring sites and the three subregions of the Estuary and Gulf of St. Lawrence (reference period 1999–2010 [2005–2010 for Rimouski station]). Blue colours indicate anomalies below the mean and reds are anomalies above the mean. The climatological means and standard deviations are also given (abundance; $\times 10^3 \text{ ind. m}^{-2}$). Small calanoids: mostly neritic species such as *Pseudocalanus spp.*, *Acartia spp.*, *Temora longicornis*, and *Centropages spp.*; large calanoids: mostly *Calanus* and *Metridia* species; cyclopoids: mostly *Oithona spp.* and *Triconia spp.*; warm-water species: *Metridia lucens*, *Centropages spp.*, *Paracalanus spp.*, and *Clausocalanus spp.*; and cold/arctic species: *Calanus glacialis* and *Metridia longa*.

APPENDICES

Appendix 1. GLM results for Rimouski and Shediac Valley stations. Significance of year and month effects as well as the adjusted R squared of the regression for each group are presented.

Region	Group	year (p)	month (p)	R ²
Rimouski	<i>Calanus finmarchicus</i>	<0.0001	<0.0001	0.48
	<i>Pseudocalanus</i> spp.	<0.0001	<0.0001	0.57
	Total copepods	<0.0001	<0.0001	0.57
	Non copepods	<0.0001	<0.0001	0.43
	<i>Calanus hyperboreus</i>	<0.0001	<0.0001	0.40
	Small calanoids	<0.0001	<0.0001	0.65
	Large calanoids	<0.0001	<0.0001	0.25
	Cyclopoids	<0.0001	<0.0001	0.58
	Copepods: Warm	<0.0001	0.95	0.54
	Copepods: Cold	<0.0001	<0.0001	0.43
Shediac Valley	<i>Calanus finmarchicus</i>	<0.0001	<0.0001	0.36
	<i>Pseudocalanus</i> spp.	0.2	0.3	0.03
	Total copepods	0.4	<0.0001	0.18
	Non copepods	0.0007	0.0001	0.24
	<i>Calanus hyperboreus</i>	<0.0001	<0.0001	0.66
	Small calanoids	0.01	0.0004	0.18
	Large calanoids	<0.0001	<0.0001	0.38
	Cyclopoids	0.3	<0.0001	0.26
	Copepods: Warm	0.1	0.03	0.09
	Copepods: Cold	0.2	<0.0001	0.29

Appendix 2. GLM results for sections. Significance of year, season, and station effects as well as the adjusted R squared of the regression for each group are presented.

Region	Group	year (p)	season (p)	station(p)	R ²
wGSL	<i>Calanus finmarchicus</i>	<0.0001	0.002	<0.0001	0.66
	<i>Pseudocalanus</i> spp.	<0.0001	<0.0001	<0.0001	0.52
	Total copepods	<0.0001	<0.0001	<0.0001	0.76
	Non copepods	<0.0001	<0.0001	<0.0001	0.60
	<i>Calanus hyperboreus</i>	0.001	<0.0001	<0.0001	0.60
	Small calanoids	<0.0001	<0.0001	<0.0001	0.68
	Large calanoids	<0.0001	0.07	<0.0001	0.78
	Cyclopoids	<0.0001	<0.0001	<0.0001	0.70
	Copepods: Warm	<0.0001	0.3	<0.0001	0.47
	Copepods: Cold	<0.0001	<0.0001	<0.0001	0.66
sGSL	<i>Calanus finmarchicus</i>	<0.0001	<0.0001	<0.0001	0.32
	<i>Pseudocalanus</i> spp.	<0.0001	<0.0001	0.7	0.16
	Total copepods	<0.0001	<0.0001	0.003	0.29
	Non copepods	<0.0001	<0.0001	<0.0001	0.49
	<i>Calanus hyperboreus</i>	<0.0001	<0.0001	<0.0001	0.48
	Small calanoids	<0.0001	0.003	0.01	0.27
	Large calanoids	<0.0001	<0.0001	<0.0001	0.48
	Cyclopoids	<0.0001	<0.0001	0.0009	0.35
	Copepods: Warm	<0.0001	<0.0001	0.3	0.52
	Copepods: Cold	<0.0001	<0.0001	<0.0001	0.39
eGSL	<i>Calanus finmarchicus</i>	<0.0001	0.6	<0.0001	0.21
	<i>Pseudocalanus</i> spp.	<0.0001	<0.0001	<0.0001	0.27
	Total copepods	<0.0001	<0.0001	<0.0001	0.28
	Non copepods	<0.0001	<0.0001	<0.0001	0.45
	<i>Calanus hyperboreus</i>	0.05	<0.0001	<0.0001	0.53
	Small calanoids	<0.0001	0.96	<0.0001	0.40
	Large calanoids	<0.0001	<0.0001	<0.0001	0.45
	Cyclopoids	<0.0001	<0.0001	0.0008	0.32
	Copepods: Warm	<0.0001	<0.0001	<0.0001	0.51
	Copepods: Cold	<0.0001	0.0004	<0.0001	0.37